République Algérienne Démocratique et Populaire
Ministère de l'Enseignement Supérieur et de la Recherche Scientifique
Université 8 Mai 1945 Guelma

Faculté des Sciences et de la Technologie
Département d'Architecture
Laboratoire de Génie Civile et Hydraulique (LGCH)

THÈSE

EN VUE DE L'OBTENTION DU DIPLOME DE DOCTORAT EN 3ème CYCLE

Faculté des Sciences et de Technologies
Département de Génie Civil et d'Hydraulique
Spécialité : Structure

Présentée par

Oussama Nedjhioui

Intitulée

Étude expérimentale et numérique d'une poutre en béton armé renforcée par des matériaux composites

Sous la direction de: Madi Rafik

Jury

Nom et Prénom	Grade		
Mr Benmalek Mohamed Larbi	Professeur	Univ. du 8 Mai 1945 Guelma	Président
Mr Madi Rafik	Professeur	Univ. du 8 Mai 1945 Guelma	Rapporteur
Mr NAFA Zahreddine	Professeur	Univ. du 8 Mai 1945 Guelma	Examinateur
Mr Bouziane Salah	Professeur	Univ. du 20 août 1955 Skikda	Examinateur
Mr Guenfoud Mohamed	Professeur	Univ. du 8 Mai 1945 Guelma	Invité

Année Universitaire : 2023/2024

Dedication

*To my beloved **parents**, whose unwavering love, guidance, and support have been the foundation of my journey.*

*To my respected **teachers**, whose wisdom and knowledge have illuminated my path and enriched my mind.*

*To my loyal **brothers**, who have shared both the challenges and the joys of life's adventures with me.*

*And especially to those who supported me in this research: **Sofiane BENSEHLA**, **Oussama Merabat**, and **Ilyes Guendouz**. Your contributions and encouragement have been invaluable.*

May Allah make us all blessed wherever we are and grant us the ability to make a positive impact on Islam and Muslims through our collective efforts.

Acknowledgments

In the light of this work, I would first like to thank ALLAH All-Powerful for all the wonders he does in my life and for giving me the courage, strength, goodwill and especially the patience to complete this modest scientific contribution.

Then, I am extremely grateful to many people who made the completion of this Ph.D. thesis possible. I would like to address my warmest thanks to:

My supervisor ***Pr. Rafik Madi*** *for his guidance and support during these years, his expertise, understanding, and patience added considerably to my research study experience.*

The team of the Civil and Hydraulic Engineering Laboratory (LGCH), where I belong and its director ***Pr. Nouaouria Mohamed Salah*** *for their scientific services and orientations*

Pr. Fathe Bouteldja*, who devoted a lot of time and effort to assist us in completing the laboratory work, and whose valuable guidance and instructions resulted in the success of the laboratory work.*

I would also like to express my deep gratitude to the members of the jury.

I would like to thank all those who have helped me from near or far during these years of research and study.

I cannot conclude without a word of thanks to all my teachers and colleagues.

Table of Contents

ملخص

تستكشف هذه الدراسة تأثير الفتحات الطولية المستطيلة على أداء الانحناء للروافد الخرسانية المسلحة من النوع T، وتحديدًا عند تقويتها أو إعادة تجديدها باستخدام طبقات البوليمر المُقواة بالألياف الكربونية الخارجية. تضمنت الدراسة ثمانية روافد من النوع T مسلحة بالخرسانة، حيث كانت كل مجموعة من أربع مجموعات تحتوي على رافدة واحدة من النوع المملوء غير المجوّف ورافدة واحدة من النوع المُجوَّف. خضعت هذه الروافد لاختبارات دقيقة من خلال تجربة الانحناء بثلاث نقاط. جميع الروافد كانت مجهزة بالتساوي بطبقة بوليمر مُقواة بالألياف الكربونية مماثلة، وكانت نسب التسليح الطولية متطابقة. أظهرت النتائج التجريبية أن القدرة على التحمل النهائية للروافد الخرسانية المسلّحة من النوع T المُجوَّف والتي تم تقويتها تراجعت بنسبة 9% مقارنة بأقرانها من النوع المملوء. بالإضافة إلى ذلك، أظهرت الروافد المُجوّفة التي تم إعادة تجديدها والتي تعرضت لتحميل بنسبة 100% انخفاضًا بنسبة 24% في القدرة على التحمل النهائية مقارنة بالروافد المملوءة التي تم إعادة تجديدها. يجدر بالذكر أن طبقة CFRP قد كان لها تأثير إيجابي على تقليل التشوّه في الروافد المُجوَّفة مقارنة بالروافد المملوءة. فيما يتعلق بسلوك الانحناء، أظهرت الروافد المُجوَّفة التي تم تقويتها بطبقة البوليمر المُقواة بالألياف الكربونية والتي تحتوي على نسبة 5% من منطقة النواة المُجوَّفة عرضية أداءً مشابهًا للروافد الصلبة التي تم تقويتها. ومع ذلك، بعد تعرضها للتحميل المسبق، أظهرت الروافد المُجوَّفة التي تم إعادة تجديدها انخفاضًا في الكفاءة الانحنائية مقارنة بالروافد المملوء التي تم إعادة تجديدها. لتعزيز عمق فهمنا، تم إنشاء نموذج عددي معتمد باستخدام Abaqus لمحاكاة سلوك الروافد المجوَّفة من النوع T بدقة. فيما بعد، تمت إجراء دراسة تعميمية باستخدام النموذج المعتمد لاستكشاف تأثير تغيير موقع وحجم القسم المُجوَّف على استجابة الروافد من النوع T.

الكلمات المفتاحية:

الروافد، التجريبية، المسلحة ، بوليمر مُقواة بالألياف الكربونية، نموذج عددي، دراسة تعميمية.

Abstract

This research investigates the effect of longitudinal rectangular holes on the bending capacity of T-beams constructed with reinforced concrete (RC), especially when they undergo strengthening or retrofitting using external laminates made of carbon-fiber-reinforced polymer (CFRP). The study involved eight RC T-beams, organized into four groups, each comprising one hollow and one solid beam. A three-point bending experiment was employed for a comprehensive examination of these beams. All beams were consistently equipped with an identical CFRP laminate and shared the same longitudinal reinforcement ratios. The experimental results showed that the ultimate load-bearing capacity of strengthened hollow RC T-beams was reduced overall by 9% in comparison with solid RC T-beams. In contrast, retrofitted hollow RC T-beams, subjected to 100% preload, showed a 24% decrease in ultimate load bearing capacity versus retrofitted solid RC T-beams. In particular, CFRP laminate has been shown to reduce strains in hollow T-beams effectively compared with solid beams. Retrofitted hollow RC T-beams showed a decrease in flexural efficiency post-preloading, despite the fact that strengthened solid RC T-beams and CFRP-strengthened reinforced concrete hollow T-beams with a 5% hollow cross-section displayed largely similar bending behavior. To enhance our understanding, a numerical model was developed in ABAQUS, providing an accurate simulation of hollow RC T-beam behavior. Subsequently, the validated model was employed in a parametric study to explore the impact of changing the size and location of the hollow section on the response of RC T-beams.

Keywords:

Beams, experimental, numerical, reinforced, CFRP, parametric.

Résumé

Cette recherche explore l'impact des ouvertures rectangulaires longitudinales sur les performances en flexion des poutres en béton armé (BA) de type T, notamment lorsqu'elles sont renforcées ou rénovées avec des laminés polymères renforcés de fibres de carbone (CFRP) externes. L'étude a porté sur huit poutres en BA de type T. Chacun des quatre groupes comprenant une poutre pleine et une poutre creuse. Ces poutres ont été soumises à des tests rigoureux grâce à une expérience de flexion trois points. Toutes les poutres étaient renforcées par un laminé CFRP similaire et présentaient des taux de renforcement longitudinal identiques. Les résultats expérimentaux ont révélé que la capacité de charge ultime des poutres creuses renforcées en BA diminuait de 9 % par rapport à leurs homologues pleines. De plus, les poutres creuses rénovées en BA, soumises à une précharge de 100 %, présentaient une diminution de 24 % de la capacité de charge ultime par rapport aux poutres rénovées pleines en BA. Notamment, le laminé CFRP réduisait efficacement la déformation des poutres creuses en BA par rapport aux poutres pleines. Bien que le comportement en flexion des poutres creuses en BA renforcées par le CFRP avec une zone de noyau creux de 5 % en coupe transversale ressemblait étroitement à celui des poutres pleines renforcées en BA, les poutres creuses rénovées en BA présentaient une diminution de l'efficacité en flexion après la précharge. Afin d'approfondir notre compréhension, un modèle numérique validé a été créé à l'aide du logiciel ABAQUS, fournissant une simulation précise du comportement des poutres en BA de type T creuses. Par la suite, une étude paramétrique a été réalisée avec le modèle validé pour explorer l'influence de la variation de la position et de la taille de la section creuse sur la réponse des poutres en BA.

Key words:

Poutres, expérimentaux, numérique, renforcée, CFRP, paramétrique.

List of Figures

List of Tables

Introduction

Introduction

The field of civil engineering stands at the intersection of innovation and tradition, constantly evolving to meet the demands of modern society while preserving the integrity and safety of our structures. One of the most critical elements in civil engineering is the design and analysis of reinforced concrete (RC) T-beams, which play an integral role in supporting various infrastructure elements, from buildings and bridges to industrial facilities. As our built environment continues to grow and diversify, so too must our understanding and techniques for optimizing the performance of these structural components.

One pressing challenge in the realm of RC T-beams is the incorporation of openings and voids within these structures. While these openings serve vital functions like accommodating utility conduits, they often diminish the beams' load-bearing capacity, raising concerns about structural integrity and stability. In addressing this issue, engineers and researchers are compelled to explore innovative strategies to strengthen or retrofit these elements to restore and even enhance their performance.

The primary objective of this study is to comprehensively investigate the impact of longitudinal rectangular openings on the flexural behavior of RC T-beams. Through experimentation and numerical simulations, this research delves into the effectiveness of external carbon-fiber-reinforced polymer (CFRP) laminates in strengthening or retrofitting hollow RC T-beams, offering a multifaceted approach to tackling this prevalent issue.

Our working hypothesis posits that CFRP laminates can significantly enhance the load-bearing capacity and resilience of hollow RC T-beams with longitudinal openings. Additionally, we anticipate that specific parameters, such as the size and location of the openings and the type of CFRP strengthening, will influence the structural response of these beams.

The work presented in this thesis comprises a general introduction, five chapters, and a general conclusion.

Chapter I: Durability of Reinforced Concrete Structures

Within this chapter, we take our first steps into the domain of reinforced concrete structures, with a primary focus on the aspect of durability. Durability, in the context of structural performance, defines a structure's ability to fulfill its intended functions over an extended period, including its expected service life. We examine the dynamic interplay between these structures and the surrounding environment, a relationship fraught with profound implications for their longevity and

functionality. The environmental influences on reinforced concrete structures are pivotal in shaping their durability. This, however, poses an inherent risk, with the potential for concrete degradation and steel reinforcement corrosion as the most pressing concerns.

Concrete degradation and steel reinforcement corrosion represent two overarching risks that can introduce a medley of mechanical, physical, structural, chemical, or even biological effects, ranging from cracks and structural weakening to reduced load-bearing capacity. The significance of mitigating these risks and adhering to sound construction methods cannot be overstated in the pursuit of structural longevity. By exploring the multifaceted challenges associated with the durability of reinforced concrete structures, we set the stage for a comprehensive examination of potential solutions and strategies to safeguard their integrity.

Chapter II: Strengthened RC Beams

The second chapter of our exploration is dedicated to the world of reinforced concrete beams, with a specific focus on the concept of strengthening these structural elements in construction. While traditional repair methods have been employed with some degree of success, they are not without their limitations and challenges. This chapter introduces the need for innovative strengthening techniques, shedding light on the substantial drawbacks associated with conventional approaches.

The central spotlight shines on the use of composite materials, particularly Carbon Fiber Reinforced Polymer (CFRP), as a revolutionary means of reinforcement. The advantages of this approach are manifold, offering enhanced strength, ductility, and load-bearing capacity to aging or degraded RC beams. The introduction of CFRP composite materials signifies a paradigm shift in the realm of structural reinforcement, as we seek to overcome the limitations of traditional methods and usher in a new era of structural fortitude.

Chapter III: Materials and Methods

Within this chapter, we delve into the critical aspects of materials and methods that underpin our research. The reinforced concrete T-beams at the heart of our study have been carefully sourced and manufactured under stringent conditions to ensure consistency and reliability. This standardized production process is integral to our research, as it minimizes external variables that could impact our test results. It is worth noting that this rigorous protocol is part of our overarching strategy to ensure the precision and accuracy of our findings.

The primary objective of our experimental study is to assess the impact of longitudinal openings on the flexural behavior of these reinforced concrete T-beams. These openings are a key focus of our research, as they represent a potential vulnerability in the structural integrity of these beams. Furthermore, our study endeavors to evaluate the efficacy of external Carbon Fiber Reinforced Polymer (CFRP) laminates as a means of reinforcement and repair for these hollow RC T-beams. As we journey through this chapter, we lay the foundation for the extensive experimentation and analysis that forms the core of our research.

Chapter IV: Experimental Testing and Analysis Results

This chapter is dedicated to the rigorous testing and analysis of the reinforced concrete T-beams that constitute the subject of our research. Our work begins with the purposeful conduction of three-point bending tests, a critical avenue for exploring the flexural performance and structural characteristics of these T-beams. Within the confines of these tests, we aim to meticulously examine a comprehensive array of parameters, each contributing to our understanding of the beams' behavior.

These parameters include the first cracking load, yielding, ultimate load, crack patterns, failure modes, load-displacement profiles, and the Load-Strain response. Through these tests, we delve into the intricacies of the beams' mechanical responses, unearthing insights that are instrumental in shaping our research findings. Our analytical exploration extends beyond the confines of theoretical knowledge, offering a hands-on perspective into the dynamic world of structural performance.

Chapter V: Numerical Analysis

In the fifth chapter of our work, we transition from the experimental testing to the numerical analysis, driven by the overarching goal of optimizing the performance of reinforced concrete hollow T-beams strengthened with CFRP.

In our concluding chapter, we will synthesize the insights gained from our multifaceted research and propose recommendations that can further enrich the field.

Chapter I

DURABILITY OF REINFORCED CONCRETE STRUCTURES

Chapter I. Durability of reinforced concrete structures.

I.1. Introduction

The durability of structures is their ability to perform their required functions for the longest possible period, including their expected life [1].

The environment around reinforced concrete structures is the first place that affects their durability resulting in the loss of their functionality and the loss of the structure's integrity in the worst case. Concrete deterioration can be divided into two main categories: concrete degradation and steel reinforcement corrosion. These two risks can include one or more mechanical, physical, structural, chemical, or biological effects on concrete or the corrosion process of steel reinforcement [2]. The types of concrete deterioration are summarized in the **Figure I-1**.

The optimum durability of structures is achieved by avoiding these influences and using the correct execution method.

This chapter deals with the main factors affecting the durability of structures and concrete and ways to avoid them.

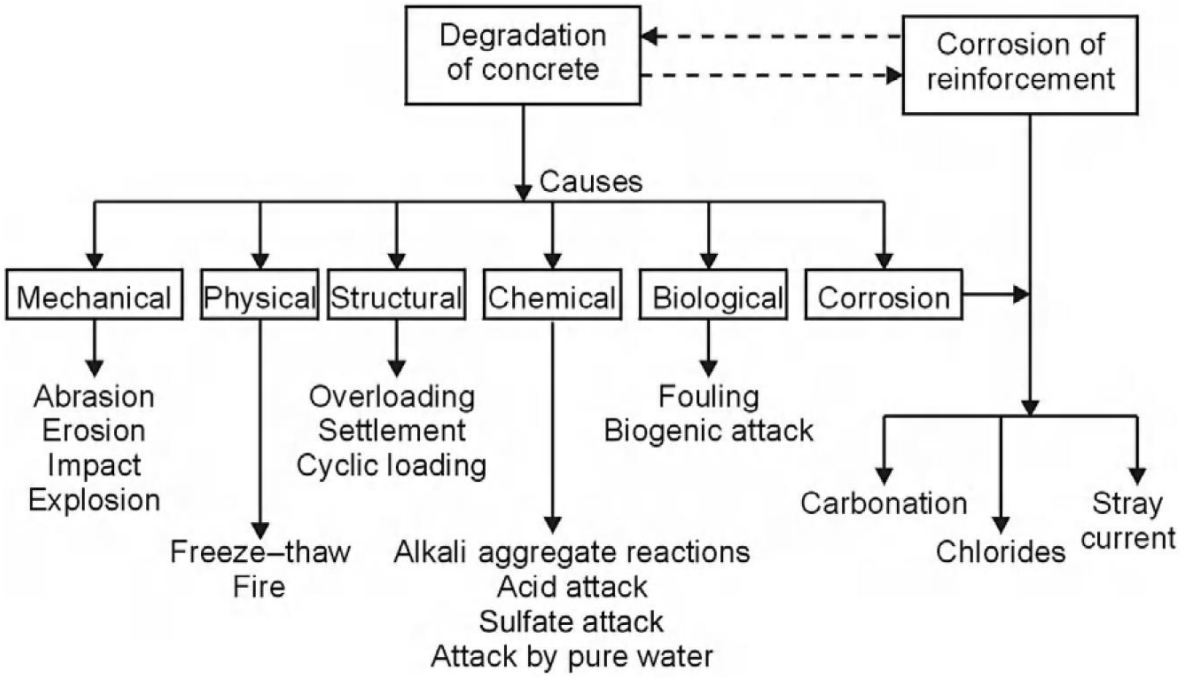

Figure I-1. types of concrete deterioration [3].

I.2. Durability of reinforced concrete structures against influencing factors

I.2.1. Durability from mechanical factors

I.2.1.1. Abrasion

Abrasion, as defined by ASTM, "is the wear due to hard particles or hard protuberances forced against and moving along a solid surface" [4] (**Figure I-2**). As a result, Abrasion resistance can therefore be defined as the ability of a surface to resist frictional wear [5].

According to ACI, abrasion can be caused by four different factors: human traffic on concrete floors, vehicle traffic with studded tires and snow tire chains, abrasive materials in water that affect hydraulic structures like dam spillways, and high-water velocities that cause cavitation at the concrete surface [5].

Several elements are necessary to provide excellent abrasion resistance in concrete. The materials chosen (aggregate, supplementary cementitious materials and reinforcing fibers), the mix composition (Water-to-cementitious materials (w/cm) ratio and compressive strength versus abrasion resistance), strength growth, and building techniques all have a significant impact on the resistance level [6].

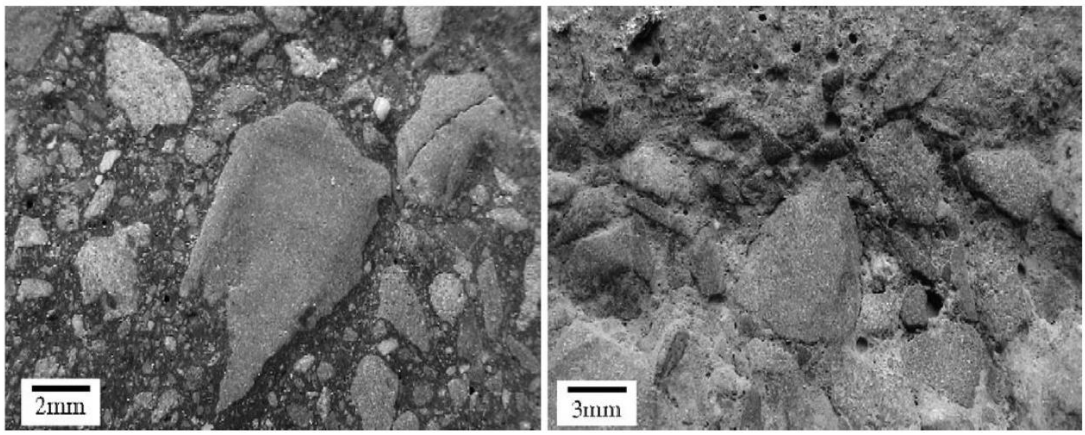

(a) (b)

Figure I-2. Abraded surface of concrete: (a) 2mm et (b) 3mm [7].

I.2.2. Durability from physical factors

I.2.2.1. Freeze-Thaw:

Freezing-thawing damage occurs by the rapid freezing and thawing of water accumulation in cracks, voids, or pores of the concrete, which leads to concrete expansion and thus cracking or spalling. The air entrainment process in the pores and voids of the concrete is a way to prevent freezing and thawing [8].

Freeze-thaw cycles cause the following disorders:

- microcracking or cracking of the concrete mass in the case of internal freezing.
- spalling of the concrete surface under the combined action of freeze-thaw cycles and the use of de-icing salts . (**Figure I-3**).

The following Preventive measures must be considered to ensure the freeze-thaw durability of concrete:

The following principles must govern the formulation of a freeze-thaw-resistant concrete:

- It is necessary to reduce the total volume of the pores and their capillary dimension to reduce permeability, prevent water from entering, have a well-distributed network of air bubbles, and ensure good mechanical resistance.
- Use a high cement dosage to increase compactness, a W/C ratio (water to cement mot), must be below a specific limit.
- A network of entrained air bubbles must be provided.
- The aggregates used must be non-freezing.
- It is also advisable to respect the covers of the reinforcements when placing the concrete.
- Effectively cure the fresh concrete after its implementation using a curing product, for example.
- If possible, design the structures by keeping the water away so as not to saturate the concrete with water (provide for forms of laying of 2% minimum).
- Do not expose young concrete to negative temperatures.
- Not apply de-icing salts until the concrete has reached sufficient strength.

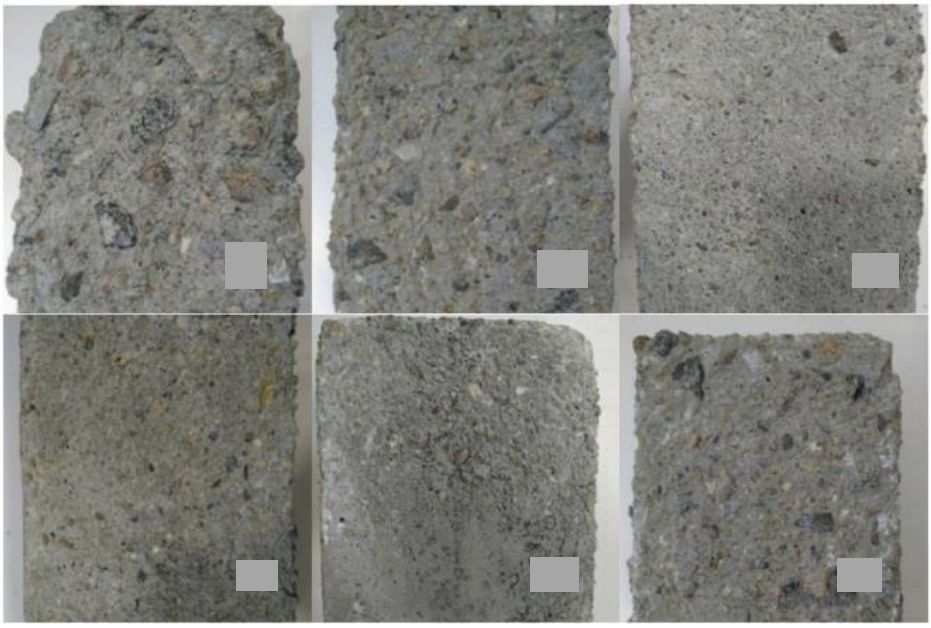

Figure I-3. Concrete surface after freezing-thawing cycles (spalling of the concrete surface) [9].

I.2.2.2. Fire:

Exposing concrete to a high temperature causes water to evaporate, which leads to concrete shrinkage in one direction and the expansion of aggregates in another. This causes microcracks to occur inside the concrete and thus to its deterioration.

The fire resistance of cementitious materials (mortar, concrete) depends on their formulation, physicomechanical characteristics, and the environmental conditions to which it is subjected, such as the rate of rising in temperature, the maximum temperature reached, and the exposure time. Exposure of concrete structures to fire generates several forms of thermal damage (instability), such as spalling and detachment of surface concrete (**Figure I-4**) [10].

Different forms of thermal damage:

In the event of a fire in buildings or tunnels, the concrete may exhibit thermal instability above a certain temperature. The thermal instability of concrete can present itself in various forms [11], [12]:

- **Explosive spalling**: This type of burst occurs during the first thirty minutes of the fire or a standard test. It can occur at a temperature above 100°C. The explosive burst is characterized by a sudden detachment of small or large pieces of concrete, accompanied by a loud noise.

- **Surface spalling**: commonly called spalling, surface spalling is characterized by the detachment of small pieces (up to approximately 20 mm) of the facing exposed to fire. It is less violent than the explosive burst.
- **Bursting of aggregates**: this bursting is caused by the thermal expansion of the aggregates close to the surface due to the temperature rise. The main causes of this phenomenon are the conversion of quartz at 570°C. The damage caused by the bursting of aggregates is only superficial.
- **Corner spall**: This is seen in the advanced stages of fire when the concrete is weakened, and cracks develop due to tensile stresses along the edges and corners of the structure.
- **Bursting by the detachment of the aggregates**: this type of instability results from the modification of the microstructure of the cement paste with the temperature rise and the internal cracks generated by the differential thermal expansion between the cement paste and the aggregates.
- **Bursting in the cooling phase**: it is non-violent and noiseless. This phenomenon is caused by the presence of limestone aggregates and the rehydration of the lime during the cooling phase.

Figure I-4. Spalling in RC slab exposed to fire [13].

I.2.3. Durability from chemical factors

I.2.3.1. Alkali–aggregate reaction (AAR)

The aggregates and alkaline cement paste react, resulting in the growth of an expanding crystalline gel strong enough to produce cracks in the aggregates and the concrete matrix. (Also known as the alkali-silica reaction, ASR). Silica gels are created when soluble silicates in the aggregates react. These gels enlarge after absorbing water and cause a "map cracking" and gel efflorescence [8] As seen in **Figure I-5**.

Figure I-5. Map cracking due to an alkali-silica reaction [14].

Concrete durability from Alkali–aggregate reaction:

It is possible to avoid the worst impacts of these reactions by taking appropriate preventative steps prior to pouring concrete [14], [15]:

- Making Use of Nonreactive Aggregates: The aggregates must undergo stringent testing, thorough quality control must be assured, and ideally, field performance should be well-documented to ensure non-reactivity.
- Utilization of cement with a low-alkali content.
- Incorporation of a suitable pozzolan: Most alkali-aggregate reactions are affected by pozzolans, and expansion due to an alkali-silica reaction can frequently be avoided or reduced by substituting 20–30% of the Portland cement with an appropriate pozzolan. The quantity and arrangement of the exposed hydroxyl groups on the surface of the individual particles are likely connected to the activity of fine siliceous powders and pozzolans. The combination of pairs of hydroxyls connected to nearby silicon atoms on the surface, leaving

strained silicon-oxygen groups (siloxane bridge systems) at the surfaces, is hypothesised to drive off water.

- Design to reduce aggregate wetting.

There are known approaches that can aid in extending the service life of the structure after ASR-induced expansion and degradation have occurred in concrete [14]:

- Reducing moisture by applying suitable outer layers of insulation.
- Reduce moisture by using drainage.
- Treating existing cracks to reduce expansion and direct moisture ingress, deicing salts.
- The use of deicing agents that raise the alkalinity of concrete should be avoided.

I.2.3.2. Acid attack:

The pH of the pore water in hardened cement paste is roughly 13, making it an alkaline substance. This means that liquid acids can attack concrete.

The hydrated cement's calcium hydroxide, Ca(OH)2, is particularly vulnerable to acid attack, but the C-S-H and, in rare cases, the aggregate are also susceptible. When the liquid's pH falls below 6.5, the attack will start.

The main activity of hydrogen ions in acid attack is to leach calcium hydroxide by the following reaction:

$$Ca(OH)_2 + 2H^+ \rightarrow Ca^{2+} + 2H_2O$$

Attacks on C-S-H are also possible when the acid is more concentrated, Creating silica gel:

$$3CaO \cdot 2SiO_2 \cdot 3H_2O + 6H^+ \rightarrow 3Ca^{2+} + 2(SiO_2 \cdot nH_2O) + 6H_2O$$

C–S–H; Silica gel

Concrete exposure to acid leads to its erosion and thus severe damage to the structure (**Figure I-6**).

Several preventive measures should be taken into consideration to ensure the durability of concrete from acid attacks:

- Using calcareous aggregates, such as limestone or dolomite, rather than siliceous aggregate helps neutralise the acid.
- Filling the pores of the concrete surface or coating it with resistant chemicals such as sodium silicate (water glass), fluoride salts, and some iron compounds.

- Carbon dioxide gas or vaporised silicon tetrafluoride can be used to treat the surface. These gases seal the surfaces by forming very insoluble CaCO3 or CaF2.
- Portland cement can be efficiently reduced in Ca(OH)2 content by combining SCMs, such as fly ash, GGBFS, silica fume, or metakaolin, at replacement levels up to roughly 60% [16].

Figure I-6. tank damage containing hydrochloric acid [17].

I.2.3.3. Sulfate attack:

The expanding attack of the calcium hydroxide and calcium aluminates in the concrete by Sulfates of sodium, calcium, potassium, and aluminum present in groundwater, soils and industrially derived sulfate from chemical processes can degrade the concrete matrix [8].

The presence of sulfate in concrete in sufficient concentration causes it to crack and spall, which ultimately causes concrete to disintegrate (**Figure I-7**). The concrete spalling and cracking result from the creation of expansive products such as gypsum and ettringite, loss of C-S-H bonding properties by decalcification of C-S-H (**Figure I-8**) and the breakdown of the concrete microstructure [16].

Figure I-7. Effect of sulfate-rich soil on concrete (concrete spalling) [16].

Figure I-8. Example of attack by sulfuric acid dosed at 5% for ordinary concrete for four months [18].

Several steps can be identified to ensure a durable structure that is resistant to sulfate attack:

- Design according to the code standards.
- Cement modification.
- External structures protection.

Building code standards specify many things that can reduce sulfate attacks, such as:

- Selection of cement content, grade of concrete.

- Determine the aggressive chemical environment.
- Determine the concrete cover for reinforcement.
- Service life and other exposure classes.

Cement modifications can include the following:

- Reduce C_3A content in cement.
- The use of sulfate-resistant cement.
- Use of pozzolan: Incorporating or replacing part of the cement with pozzolanic material reduces sulfate attack. Mixing pozzolan turns leached calcium hydroxide into a non-leaching cement product. This pozzolanic action is responsible for the impermeability of concrete. Second, removing calcium hydroxide reduces the susceptibility of concrete to attack by magnesium sulfate.
- Use of high-quality concrete: using dense well-compacted concrete shows higher resistance to sulfate attack. Similarly, concrete with a lower water/cement ratio also shows higher resistance to sulfate attack.

The following External structure protections are possible:

- Structure foundations can be placed above the groundwater table, reducing groundwater contact with the concrete surface.
- A waterproof membrane can be provided to avoid exposure of the structure to the external environment.
- Exterior coating application.
- Determine the appropriate concrete cover for reinforcement BS EN 1008: 2002.

I.2.3.4. Attack by pure water

Pure water is quite aggressive toward concrete despite being essentially ion-free. Since concrete contains soluble species like portlandite $Ca(OH)_2$ that can be leached from the matrix, these fluids' ion-hungry character makes them hostile. In some circumstances, the cement hydration products may be dissolved and leached from the concrete matrix, destroying the CSH gel and reducing concrete strength. Calcium hydroxide is the most easily soluble product; hence, it is frequently the first substance to be dissolved or removed. This degradation is frequently caused by an attack from pure water [16]. Avoiding pure water attacks can be made by well-compacted and cured concrete and providing proper drainage after concrete pouring.

I.2.4. Durability from structural factors

I.2.4.1. Overloading and cyclic loading:

Building codes are used to design the cross-sections of concrete using calculated and estimated loads. Concrete may sustain damage or fail when a structure is overloaded to the degree that is not protected by safety considerations. Shear, flexure, or tension overloading are all possible, and there are several cracking patterns to watch for. A concrete part that has been overloaded may develop many forms of cracks. The type of loading stress can be determined based on the orientation and location of the crack (vertical, diagonal, top, bottom, etc.). Positive flexural cracks, for instance, are indicated by vertical fissures at a beam's centre and bottom [19] (**Figure I-9**).

To avoid cracks overloading on concrete:

- The structure must be designed to be strong enough to withstand any load at any time it is likely to encounter during its life cycle. Therefore, the estimate of the total load acting on the structure or the total load likely to run on the structure is calculated accurately and must be designed.
- Use a low percentage of water-cement and increase the coarse aggregate in the concrete mixture,
- Additives containing calcium chloride should be avoided.
- The surface should be prevented from the rapid evaporation of water content.
- Loads should be applied to the concrete surface only after it has gained its maximum strength.
- Sealing cracks by injection method.
- Repair of damaged members by FRP materials.

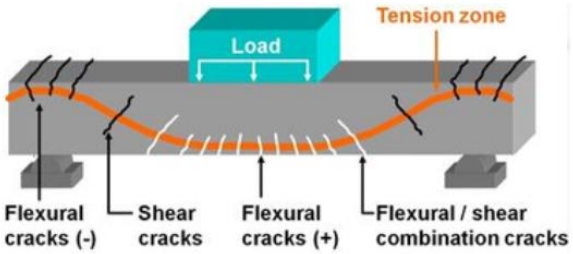

Figure I-9. overloading cracks on concrete beam.

I.2.4.2. Settlement

Fresh concrete might develop plastic settlement cracks or subsidence cracks. Bleed water rises, and solid particles settle after the concrete has consolidated. A variation in settlement occurs when this vertical displacement is opposed by a rigid inclusion, like a reinforcing bar close to the concrete surface. This differential settlement produces tensile stresses that form exactly above the reinforcement, leading to settlement cracks above and parallel to the bar and a weakened concrete zone above the reinforcement [20].

Settlement may also affect the local bond and leave a gap under the reinforcing bar. Because these cracks develop above and parallel to the bar, they enhance the chance of corrosion by giving water and deicing agents a direct route to the bar [21] (**Figure I-10**).

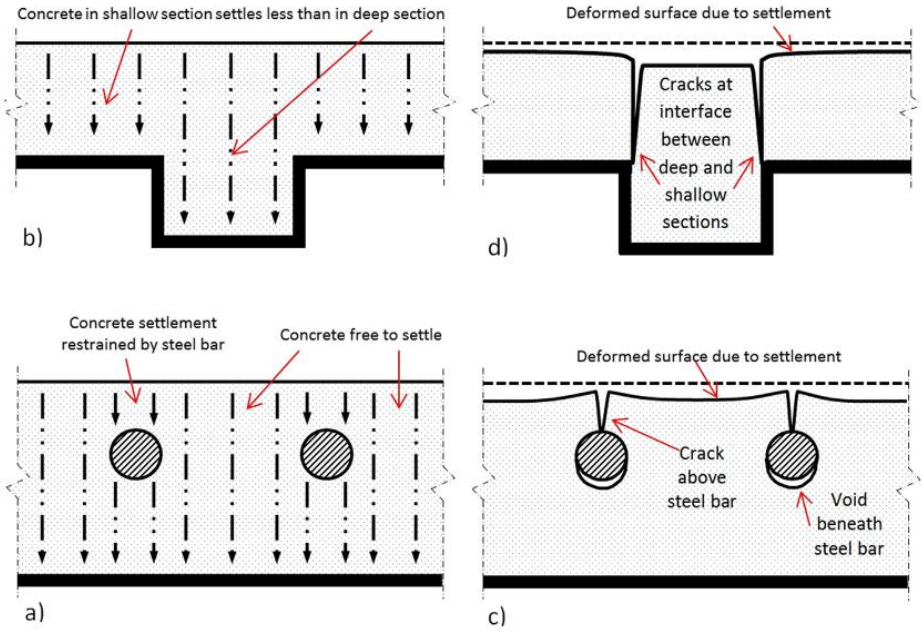

Figure I-10. Plastic settlement cracking in a slab and T-beam due to presence of steel reinforcement [22].

Much research has been conducted to prevent settlement cracking in concrete, such as:

- The displacement of settlement is significantly reduced when synthetic fine fibrillated polypropylene and coarse polypropylene fibres are added to the concrete mixtures [23].
- Compared to mortar that only contains sand, settlement is reduced when Lightweight Aggregate (LWA) is added, and the reduction in settlement gets more when more LWA is added. Additionally, internal curing, which supplied water to the mortar when moisture

was lost due to evaporation and cement hydration, contributed to improving settlement performance [24].

- Re-vibration usually performed 1-2 hours after the concrete pouring, is a technique that, when used properly, can help improve the in-situ quality of the concrete by removing defects from bleeding, plastic shrinkage, and constrained settlement [16].

I.2.5. Durability from corrosion of reinforcement

There are two main mechanisms for steel corrosion in concrete that don't necessitate the deterioration of the concrete first. Carbonation and chloride attack are the first and second of them, respectively [8]. The results of corrosion on reinforced concrete structures are: (**Figure I-11** and **Figure I-12**)

a) Column and beam cracking.
b) concrete cover spalling and delamination.
c) the rebar's cross section reduction due to pitting corrosion.
d) brittle failure of prestressing tendons due to hydrogen embrittlement.

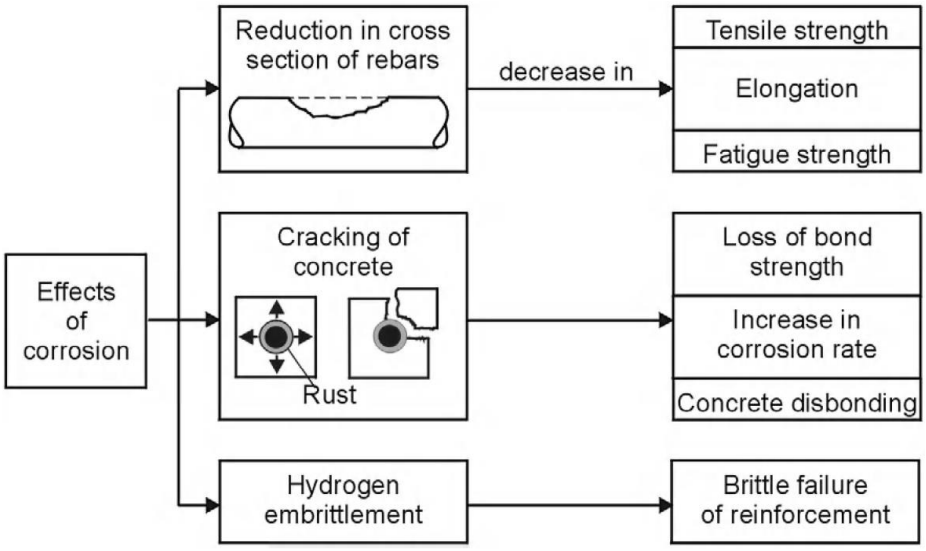

Figure I-11. Corrosion consequence in reinforced concrete structures [25].

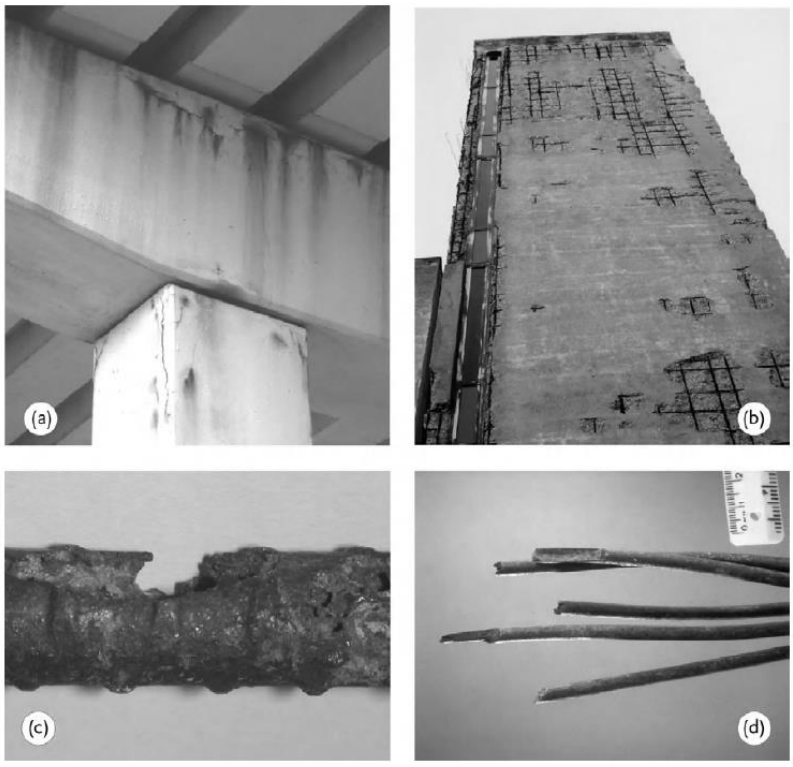

Figure I-12. Examples of consequences of corrosion of steel in concrete [3].

I.2.5.1. Carbonatation

Carbonation occurs when carbon dioxide in the air reacts with the alkaline constituents of the concrete [26]. When hydrated cement paste reacts with the carbon dioxide in the air in moist settings, it produces an acidic aqueous solution that tends to neutralize the alkalinity of concrete (This action is referred to as carbonation).

When it comes to the corrosion of embedded steel, carbonatation has a significant impact:

- As the initial effect, the pH of the pore fluid decreases from its typical range of pH 13 to 14 to ranges that are close to neutrality. If chlorides are not initially present in the concrete, the pore solution is entirely made up of pure water following carbonation. As a result, the steel in humid carbonated concrete corrodes just like it would if it came into touch with water.
- As a second effect of carbonation, chlorides that are normally attached to hydrated phases and in the form of calcium chloroaluminate hydrates may also be freed, increasing the aggressivity of the pore solution.

The component of cement paste that reacts with CO2 most readily is calcium hydroxide. The reaction that occurs in an aqueous solution can be represented as follows [3]:

$$CO_2 + Ca(OH)_2 \xrightarrow{H_2O,NaOH} CaCO_3 + H_2O$$

To reduce the carbonation effect:

- Manufacture of low permeability concrete in order to reduce the rate of carbon dioxide and water permeability inside the concrete. To achieve low concrete permeability, we must: Use a low percentage of cement water, provide good compacting of concrete, and use sufficient and appropriate curing of concrete.
- Provide sufficient concrete cover (The distance from the reinforcement bar to the outer surface of the concrete). This distance is essential for structural integrity, durability, and reinforcement protection from corrosion and fire.
- Put a protective coating on the concrete cover that prevents carbon dioxide from reaching the concrete.

I.2.5.2. Chloride attack

Chloride attack is the second leading contributor to reinforcement corrosion. This is typically caused by one of the following:

- The penetration of de-icing salt by roads and vehicles.
- The penetration of sea salt into marine environments.
- Cast-in salt from contaminated mix components.
- Calcium chloride cast in as a set accelerator.

Corrosion occurs at a specific level of chloride. When the chloride content of the reinforcement surpasses 0.4% of the cement weight, there is a severe risk of corrosion, especially when there is moisture present. Chloride-ingress rates depend on the environment and concrete's quality. Chlorides can be transported quickly through wetting and drying absorption in concrete with low reinforcement cover, especially in low-quality concrete, and through capillary action that nearly suctions chloride-laden water into the concrete. The salt is subsequently left behind as the water evaporates [8].

According to ACI Committee 222 (1996) [27], there are three theories about the chloride attack:

- Chloride ions can enter the oxide film on steel more easily than other ions do through pores or flaws in the film.

- In competing with dissolved or hydroxyl ions, chloride ions are adsorbed on the metal surface.
- As a result of competition between chloride and hydroxyl ions for the ferrous ions produced by corrosion, a soluble complex of iron chloride arises and can diffuse away from the anode, shattering the protective layer and allowing corrosion to proceed. (**Figure I-13**)

Several methods are available to prevent the effect of chlorides on concrete structures. Among these methods are the following:

- Increasing the cover over the steel reinforcement is the easiest method to protect against chloride attack. Studies show that a one-inch increase in the coating can double the life expectancy of a structure.
- The rate of reinforcement degradation under the harsh conditions of chlorides can be prevented by the presence of epoxy-coated rebar, cathodic protection, or stainless steel-covered rebar. (**Figure I-14**)
- Reduce the permeability of the concrete to lessen the ingress of chloride ions into the concrete.

Figure I-13. Cracking Caused by Corrosion in Reinforced Concrete as a Result of Chloride Pollution and Ingress [28].

Figure I-14. Protective layer against corrosion [29].

Chapter II

STRENGTHENED RC BEAMS

Chapter II. Strengthened RC beams

II.1. Introduction

Most construction companies of reinforced concrete works use the technique of lining the elements degraded by the reinforced concrete for the reinforcement and the repair of the structural elements. This technique is not expensive because of the materials used and does not require skilled labor. On the other hand, it has significant drawbacks, such as:

- The considerable increase in the sections of the elements consequently increases the weight of the structure, which requires resizing the foundations.
- The need to decommission the structure to be reinforced for the duration of the works.
- Shoring of beams and floors during the rehabilitation phase.
- The problem of adhesion between the old and the new concrete.
- The redistribution of uncontrolled additive charges.

Considering these problems, the development of another process of repair and strengthening, namely that of the use of composite materials. This technique consists of bonding composite slats or fabrics to degraded areas or strengthening them to increase their resistance or ductility capacity.

II.2. Behavior of RC beams strengthened by FRP material

Using a fabric of composite materials (FRP) associated with epoxy glues on tensioned surfaces or on lateral surfaces is a very effective way to reinforce reinforced concrete beams, particularly for weakly reinforced beams. Bonding the fabric to tensioned surfaces increases the ultimate strength of the reinforced beams, and by decreasing the deflection of the structures, it also increases their stiffness (**Figure II-1**), thus limiting the propagation of cracks. This phenomenon makes it possible to reduce the reinforcements' corrosion and improve the structures' durability. One of the most common applications of composite materials for the reinforcement of reinforced concrete structures concerns structures subjected to bending or shear stresses [30].

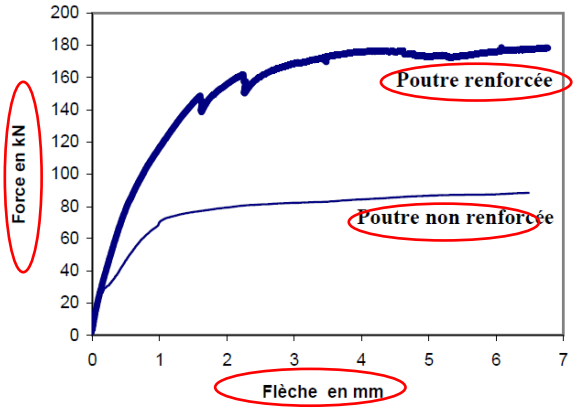

Figure II-1. Comparison of behaviour between strengthened and unstrengthened beams [30].

The composite material is an elastic material whose behaviour differs from that of concrete and steel (**Figure II-2**). The adhesion of FRP fabrics to surfaces of reinforced concrete structures causes a change in structural behaviours compared to those of unreinforced reinforced concrete structures: for example, the relationship between force and deflection or failure mode [30].

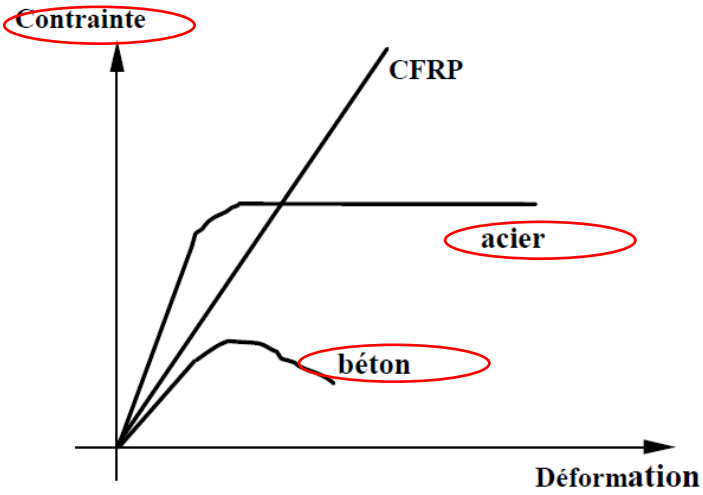

Figure II-2. Comparison of behaviour between different materials [30].

II.3. FRP constituents

FRP composites comprise two essential components: a load-bearing constituent, primarily fibres, and a polymeric matrix that serves as the fibres' binders and protectors. The matrix allows load transfer between fibres and ensures that embedded fibres keep their directional stability and orientation [31] (**Figure II-3**).

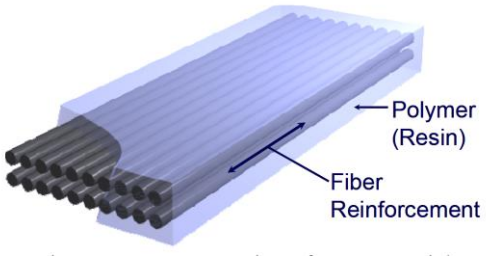

Figure II-3. FRP components: matrix and Carbon fibre [32].

II.3.1. Fibers

Composites are typically anisotropic and display different mechanical properties in three orthogonal directions. FRP composites' properties can vary depending on the method of manufacture [33].

There are three common types of reinforcing fibers: glass, aramid, and carbon. Generally, glass fibres have the lowest elasticity modulus, and carbon fibres have the highest. When tested, all fibre types behave in a linear elastic way. Basalt fibers have recently been made commercially available [34].

Table II-1 provides commercially available fibres' mechanical and physical characteristics [35]. It should be noted that the aramid and carbon fibres' negative thermal expansion coefficients show that these materials shrink when heated.

Table II-1. Properties typically found in reinforcing fibers [34].

Fiber type	Fiber identification	Density (lbs/ft.^{3})	Tensile modulus (ksi)	Tensile strength (ksi)	Failure strain (%)	Thermal expansion coefficient (310^{26}/F)	Poisson's ratio
Basalt		168	13,050	435	3.2	8.0	
Glass	E-Glass	159	10,500	500	4.80	8.99	0.20
	S-Glass	155	12,600	625	5.00	5.22	0.22
Aramid	Kevlar 49	91	19,000	525	2.80	23.60	0.35
	Technora	88	10,100	435	4.60	210.79	0.35
Carbon	T-300	110	33,500	530	1.40	21.08	0.20
	P-100	134	10,000	350	0.32	22.61	0.20
	AS-4	112	36,000	590	1.65	21.08	0.20
	IM-7	111	43,500	770	1.81	21.35	0.20

II.3.2. Matrix

Thermosetting polymer is the most often utilised matrix for structural composites. Polyester, vinyl ester, and epoxy are the most popular polymeric matrix materials utilised with high-performance reinforcing fibres. They are all thermosetting polymers that are chemically resistant and have good processability. Epoxies cost more than polyesters and vinyl-esters but generally offer superior mechanical qualities and exceptional durability. Chemical reaction processes are used to cure thermoset polymers, including epoxy, and the curing process is irreversible. The mechanical characteristics of two commercially available epoxies often employed in FRP composites are listed in **Table II-2** [34].

Table II-2. FRP epoxy mechanical characteristics [34].

Epoxy type	Sikadur	Tyfo S epoxy (psi)
Tensile strength	8000	10,500
Tensile modulus	250,000	461,000
Tensile elongation	3%	5%
Flexural strength	11,500	17,900
Flexural modulus	500,000	452,000

II.3.3. Composite interfacial adhesion and debonding

Utilizing the composite constituents depends on the quality of the adhesive bonds at the interfaces between plies and concrete and the strengthening FRP layers.

The concept of "adhesion" refers to intermolecular forces that act across an interface and takes surface energies and interfacial tensions into account. Adhesives interact with a solid surface's molecular forces when they come into touch with it as a liquid and flow over and through the surface's irregularities. The "joint" is then created when the adhesive hardens. Thus, the fundamental conditions for good adherence are the close contact between the adhesive and the substrates and the absence of any weak layers or contamination at the interface. Essentially, the treated surface of FRP and the exposed components of concrete should have more significant surface energy than the adhesive's surface tension [36], [37], [38].

II.4. Forms of plating beams

Existing reinforced concrete structures frequently need to be strengthened or repaired. Adhesively bonding plates or fabrics to the surfaces is a typical retrofitting technique. This section will give a thorough overview of all kinds of plating.

II.4.1. Plate position

Through an adhesive bond, bolts, or wraps, forces from the RC structure can be transferred to the external plates. Any beam surface may be covered with plates, which can be shaped as flat plates, channels, or angle sections.

II.4.1.1. Tension face plates

The tension face plate is the position most frequently utilised because it maximizes the bending lever arm and increases the bending strength brought on by plating. However, tension plates are more susceptible to early delamination, as delamination stress concentrations are likely to be interacting with nearby tensile reinforcement bars. It is also important to remember that adding tension reinforcement decreases the RC cross-ductility, sections which can restrict how much strength can be added by tension face plates. The sides of the beam could be plated as a substitute [39] (**Figure II-4**).

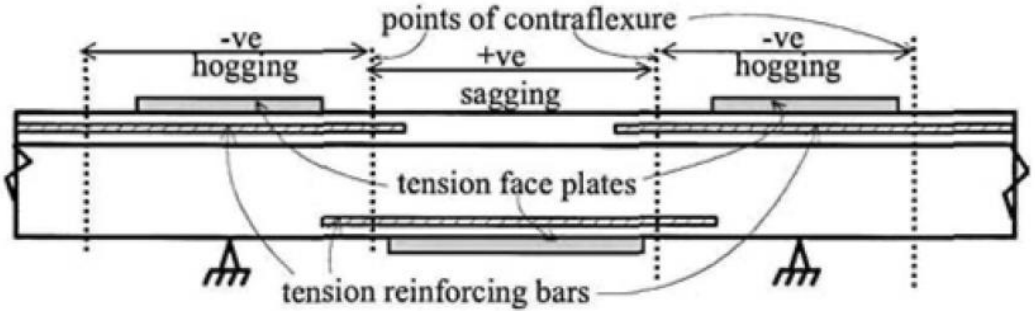

Figure II-4. Tension face plated beam [39].

II.4.1.2. Side plate:

Due to the smaller lever arm, side plates are less effective at boosting bending capacity than plates on the tension side. However, since beams clad on the sides tend to be more ductile than girders clad on the tension face, it may be possible to bond a larger surface area of the plate to the sides than to the tension face of the girder; this is especially true if the plate is extended into the compression region of the web, as in plate A in **Figure II-5**.

Due to the lack of interaction between the stresses surrounding the tension reinforcing bars and the debonding stresses, adhesively bonded side plates be less susceptible to debonding. Additionally, adhesively bonded side plates can significantly increase the concrete component of the vertical shear capacity [39].

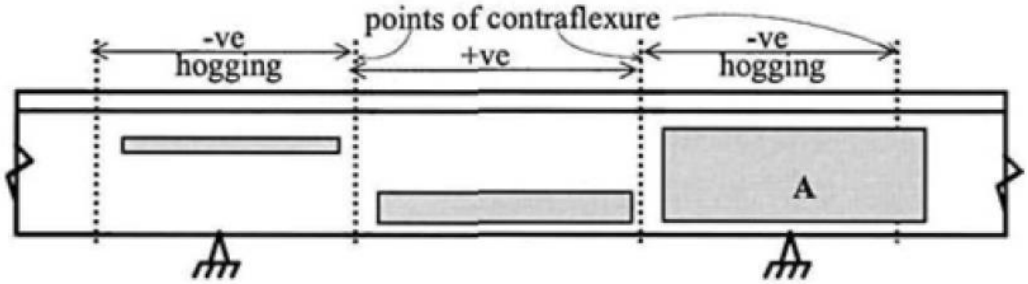

Figure II-5. Side plated beam [39].

II.4.1.3. Compression face plates

As shown in **Figure II-6**, plates may also be bonded to the compression face. It is possible to use compression face plates, like those in position A, to improve beams' ductility and vertical shear resistance. Extending tension face plates into the compression faces, as seen at B, is another typical procedure that discourages but does not always prevent debonding. Because there is no interaction between delamination loads and those exerted around compression armatures, so compression surface sheets are less prone to early delamination than tension surface sheets [39].

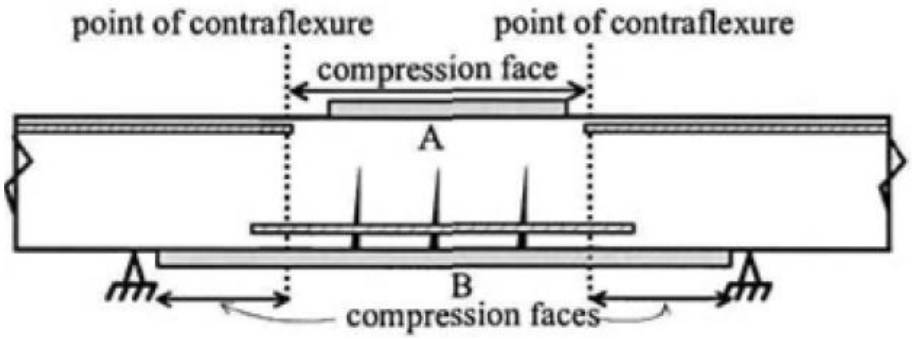

Figure II-6. Compression face plated beams [39].

II.4.2. Bonding or joining techniques

II.4.2.1. Bolted and adhesively bonded plates

Adhesively bonding plates to the tension faces or the sides of beam structures is the common procedure, as shown in **Figure II-7** (a) and Section A-A of **Figure II-8**.

Nevertheless, the plate can be bolted if a flexible joint is required, or if the bonded sheet is subject to early delamination, as indicated in **Figure II-7** (b) and **Figure II-8**.

While plates could be directly bolted onto the tension side, as shown in **Figure II-8**, this may be challenging in girders because of the bulkiness of the tensile bars. In this situation, the plates can be bolted to the sides of the beam, where only the stirrups must be omitted.

Bolting allows for the maximum resistance of the sheet to be achieved, while glued FRP sheets frequently delaminate at strains of a quarter to a third of their breaking strain. Bolting is presumably more expensive to install than adhesive bonding [39].

(a) (b)

Figure II-7. bonding plates: (a) by adhesion (current study); (b) by bolting [40].

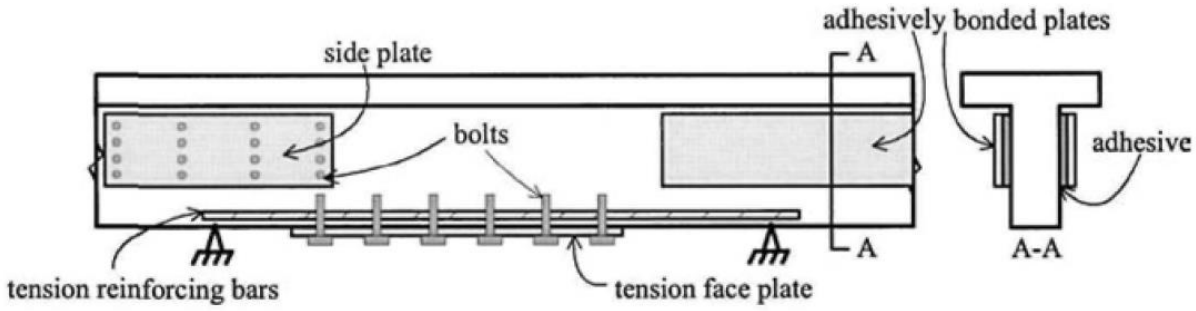

Figure II-8. Types of plate bonding [39].

II.4.2.2. Wrapping and mechanical end anchorage

As demonstrated in **Figure II-9**, wrapping provides an alternative method to bolting or adhesion for transferring the force into the plate.

Different wrapping types can be used:

- **Fully wrap**: It is the most effective form, where the cross-section should be completely wrapped, as indicated in A-A in **Figure II-9**. The vertical wrap takes over transferring the force, such as at C after the plate debonds but neither prevents nor inhibits it from debonding. As the fully wrapped section has enough ductility to allow the stirrups to yield or at least get considerably stressed while the wrap is still resisting vertical shear force, it is a particularly effective solution for improving the vertical shear capacity of a beam with stirrups. However, because the plate must penetrate the flange of the beam, the method is challenging to implement. (**Figure II-10**)
- **Partially wrap**: Another strategy is to wrap as in B-B partially (**Figure II-9**), but because the system is brittle and the resistance to the force D is often low, the plate will likely debond before the stirrups are subjected to any significant stress. (**Figure II-11**)
- **Compromise wrap**: the plate is bonded within the flange on both surfaces, creating a ductile system that may enable some straining of the stirrups prior to debonding and a relatively strong joint as in E-E in **Figure II-9** [39].

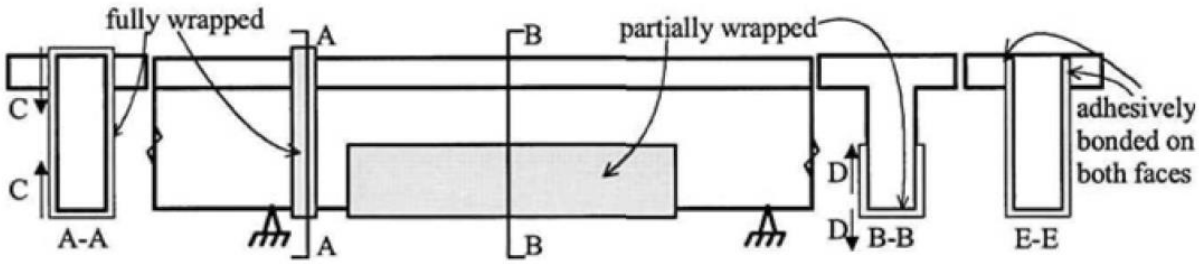

Figure II-9. Vertically wrapped plates [39].

Figure II-10. Full wrapped RC beam by CFRP [41].

Figure II-11. Partially wrapped RC beam by CFRP [42].

II.5. Failure mode of strengthened RC beams by FRP

Experimental studies have so far discovered several failure modes for RC beams strengthened in flexure with FRP plates. According to Yao and Teng [43], the failure types are as follows:

- Concrete crushing.
- FRP rupture.
- Shear failure.
- Intermediate crack (IC) debonding
- Critical diagonal crack (CDC) debonding
- Concrete cover separation failure.
- Plate-end interfacial failure, which are depicted in **Figure II-12**.

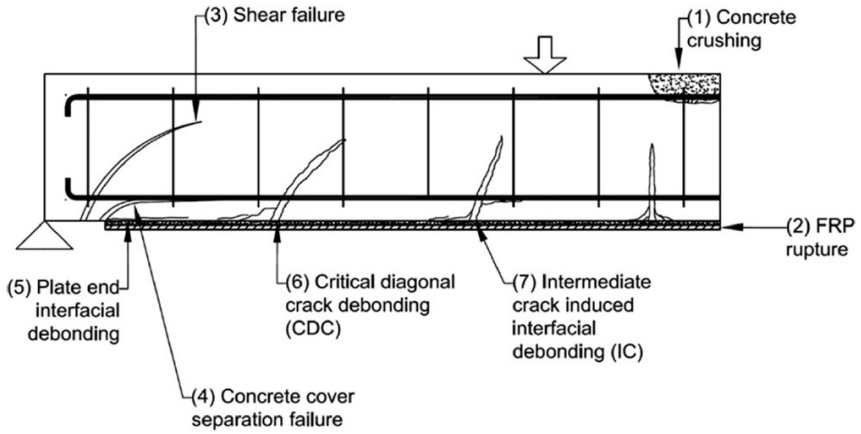

Figure II-12. Failure mode types of RC beam strengthened by CFRP [44].

II.5.1. Concrete crushing

Concrete crushing after yielding steel reinforcement indicates an inadequately reinforced member, according to contemporary reinforced concrete design requirements. This failure mode ensures that the member's ductility is maintained at a high level before it fails, giving plenty of time for evacuation before the collapse. Concrete crushing may only happen in lightly strengthened members when the FRP has not yet debonded at the moment of failure in the case of FRP-strengthened members. In this case, the bending moment capacity is calculated as follows [45]:

$$M_{\mathrm{u}} = A_{\mathrm{st}} f_{\mathrm{sy}} \left(d_{\mathrm{st}} - \frac{\delta c}{2}\right) + A_{\mathrm{f}} E_{\mathrm{f}} \varepsilon_{\mathrm{f}} \left(h - \frac{\delta c}{2}\right) - A_{\mathrm{sc}} E_{\mathrm{sc}} \varepsilon_{\mathrm{sc}} \left(d_{\mathrm{sc}} - \frac{\delta c}{2}\right)$$

Where:

M_{u}: ultimate moment of resistance, $N.mm$;

A_{st}: area of longitudinal steel in tension, mm^2;

f_{sy}: yield strength of reinforcement steel, MPa;

d_{st}: effective depth of tension steel reinforcement, mm;

δ: factor for concrete stress block depth;

c: depth of the neutral axis used in ACI 440.2 (2017), mm;

A_{f}: area of FRP longitudinal FRP, mm^2;

E_{f}: static modulus of elasticity of FRP reinforcement, MPa;

ε_{f}: strain in FRP reinforcement;

h: depth of section, mm;

A_{sc}: area of longitudinal steel in compression, mm^2;

E_{sc}: modulus of elasticity of longitudinal steel in compression, MPa;

$\varepsilon_{\mathrm{sc}}$: strain of longitudinal steel in compression;

d_{sc}: effective depth of longitudinal steel in compression, mm.

II.5.2. FRP Rupture

It is conceivable under some circumstances for the FRP material to rupture prior to concrete crushing but after the steel tension reinforcement has yielded, as seen in **Figure II-13**. In this instance, the FRP rupture controls the member failure. In this scenario, the following equation is employed to calculate the member's moment capacity [45]:

$$M_{\mathrm{u}} = A_{\mathrm{st}} f_{\mathrm{sy}} \left(d_{\mathrm{st}} - \frac{\delta c}{2}\right) + A_{\mathrm{f}} E_{\mathrm{f}} \varepsilon_{\mathrm{fu}} \left(h - \frac{\delta c}{2}\right) - A_{\mathrm{sc}} E_{\mathrm{sc}} \varepsilon_{\mathrm{sc}} \left(d_{\mathrm{sc}} - \frac{\delta c}{2}\right)$$

Where:

$$\varepsilon_{sc} = \varepsilon_{fu}\left(\frac{c - d_{Sc}}{h - c}\right) - \varepsilon_{o}$$

ε_{fu}: ultimate tensile strain of FRP;

ε_{o}: existing strain in the concrete on the surface where the FRP is applied.

Figure II-13. FRP rupture in RC beam specimen [46].

II.5.3. Intermediate crack (IC) debonding

Slender elements reinforced with relatively thin FRP plates or sheets are most frequently reported to experience intermediate crack-induced debonding, also known as IC debonding. The mechanism of IC debonding is caused by the occurrence of a significant flexural or shear crack. As the crack opens, tensile stresses are produced, which are then transmitted to the FRP plate, resulting in high interfacial tensions between the FRP and the concrete. Debonding begins at the crack site and spreads toward the closest plate end once the interfacial stresses exceed the interface's bond strength [47] (**Figure II-14**).

Restricting the maximum strain in the FRP tension plate prevents IC from debonding during the design stage [45].

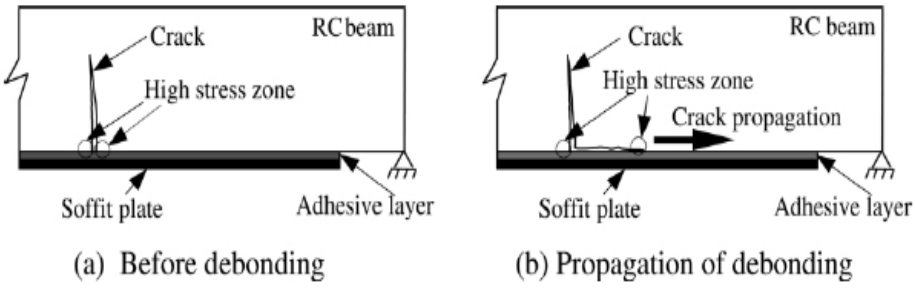

Figure II-14. Intermediate crack-induced debonding [47].

II.5.4. Critical diagonal crack (CDC) debonding

Critical diagonal fissure crack (CDC) is caused by the vertical shear force that displaces the rigid body across the critical diagonal crack. This results in the diagonal crack sliding or opening, which starts the FRP plate debonding from the diagonal crack's root and spreads to the plate's end as demonstrated in the **Figure II-15**. The debonding occurs immediately because of the sudden occurrence of the CDC debonding cracks [48].

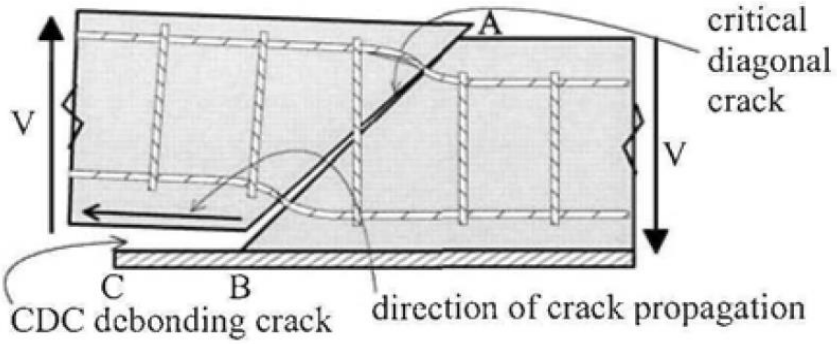

Figure II-15. Critical diagonal crack (CDC) debonding mechanism [39].

There are two ways of the end debonding of the FRP tension plate from the concrete: end interfacial delamination or concrete cover separation failure. Concrete cover separation has been recorded far more frequently than the end interfacial delamination of end debonding failure stated above. Depending on which the weakest interface, delamination begins at the interface between the FRP and the adhesive or the FRP and the concrete and spreads away from the plate-free end [45].

II.5.4.1. Concrete cover separation

The greater interfacial shear and debonding forces generated at the end of the FRP are assumed to be the starting point for failure of the concrete shell. These elevated shear stresses at or near the FRP end cause cracks to appear in the concrete. These cracks propagate vertically to the level of the tension steel reinforcement and then horizontally along that level of reinforcement, causing the concrete cover to separate [45], as shown in **Figure II-16**.

Figure II-16. Concrete cover separation of RC beam specimen strengthened by FRP (current study).

II.5.4.2. End interfacial delamination

Shear cracking may not happen in areas where the concrete has a high shear capacity. High interfacial shear and peeling stresses in this situation could cause an end interfacial delamination failure [45] (**Figure II-17**).

Figure II-17. FRP Plate end interfacial debonding [49].

II.6. Durability of strengthened RC structure by FRP:

The success of most applications involving the structural reinforcement of FRP relies significantly on the interface between FRP and concrete. This interface is crucial as it facilitates the transfer of stresses. Yet, practical experience in the field reveals that ensuring a reliable bond between FRP and concrete is not always assured. Several factors influence the quality of this bond, including the condition of the existing concrete, the preparation of the concrete surface, the excellence of the FRP application, the quality of the FRP material itself, and the durability of the resin. In the subsequent section, the primary focus will be on evaluating the durability of the FRP, followed by an examination of the overall durability of the entire strengthened system [50].

II.6.1. Glass transition temperature

The temperature above which it is reasonable to anticipate a significant drop in FRP performance is known as the glass transition temperature T_g. The resin chains can move and become more flexible if the thermal energy is above T_g. The bond capacity will be decreased as a result. Additionally, it decreases the resin's load or sharing capacity and causes preferential loading of specific fibres (the shorter ones). These individual fibres may be loaded beyond their capacity and break because the load is no longer distributed among the group of fibres. In the most severe circumstances, the FRP's maximum load carrying capability may be reduced by 30-40% [51]. To avoid premature debonding resulting from excessive temperature rise, it is imperative that the maximum service temperature remains below the glass transition temperature T_g of both the resin and the adhesive. Opting for an adhesive with an elevated T_g is essential when the reinforced element will be subjected to elevated temperatures. Two potential strategies exist: employing a cold-cure resin with a high T_g or subjecting the resin to post-curing to elevate its T_g [50].

II.6.2. Moisture

II.6.2.1. Effect of water absorption on FRP

For all structural materials, the presence of moisture is a particularly harsh environmental factor. As a result, resin chains have a chance of splitting and losing tensile strength. Therefore, the first issue with FRP materials is how well the resin matrix withstands the impacts of repeated exposure to fresh or salt water. It has been demonstrated via experience in the boat and military industries that the effects are felt over a very long period [52].

Water will be absorbed by the resin matrix. The type of resin and water temperature affect how much water is used. The principal outcomes of water absorption on the matrix include a lowered glass transition temperature and increased stiffness of the resin. [50].

II.6.3. Durability of an FRP-concrete system

Prior to strengthening, it is crucial to assess the condition of the existing concrete, including the state of the internal steel, to guarantee the bond quality and the long-term durability of the system. Addressing fundamental concerns is imperative before the implementation of FRP systems. Otherwise, there is a risk of water and chemicals permeating the concrete, leading to potential system damage through debonding or peeling in areas of localized stresses. Environmental factors, such as temporary water pooling in the FRP-concrete interface, could contribute to these stress-related issues. **Figure II-18** depicts the interactions at the system level [53].

Another significant issue with the FRP's moisture barrier qualities is the internal pore pressure. This internal pressure will be locally build-up since the secondary impact of the FRP strengthening system is to seal the concrete. As a result, there may be a need for sufficient gaps (zones without externally bonded FRP) to allow moisture transfer in FRP-strengthened parts. Additionally, these openings could let deleterious substances or excessive moisture access [50].

The effects of encapsulating concrete with FRP in interior applications and mild climates, especially with well-rehabilitated concrete, are minimal. In fact, completely enclosing a concrete member in FRP can potentially enhance its lifespan, providing protection against detrimental elements like marine and chemical environments. Nevertheless, if the structure is exposed to severe weather fluctuations and/or excessive moisture due to poor concrete conditions, the encapsulation may pose a risk. Consequently, it is not advisable to fully encapsulate concrete when installing FRP on a structural member prone to water accumulation. These risks can be substantially mitigated through maintaining favorable internal and external concrete surface conditions, thorough surface preparation, proper exposure of the concrete substrate, and the correct implementation of an appropriate FRP system [51].

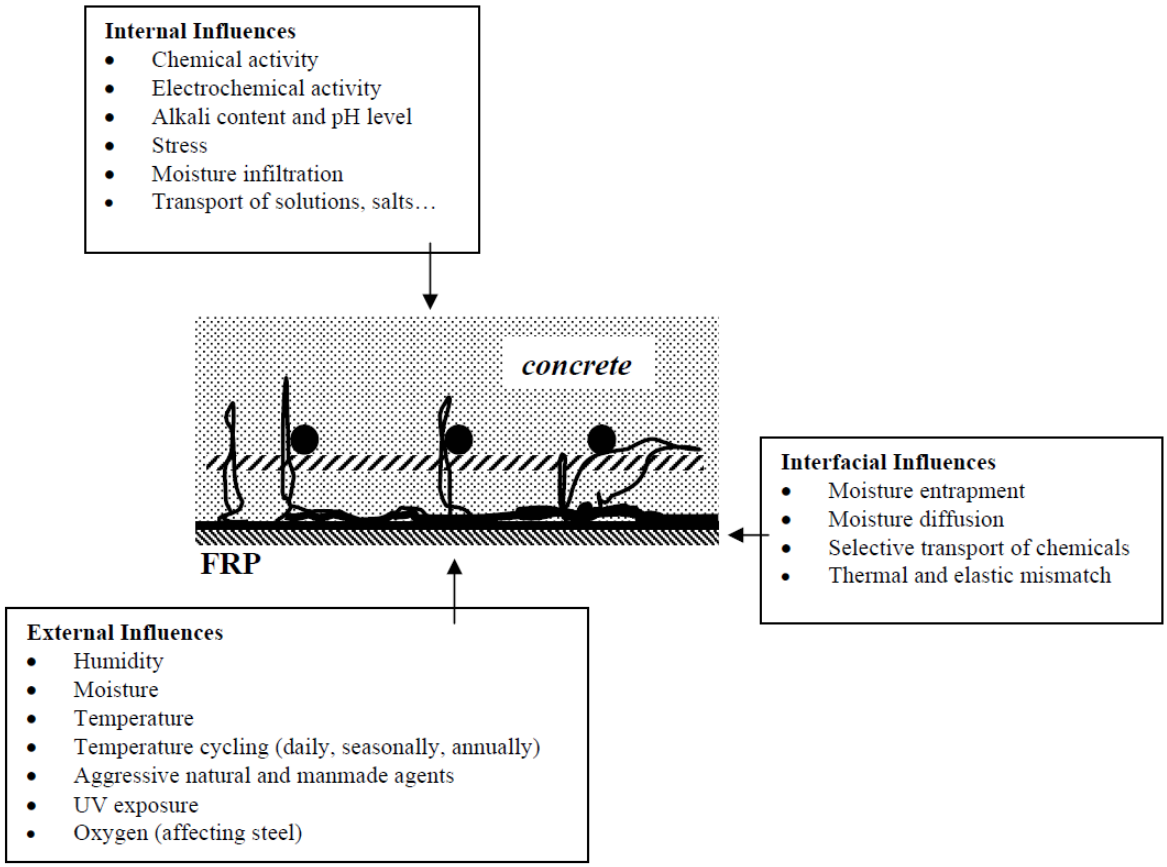

Figure II-18. The interactions at the FRP system level [53].

II.6.4. Temperature Effects

II.6.4.1. Freeze-Thaw

Structures may be cracked before strengthening FRP is applied to them. As a result, The FRP may not be completely bonded to the concrete, and the interface layer between the two materials (concrete and FRP) may contain some voids. Furthermore, delamination of the FRP at the concrete-FRP interface may result from the expansion of freezing water in these cracks or voids. Therefore, it is necessary to consider how freeze/thaw cycles affect the behaviour of strengthened structures by FRP [50].

Kaiser examined the behaviour of strengthened beams that had been put through 100 cycles of freeze-thaw (with water at 20°C) between -25°C and 20°C. Strengthened beams with and without cracks underwent testing. In comparison to the behaviour of the reference elements, he found no adverse effects of frost and thaw on the behaviour of the tested elements [54].

To investigate the impact of these defects on freeze and thaw action, Tysl et al. added certain delaminations and voids in the bond layer. They determined that frost and thaw did not significantly affect the bonding behavior [55].

When high-quality, moisture-resistant epoxies are employed, Yagi et al. found that repeated freeze-thaw cycles have little to no effect on the FRP [56]. However, the same freeze-thaw tests on FRP-wrapped concrete cylinders revealed a considerable decline in strength and ductility [57]. When the concrete's quality is poor, freeze-thaw cycling could cause issues [58].

II.6.4.2. Bond Behaviour at high and low temperatures

The behaviour and integrity of the plate-adhesive concrete system depend on both the properties of the interfaces used in the joint when FRPs and concrete are combined to create a plate-bonded composite beam, specifically the plate-adhesive and concrete-adhesive interfaces, in addition to the properties of the individual materials [50].

Pantuso et al. investigated the behaviour of strengthened specimens using two distinct types of unidirectional CFRP strips (E=175 GPa and E=300 GPa), evaluated at room temperature. They tested to failure at three different temperatures: -100°C, - 30°C, and 40°C, without internal steel reinforcement. The load-deflection diagrams for test specimens tested at -100°C and -30°C indicated a partly sudden reduction in the load. On the other hand, test samples evaluated at +40°C displayed consistent behaviour. Additionally, test specimens demonstrated several types of failure with temperature variations. The bond failure occurred in the thickness of the adhesive in the

specimens tested at +40°C (cohesive failure). In addition, interlaminar plate failure was manifested in specimens strengthened with high elastic modulus strips during testing at -30°C; concrete shear failure was observed in specimens reinforced with low elastic modulus strips; and interlaminar plate failure was manifested in both cases during testing at -100°C. In summary, experiments have demonstrated that specimens tested to failure at low or high temperatures exhibit changes in both the ultimate bond force and significant differences in the form of debonding [59].

II.6.5. Alkalinity/Acidity

Both the matrix and the reinforcing fibre will play a role in how well the FRP strengthening holds up over time in an alkaline or acidic environment. Glass fibre can disintegrate in alkali and acid environments. In contrast, carbon fibre is resistant to these conditions. However, a correctly placed resin matrix will isolate and safeguard the fibre and delay the deterioration. However, carbon fibres should strengthen RC structures in situations with high alkalinity and high moisture or relative humidity environments [51].

II.6.6. Fatigue

Modern unidirectional composites, such as CFRP, perform better against fatigue than steel. However, according to studies, the existing steel reinforcement fatigue is the leading cause of the fatigue of FRP-strengthened beams. Therefore, it is advised that the stress range in the rebars be restricted to that allowed in an unstrengthened beam as the criteria for the fatigue design of CFRP strengthened beams [54], [60], [61].

II.6.7. Impact

Typically, two different types of loads are applied: gradually applied loads and suddenly applied/impact loads. For example, falling or hitting an object on another produces an impact load.

Little is known about the impact behaviour of RC elements strengthened by FRP. Erki and Meier investigated the impact response of four 8-meter beams externally strengthened for flexure, two with CFRP laminates and two with steel plates. The impact load was created by raising one end of the beams and dropping it from specified heights. The findings were compared, and it was found that although the CFRP laminate-strengthened beams performed well under impact loading, they could not absorb as much energy as the steel-plate-strengthened beams. The impact resistance of the RC elements would be enhanced by additional anchoring, at least at the ends of the externally bonded reinforcement, to supplement the epoxy bonding and prevent early debonding of the CFRP [62].

II.6.8. Lightning, galvanic corrosion

CFRP has a high resistance despite being a conductor, which makes it warms up when the current flows across it. According to research carried out by the aviation industry, unprotected CFRP is subject to two main effects from lightning strikes: first, the main body of the material heats up to the point where the resin evaporates; secondly, after the carbon cools, the CFRP material's structural characteristics are adversely impacted [36]. The interlaminar shear and compressive strength will be reduced, but the tensile strength should not be much impacted. As it is commonly known that lightning will not strike an object placed in a grounded metal cage, aluminum grids are employed in the aircraft industry to safeguard the composite in its outermost layers. FRP composites will not be vulnerable to lightning strikes in many FRP-strengthening applications because they are inside buildings, which are equivalent to grounded cages. When strengthening a bridge, composite materials are either placed around columns where CFRP need protection or on the soffits of the beams, where lightning cannot access them. Composites should be protected with metal grids in any circumstances where lightning might be a problem. Lastly, carbon-based FRP should not come into direct contact with steel to prevent the steel reinforcement's potential galvanic corrosion [50].

II.7. Bibliographic review on the strengthened hollow RC beams

RC beams are divided according to their cross section into two parts: solid (filled) and hollow cross sections. Furthermore, Hollow beams are divided into two parts: beams with longitudinal openings and transverse openings. We will discuss in this section the previous research on the design of hollow RC rectangular and T-beams, their behaviour, and their strengthening.

II.7.1. Hollow beam design

II.7.2. Behaviour of hollow RC beam

An experimental comparison between seven hollow and seven solid beams was carried out by Alnuaimi et al [63]. Beams had a 3800 mm length and a 300x300 mm cross-section with a 200x200 mm interior cavity. This study focused on the ratio as the primary variable of bending to torsion, which ranged from 0.19 to 2.62, and the ratio in the web of shear stress due to torsion to shear stress due to shear force which varied between 0.59 and 6.84. The testing of the beams was done in a test rig, a three-dimensional frame that can apply torsion, bending moment, and shear force, as seen in **Figure II-19**.

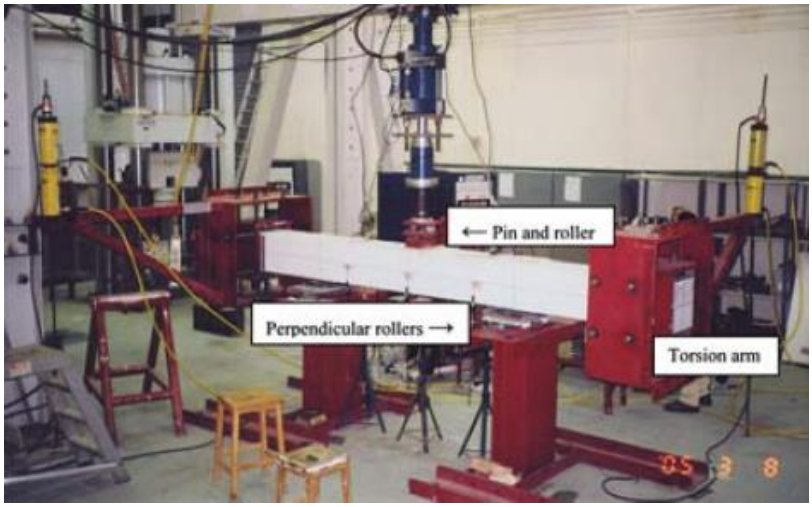

Figure II-19. Testing rig with a typical beam installed [63].

The results indicated that the solid beams cracked at much higher loads than the hollow ones. This shows that the solid beams' concrete cores contribute to an increase in the cracking load. Major cracks start on the bottom face, close to the point of failure, and failure occurs when they reach the top face, as shown in **Figure II-20**.

Figure II-20. Crack development in solid beam (BTV5-S) and hollow beam (BTV5-H) [63].

The hollow beams were often more flexible than the solid ones (i.e., more displacement for the same load value). Moreover, since the solid beams could resist more loads than the hollow ones, the maximum displacements were higher in the solid beams than in the hollow ones. (**Figure II-21**)

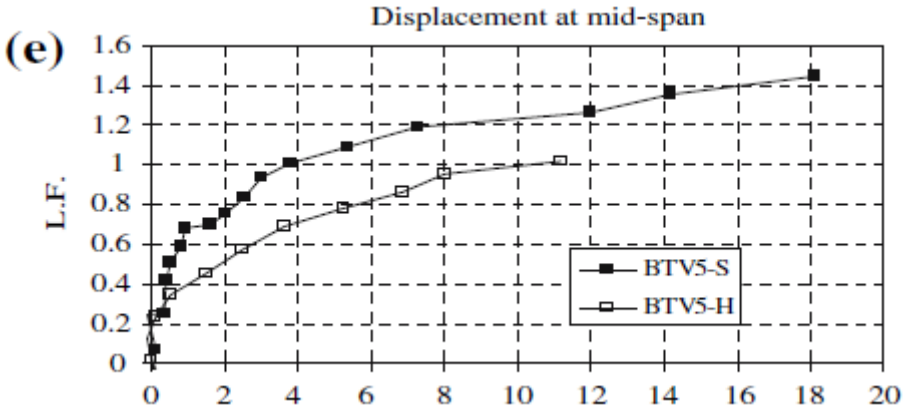

Figure II-21. Load-displacement curve at mid-span displacement of solid (BTV5-S) and hollow beam (BTV5-H) [63].

Similar curve trends were observed for both beams of each pair for the steel strain ratios closest to mid-span, with higher strain ratios reported in the hollow beams than in the solid beams for the same load as seen in (**Figure II-22**). They concluded that the concrete core plays a role in the behaviour and strength of the beams and cannot be disregarded in the presence of a combined load of bending, shear, and torsion.

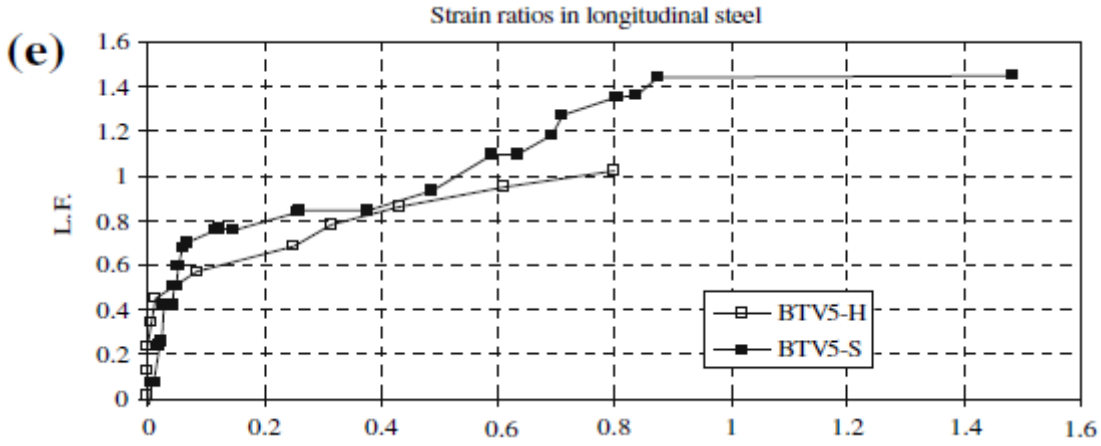

Figure II-22. Load-strain curve at mid-span of longitudinal steel [63].

Elamary et al [64] investigated how concrete's internal hollow core size affected the flexural response of hollow RC beams. Under three loading points, a control beam with a solid section and three additional specimens with hollow core areas of 3%, 7%, and 10% of the beam cross-section area were examined.

The findings showed that the failure load of the RC beams was not significantly affected by using less than 10% of the beam cross-section as the hollow section. Nevertheless, the hollow core

impacts the extent and height of the cracks. At the ultimate load, all beams failed at flexural failure mode (**Figure II-23** and **Figure II-24**).

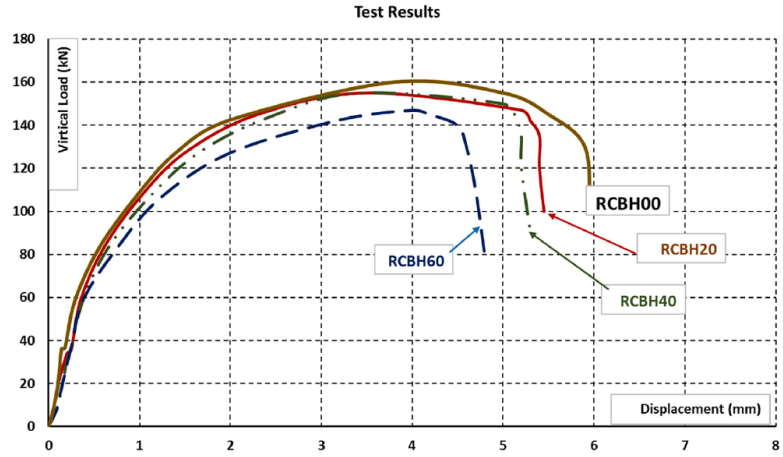

Figure II-23. Load-deflection curves of tested beams [64].

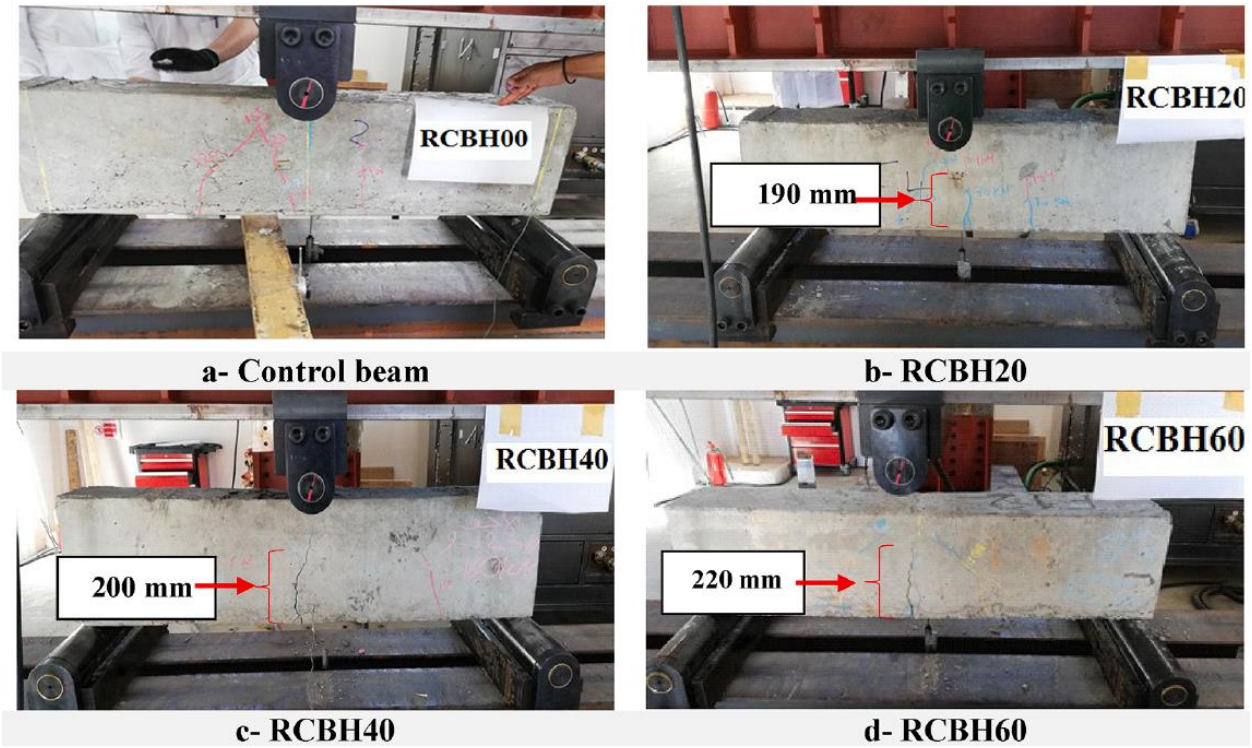

Figure II-24. Failure modes of the tested beams [64].

Abdulhusain et al [65] investigated the impact of the depth of circular cavities on the bending behaviour of six hollow reinforced concrete T-beams and one solid control beam. The cross-section of the beams measured 300 mm in height, 250 mm in flange width, 75 mm in flange depth, 150 mm in web width, and 2000 mm in length. (**Figure II-25**)

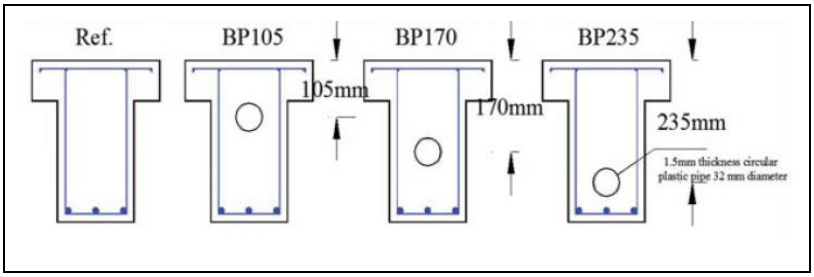

Figure II-25. Beam details [65].

According to the findings, increasing cavities' depth from 105 to 170 and 235 mm below the top fibre of the beam decreased the relevant first crack load by 3.57%, 7.14%, and 17.86%, respectively, and decreased ultimate strength by 0.39%, 1.03%, and 2.31%, respectively, as demonstrated in **Table II-3**.

Table II-3. First crack, yield load and ultimate strength of the girders tested [65].

Beam designation	Reduction in vol. of beams %	Cracking load P_{cr} (kN)	Decrease in P_{cr}%	Yield load P_y (kN)	Decrease in P_y%	Ultimate load P_u (kN)	Decrease in P_u %
Reference	/	28	/	131	/	155.6	/
BP105	4.2	27	3.57	131	0	155	0.39
BP170	4.2	26	7.14	130	0.76	154	1.03
BP235	4.2	23	17.86	125	4.58	152	2.31

The relevant yield deflection increases by 0.65%, 1.09%, and 1.85% as longitudinal cavity depth go from 105 to 170 and 235 mm; the ultimate deflection also increases by 4.90%, 6.33%, and 7.34%, as shown in **Figure II-26**. The ultimate concrete strain increases by 17.49 %, 24.47 % and 32.50 when longitudinal cavities depth increases from 105 to 170 and 235 mm, respectively, and the ultimate steel strain was also increased by 8.81 %, 11.33 % and 19.97 %. Based on the above results, they concluded that the increase in the depth of the cavities from the top fibre of the beam led to the bending behaviour of the beams being more affected.

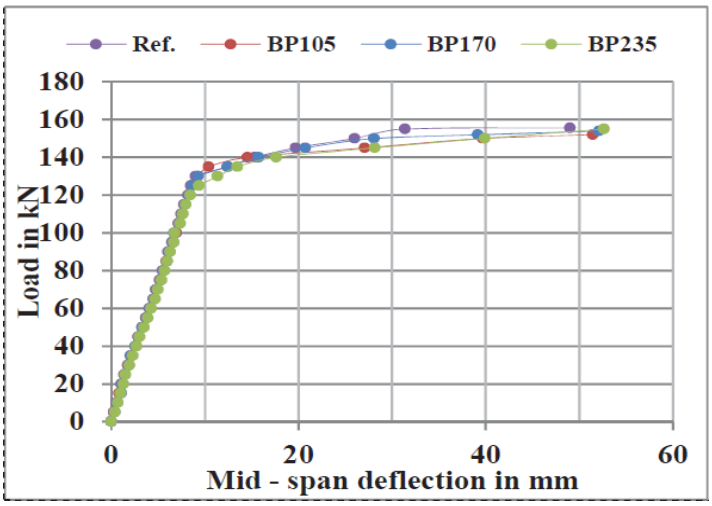

Figure II-26. Load-mid span deflection [65].

Abbass et al [66] examined the effect of different hole sizes and other parameters on flexural behaviour. They tested four solid and ten hollow RC beams with central square holes with side lengths of 60, 80, and 100mm. Beams had 150x150 mm cross-sectional dimensions and a length of 850 mm. The beams were tested under the four-point bending test (**Figure II-27**). According to the test results, the ductility of hollow beams with size reductions of 16% and 28.4% was better than that of the solid reference beam. In comparison, that of hollow beams with a 44.4% size reduction was comparable to that of the solid beam. Furthermore, compared to the reference solid beam, the toughness values of the hollow beams were 19 to 37% greater. The ultimate loads of hollow beams were around 3% lower than solid beams, as seen in **Figure II-28**.

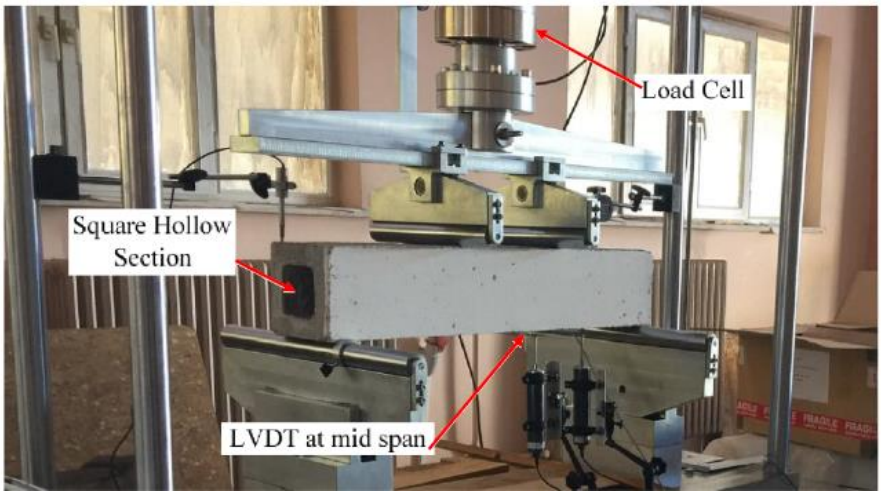

Figure II-27. Test setup (four-point bending test) [66].

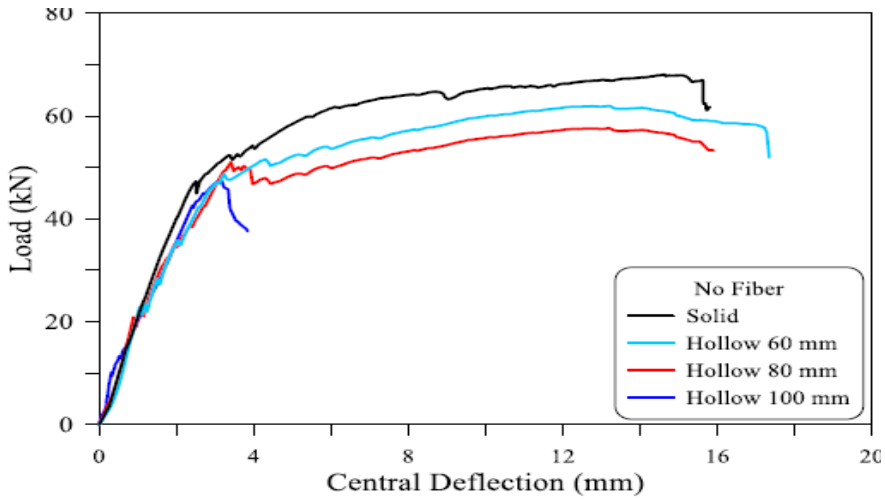

Figure II-28. Load-deflection of tested beams with different hole sizes [66].

Murugesan et al [67] tested the performance of 86 solid and hollow RC beams with 1700x150x 250 mm dimensions under a four-point bending test. The holes ranged in size from 25, 40, or 50 mm and were positioned at between 45 and 180 mm from the top. The longitudinal steel and the transverse steel amount of the beam kept constant.

Depending on the a_v/d ratio, three failure modes were observed: 13 beams failed by flexure mode with an a_v/d ratio of 2.6, Seventeen beams failed by the shear mode with an a_v/d ratio of 1.37, and 56 beams failed by flexure-shear mode when the a_v/d ratio ranged between 1.6 and 2.56, as shown in **Figure II-29**.

Deflection increases with the increase of the hole diameter at a given position of the hole and a given av/d ratio. This results from a decrease in the cross-section's moment of inertia due to the increase in hole diameter. (**Figure II-30**).

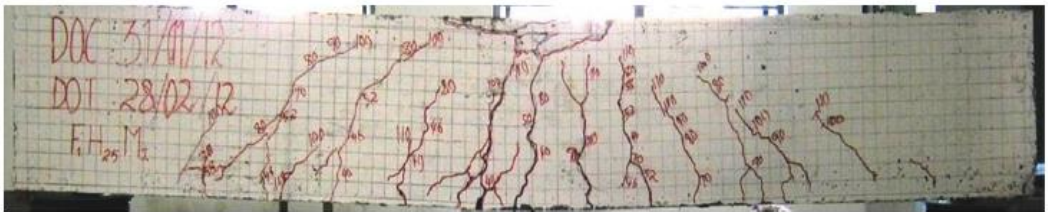

(a)

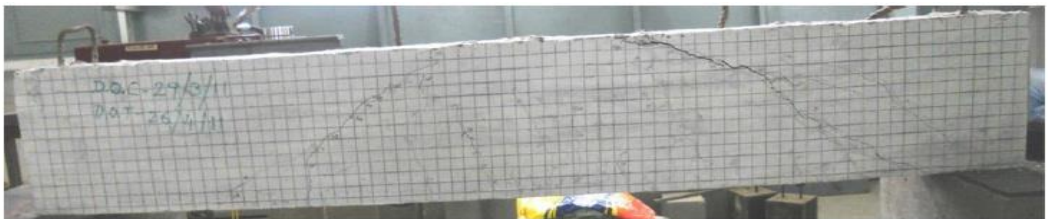

(b)

(c)

Figure II-29. Crack pattern and failure mode of hollow beams: (a) flexural failure mode; (b) shear failure mode; (c) flexural-shear failure mode [67].

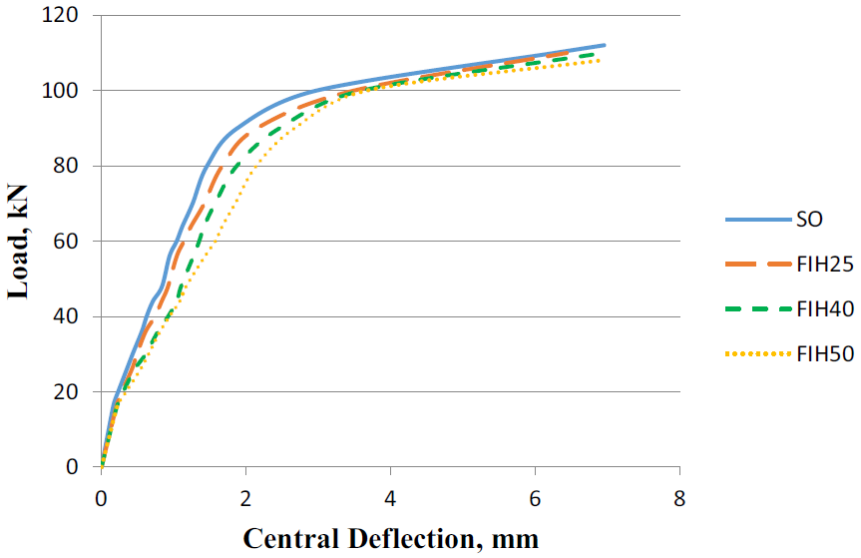

Figure II-30. Load-central deflection curves [67].

II.7.3. Behaviour of strengthened hollow RC beam

Sirisonthi et al [68] examined the flexural behaviour of nine hollow RC beams strengthened by the CFRP sheet. Three groups of beams with cross sections of 300x300 mm and lengths of 3800 mm were tested in a four-point bending test. One solid beam and two hollow beams with square openings of 50x50 mm and 100x100 mm are present in each group. The first group was not strengthened, the second group had one CFRP sheet strengthening their tension sides, and a U-shaped CFRP sheet bonded in the third group. (**Figure II-31**).

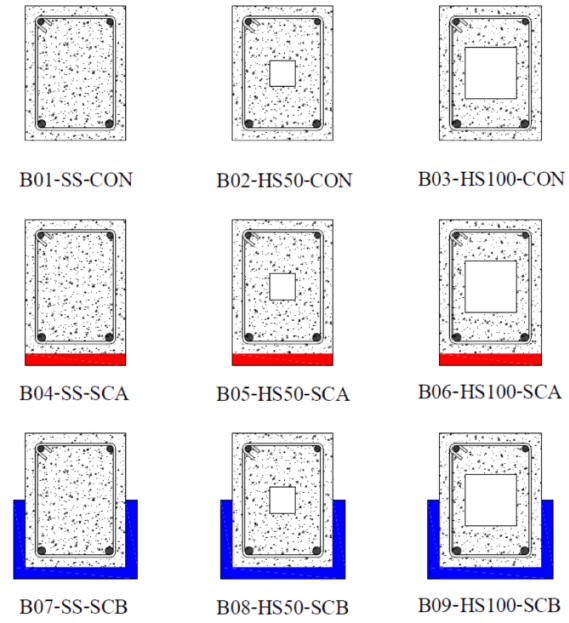

Figure 2. Layout of CFRP sheets.

Figure II-31. different types of beams configuration [68].

Unstrengthened solid beams were compared with their unstrengthened hollow counterparts first and strengthened solid and hollow beams were compared.

Internal openings decreased a structure's adequate flexural rigidity, which allowed flexural cracks to occur earlier near the midspan in hollow beams than in solid beams. Two failure mode has occurred: The crushing of concrete at the top of its midspan for both unstrengthened solid and hollow beams and the sudden de-bonding of the CFRP layer for the strengthened beams. The use of CFRP on beams enabled higher strains to be mobilised in bottom steel bars compared to control beam B01.

Previous studies have extensively investigated the shear behavior of RC deep beams with web openings strengthened with FRP composites. However, there is a notable gap in research regarding the use of CFRP to strengthen or retrofit T-shaped beams with longitudinal openings instead of web openings. Additionally, there is a need for a comprehensive investigation into the flexural

behavior of these beams. This study aims to address this gap and provide a deeper understanding of the behavior of such beams.

The research involves both experimental and numerical investigations to evaluate the effectiveness of CFRP in enhancing the flexural performance of hollow RC T-beams with longitudinal openings. The findings from this study are intended to inform the strengthening or retrofitting of hollow T-beams with longitudinal openings, contributing to the development of more sustainable and efficient structural systems. Several parameters were considered, including first cracking load, ultimate load, crack propagation, failure mode, load–deflection behavior (including stiffness and ductility), and load–strain behavior.

In the experimental phase, eight RC T-beams were subjected to a three-point bending test. These beams were divided into four groups, each containing one solid RC T-beam and one hollow RC T-beam with a 30 × 40 mm longitudinal rectangular opening. The first group served as the control group and was left un-strengthened. The second group was strengthened with a single CFRP laminate on the tension side. The third and fourth groups were preloaded to 80% and 100% of the control beams' ultimate load, respectively, before being retrofitted with one CFRP laminate on their bottom side.

Given the challenges and high costs associated with conducting extensive experiments on hollow RC beams, a more efficient approach was taken by developing a refined numerical model for hollow RC T-beams to explore a wider range of parameters. The experimental results were then compared with numerical simulations generated using ABAQUS software.

This study's results will be useful for engineers and designers in the field, providing insights into the structural performance of hollow RC T-beams with longitudinal openings and the effectiveness of CFRP strengthening methods.

EXPERIMENTAL PART

Chapter III

MATERIALS AND METHODS

Chapter III. Materials and methods

III.1. Introduction

The RC T-beams used in this study were manufactured at the Laboratory of Civil Engineering and Hydraulic Studies (LGCH) located at Guelma University.

All samples underwent a standardized production process that encompassed mixing, pouring, vibration, and storage. This rigorous protocol was followed to minimize external factors that might influence the test results.

The primary focus of this experimental study is to assess the impact of longitudinal rectangular openings on the flexural behavior of reinforced concrete (RC) T-beams. Additionally, it aims to evaluate the efficacy of external Carbon Fiber Reinforced Polymer (CFRP) laminates in the reinforcement and repair of these hollow RC T-beams.

III.2. Characteristics of the materials used

III.2.1. Concrete

The cement used is a CPJ-CEMII/A42.5 cement produced at the Hadjar El Soud cement plant (Wilaya of Skikda, Algeria).

The gravel used is 5/15 from the Bousselba-El-Fedjoudj quarry (Wilaya of Guelma, Algeria).

The sand used is rolled sand (0/5) from OUM-ALI (Wilaya of Tébessa, Algeria).

The physical characteristics of the aggregates are presented in **Table III-1**.

Table III-1. Physical characteristics of aggregates.

Characteristics	Gravel	Sand
Absolute density (g/cm^3)	2.46	2.52
Apparent density (g/cm^3)	1.41	1.55
Sand equivalent (%)	-	82
Fineness modulus	-	2.28

We used the «**Dreux-Gorisse**» formulation method for the concrete composition. The Dreux-Gorisse method is one of several techniques used to determine the proportions of the different components (sand, cement, gravel, water) of concrete [69]. (**Table III-2**).

Table III-2. Ordinary Concrete Formulation

Concrete constituents	Weight (kg/m3)
Sand 0/5	653.18
Gravel 5/15	1040.33
Water	220.27
Cement CPJ-CEMII/A42.5	350

Five (16×32 cm^2) cm specimens were tested in compression after 28 days to define the average concrete compressive strength; the average concrete compressive strength was 21.50 MPa. (**Figure III-1**).

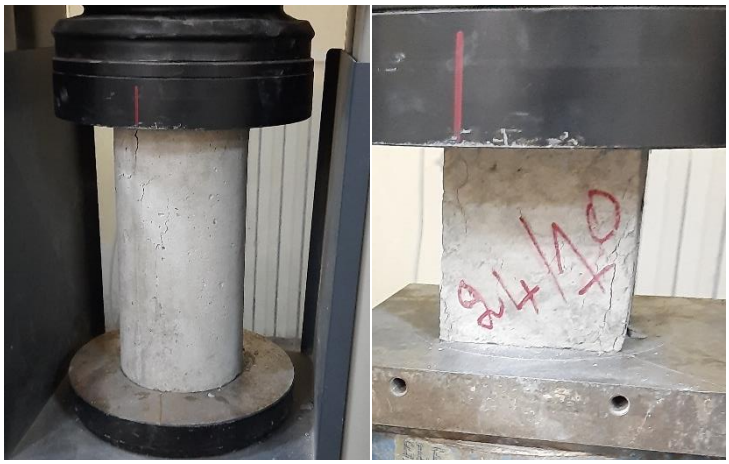

Figure III-1. Compression test specimens (cylindrical and cubic)

III.2.2. Steel bar reinforcement

The reinforcement steel bars of all RC T-beams were identical. The tension zone of beams consists of two 8 mm diameter steel bars, and the compression zone consists of four 8 and 6 mm diameter steel bars in the top flange. Along the length of the beam, 11 vertical stirrups with a 6 mm diameter and 100 mm spacing were installed, as illustrated in **Figure III-2**.

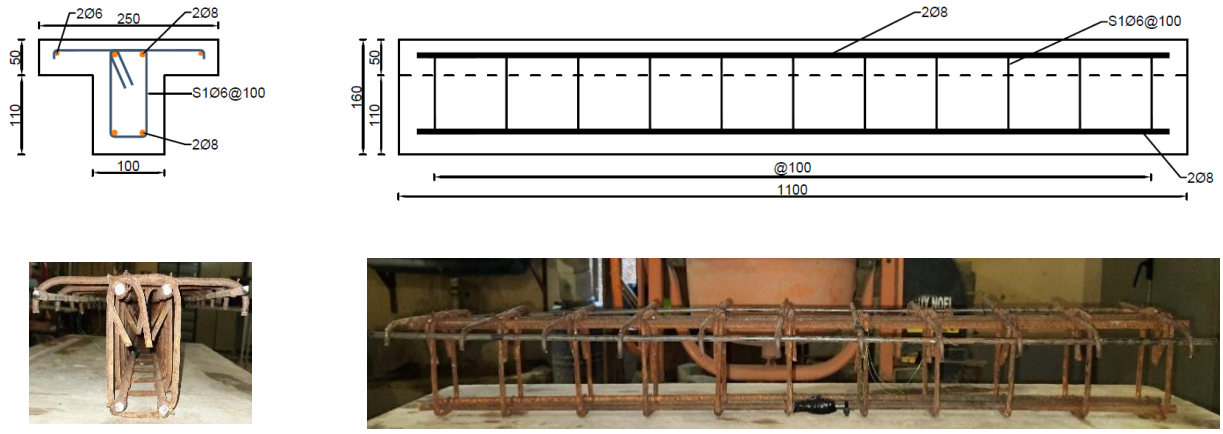

Figure III-2. reinforcement details (all dimensions in mm)

The tensile tests of the reinforcements used in the experimental study were carried out in National Center for Integrated Building Studies and Research (**Figure III-3**). The yield strength $\boldsymbol{f_y}$, the ultimate strength $\boldsymbol{f_u}$ and the young modulus $\boldsymbol{E_s}$ of steel reinforcement are mentioned in **Table III-3**.

Figure III-3. tensile tests of reinforcements bars

Table III-3. Material Characteristics of the Steel

Diameter	f_y (MPa)	f_u (MPa)	E_s (MPa)	Elongation (%)
6	323.7	407.5	2×10^5	11.4
8	519.5	616.8	2×10^5	9.8

III.2.3. Composite material

we used unidirectional carbon-fibre-reinforced polymers (CFRP) (Sika CarboDur S1012) for the external strengthening or repairing of the RC T-beams. They are made from carbon fibres embedded in an epoxy matrix. They come in the form of a factory-prefabricated laminate [70]. (**Figure III-4**)

According to manufacturer specifications, an adapted epoxy resin adhesive (Sikadur-30) was mixed at a 3:1 ratio (epoxy-hardener) as the adhesive . (**Figure III-5**)

Table III-4 lists the mechanical parameters of the CFRP and the adhesive reported by the manufacturer.

Table III-4. Properties of CFRP and the Adhesive [70]

Characteristics	CFRP	Adhesive
Modulus of elasticity in Tensile (Mpa)	170000	11200
Tensile strength (Mpa)	3100	26
Fracture elongation (%)	>1.80	-
Thickness (mm)	1.2	-
Density (Kg/l)	1.6	1.65 ± 0.1

Figure III-4. CFRP laminate (Sika CarboDur S1012)

Figure III-5. Preparation of the resin

III.3. Beams' Manufacture

We manufactured eighteen RC T-beams for our experimental work. All had the same length of 1100 mm and cross-section dimensions: 160 mm high and 100 mm wide. The flange of the RC T-beam was 250 mm wide and 50 mm high, as shown in **Figure III-6**. The choice of these dimensions is related to the dimension between the two horizontal cylindrical supports and the distance between the horizontal and vertical supports of the machine. The beam was simply supported (between pinned support and roller support). the free space between the two horizontal supports was 900 mm.

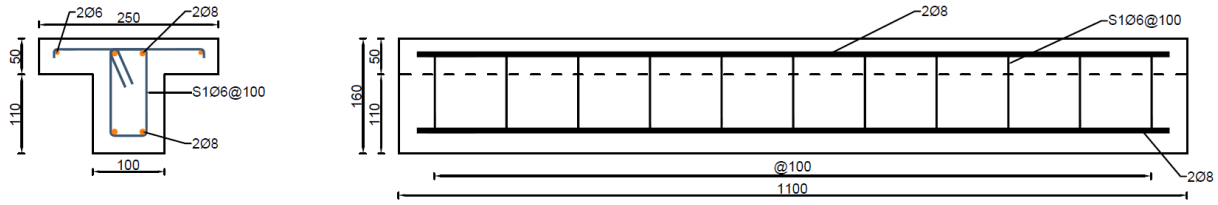

Figure III-6. RC T-beams cross-section dimensions

The tested beams are divided into four series, and each serie consists of one solid RC T-beam and one hollow RC T-beam with a longitudinal rectangle opening of 30x40 mm. In the first series (control beams), no strengthening was applied, the second series (strengthened beams) were performed by single CFRP laminate on their tension side, and the third and the fourth series (repaired beams) were pre-load by 80, and 100% of control beams ultimate load respectively as mentioned in **Table III-5**. All beams were strengthened or repaired with a similar CFRP laminate in their tension zone (**Figure III-7** and **Figure III-8**).

Table III-5. Details of tested beams

Series	Type	name	condition	strengthening	repairing	Nb of laminate
Control	Solid	CB	Not pre-loaded	unstrengthen	unrepaired	-
	Hollow	HCB	Not pre-loaded	unstrengthen	unrepaired	-
Strengthened	Solid	SCB	Not pre-loaded	Strengthened	-	1
	Hollow	SHB	Not pre-loaded	Strengthened	-	1
Repaired 80	Solid	RCB80	pre-loaded at 80%	-	Repaired	1
	Hollow	RHB80	pre-loaded at 80%	-	Repaired	1
Repaired 100	Solid	RCB100	pre-loaded at 100%	-	Repaired	1
	Hollow	RHB100	pre-loaded at 100%	-	Repaired	1

Figure III-7. experimental RC T-beams

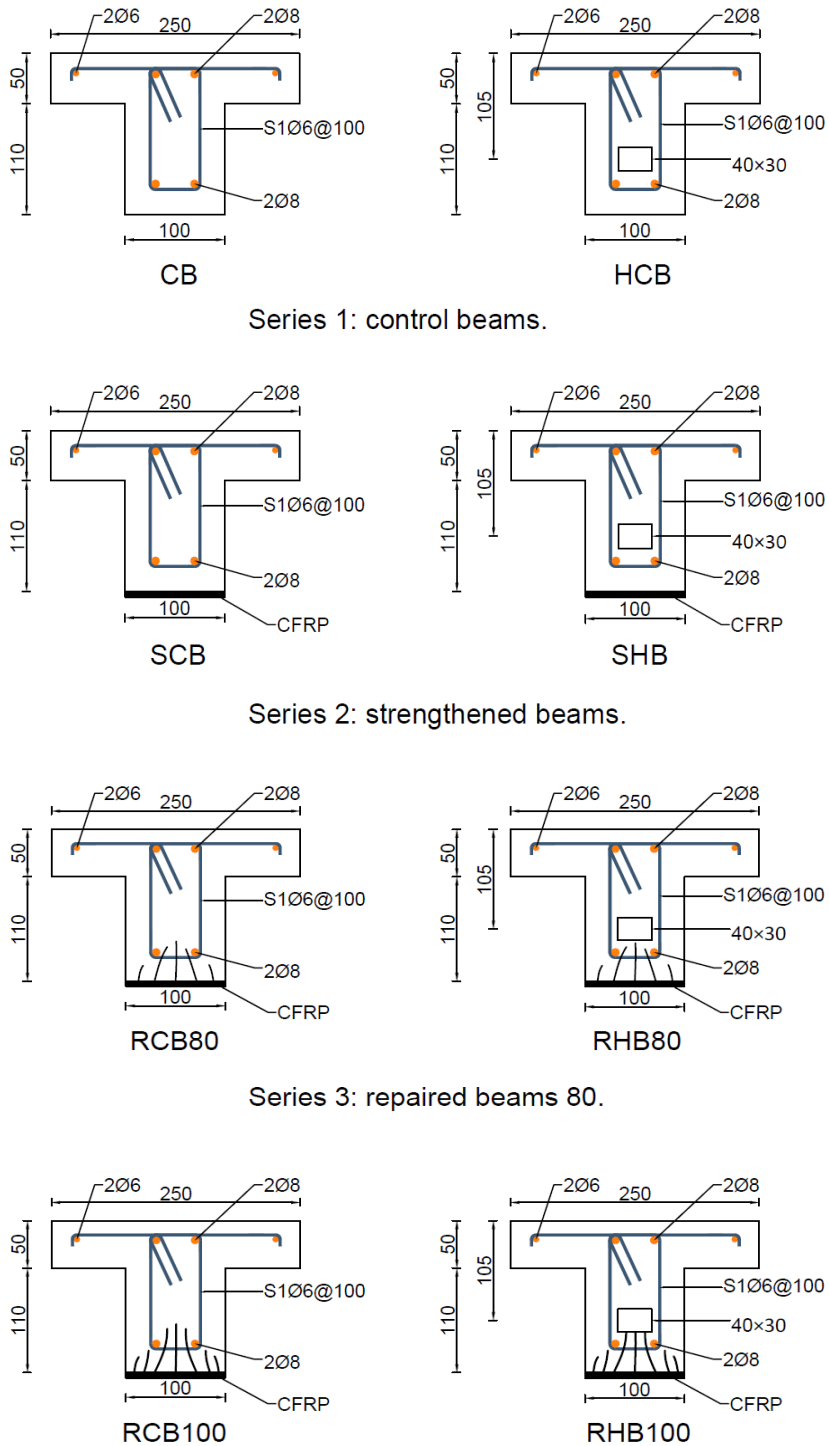

Figure III-8. Types of RC T-beam series (all dimensions in mm).

Two wooden formworks were made and used for all the tested beams. The bottom and sides of the formwork are oiled to facilitate demolding. For each beam, three cubic specimens (10×10×10

cm^3) were cast to define the compressive strength of the concrete on the day of the test. (**Figure III-9**).

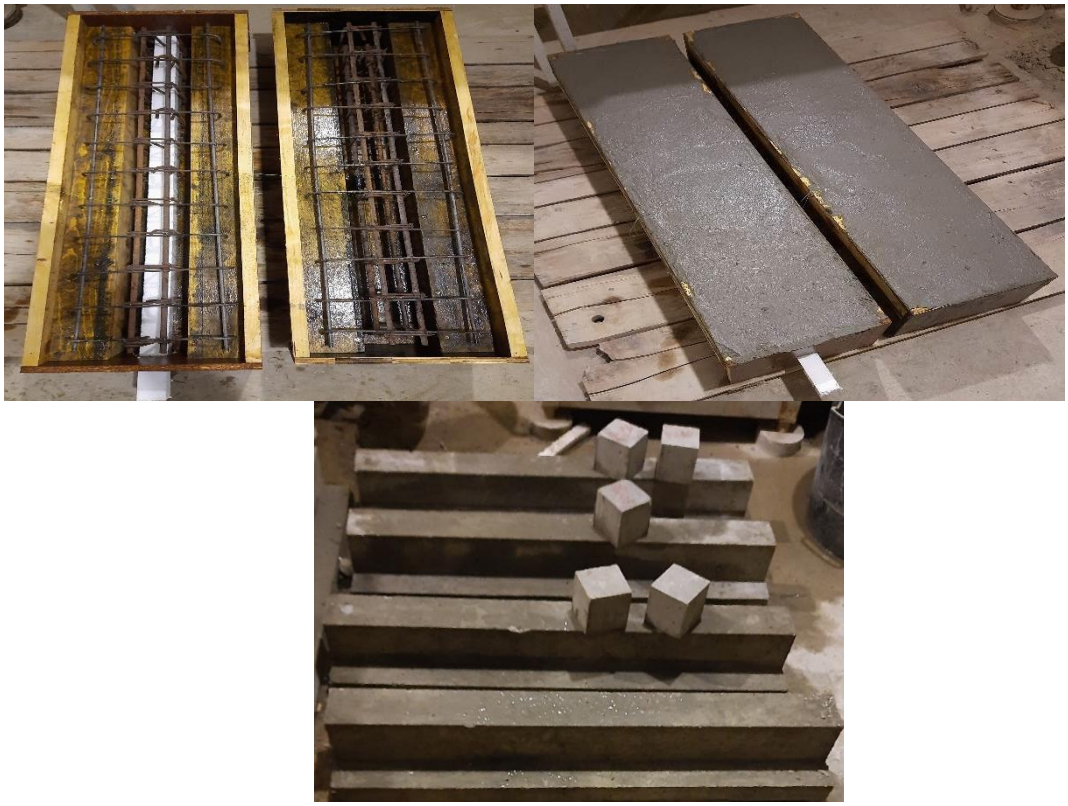

Figure III-9. Casting of beams

III.4. CFRP application:

For the strengthening or repairing tested beams, an externally bonded of CFRP laminate is applied to the concrete surface.

III.4.1. Concrete surface preparation:

We have cleaned the concrete surface of everything that would affect the bonding between the concrete surface and the adhesive used, such as oils, dust and poorly adhesive particles. The moisture content of the concrete surface should not exceed 4% [70].

III.4.2. Preparation of the CFRP laminate (Sika CarboDur S1012):

We cut the CFRP laminate to the required lengths taking care not to damage the cut end; then, we cleaned its surface with solvents to remove dirt and dust. (**Figure III-10**.a)

III.4.3. Preparation of the adhesive (Sikadur-30):

we mixed epoxy resin adhesive (Sikadur-30) at a 3:1 ratio (epoxy-hardener) with an electric stirrer fitted with a propeller for about 3 minutes until a uniform mixture of grey colors is obtained as shown in **Figure III-10**.b).

Then we applied a layer of Sikadur-30 to the concrete surface using a brush and on the cleaned CFRP laminate surface (**Figure III-10**.c). By using a rubber roller, we tight-pressed CFRP laminates onto the concrete surface to avoid air bubbles (**Figure III-10**.d)

(a)

(b)

(c)

(d)

Figure III-10. beams strengthening process

III.5. Strain gauges installation

Three types of strain gauges (SG) were used to evaluate the load-strain behaviour in the different materials: SG for concrete, steel, and CFRP laminate.

III.5.1. Reinforcement bar strain gauge

The length of the gauge in the rebar must be appropriate to the size of the diameter of the rebar so that we can easily place it. Moreover, we do special surface preparation to get the flattest possible surface and clean.

a. Surface Preparation

1. We removed a few ribs from the rebar by a grinder machine so we could bond the strain gauge in place (**Figure III-11**.a).
2. We rub the rebar surface with a coarse abrasive paper (G120) and clean it simultaneously with dry cotton wet with acetone. (**Figure III-11**.b)
3. We repeat the rubbing process, but this time with a fine abrasive paper (M04F) with cleaning with acetone until we reach a smooth surface and completely clean of all impurities (**Figure III-11**.c and **Figure III-12**)
4. We scrub the surface with wet cotton by neutralizer solution (NaOH) to get the surface to the proper pH, then we dry the surface.

b. strain gauge bonding

1. Apply the suitable adhesive on the bottom side of the gauge and in the exact location of the rebar (**Figure III-13**.a).
2. We press the gage into the adhesive and force out air bubbles (**Figure III-13**.b).
3. We apply tape under the exposed electrical wires. Electrical wires must not touch the rebar definitely (**Figure III-13**.c)

c. Waterproofing process of strain gauge

The waterproofing of the strain gauge during concrete pouring is one of the most important steps to maintain the gauge in this process.

1. We cover the entire strain gauge with a thick SB tape. (**Figure III-14**.a)
2. We cover the entire strain gauge with a melted W1 (waxy material). (**Figure III-14**.b)
3. We cover the solid waxy material with VM tape. (**Figure III-14**.c)
4. Finally, we check the electrical resistance of the strain gauge. (**Figure III-14**.d)

(a)

(b)

(c)

(d)

Figure III-11. Surface preparation process

Figure III-12. Smooth and clean surface

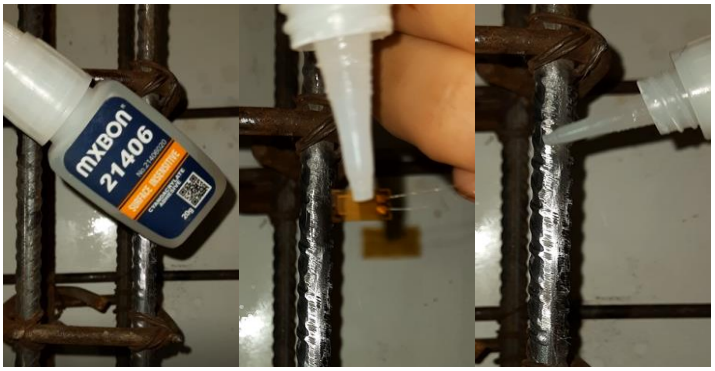

(a)

(b)

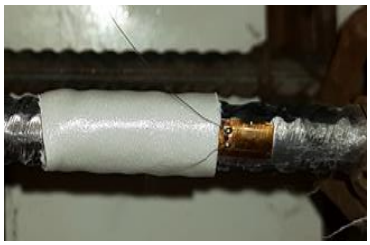

(c)

Figure III-13. strain gauge bonding on reinforcement bar

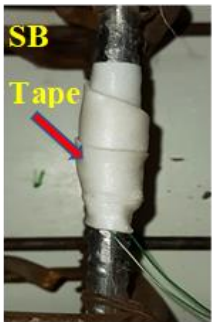

(a)

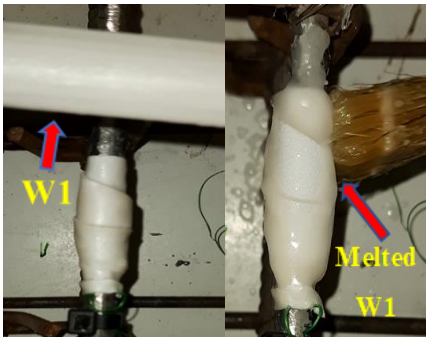

(b)

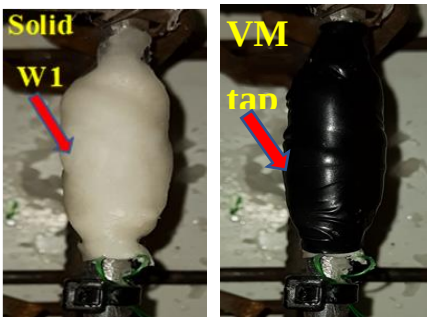

(c)

(d)

Figure III-14. Waterproofing process of strain gauge

III.5.2. Concrete strain gauges

a. Gauge Length Selection

The gauge length must be compared to the heterogeneities of the material that receives it . The manufacturer requires that the strain gauge length be at least three times greater than the largest aggregate size used in nonhomogeneous materials such as concrete . As a result, we used long strain gauges (60 mm) to perform a representative deformation measurement.

b. Surface Preparation

1. We take the concrete sample and remove with a standard wire brush all the organic contaminants represented by the clay and the excess concrete. After that, we dry the sample completely.
2. Then we prepare the surface using mild phosphoric acid solution (conditioner) by moistening the surface and removing all the loose contamination.

3. Then we warm the surface with a warm air blower to drive that conditioner off. The surface is dark when it is wet and dries when it is lighter.
4. The next step is to locate the neutralizer (the blue tip bottle), and we do the same scrubbing step. We wet a cotton gauze sponge, and then we scrub the surface. This is going to take the conditioner pH and neutralize it. It will also remove the organic components because there is a little detergent in the neutralizer.
5. Again, we take a warm air blower and drive off the excess moisture.

   The previous surface preparation process aims to eliminate the organic components and surface contamination and return the surface pH to a nominally neutral or slightly basic level so the epoxy systems will bond properly.

6. Because the concrete is rough, we must put down a pre-coat of epoxy resin to fill the surface and get a nice uniform surface thickness.

   the roughness of the surface would probably damage or change the resistance of the strain gauge. The epoxy resin takes a minimum of 24 hours to cure if we put it at room temperature

7. we do some abrasion process with thin abrasive paper to keep a nice and uniform surface thickness one more time.

c. Gauge bonding process

1. We drop a couple of ammonia solution drops onto a glass plate and clean it with a dry gauze sponge; then, we put the gauge on this clean glass plate.
2. We pull a long enough tape to transfer this gauge over to the concrete block easily. Then we place the tape over the top of the gauge and wire combination starting at the wire end, and then we lightly squeegee forward until it entrains the entire gauge.
3. We put the glue on the bonding surface of the strain gauge and the required concrete surface.
4. We reposition the gauge onto the concrete surface and lightly press it into place with a gauze sponge fold.
5. We firmly press the gauge for at least five minutes to clamp it (**Figure III-15**).

Figure III-15. strain gauge on concrete surface

III.5.3. CFRP strain gauge

For CFRP laminate, we use much shorter gauges (5mm). Their bonding is easier because, in this case, we have a perfectly flat and smooth surface [5]. The surface cleaning process remains essential (**Figure III-16**).

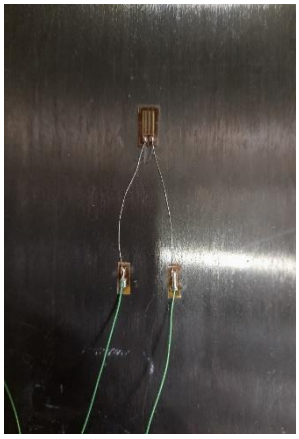

Figure III-16. strain gauge on CFRP laminate

III.6. Test instrumentation and setup:

All RC T-beams were tested under a three-point bending test by a universal testing machine (Controls model 50-C8422/MP). The three-point bending tests are commonly used to assess the mechanical properties of brittle materials. For this, we put the beam on pinned support and roller support; the distance from center to center is 900 mm. The centrally oriented loading pin begins to descend in the z-direction toward the beam at a constant strain rate during loading. The specimen begins to bend elastically as the pin continues to move; as a result, the beam's top side experiences compression, and its bottom side experiences tension. The neutral zone (intermediate section) is neither compressed nor under tension. For strain measurement in the different materials of RC T-

beams: 60 mm long SG for concrete, 5 mm long SG for steel, and 10 mm strain gauge for CFRP laminate were used. The concrete SG was attached in the concrete compression zone near the mid-span, the steel bars SG was fixed in the mid-span of tension steel bars, and the CFRP laminate SG was installed in the mid-span of the CFRP. The mid-span displacement is measured using Linear voltage displacement transducers (LVDT). (**Figure III-17**).

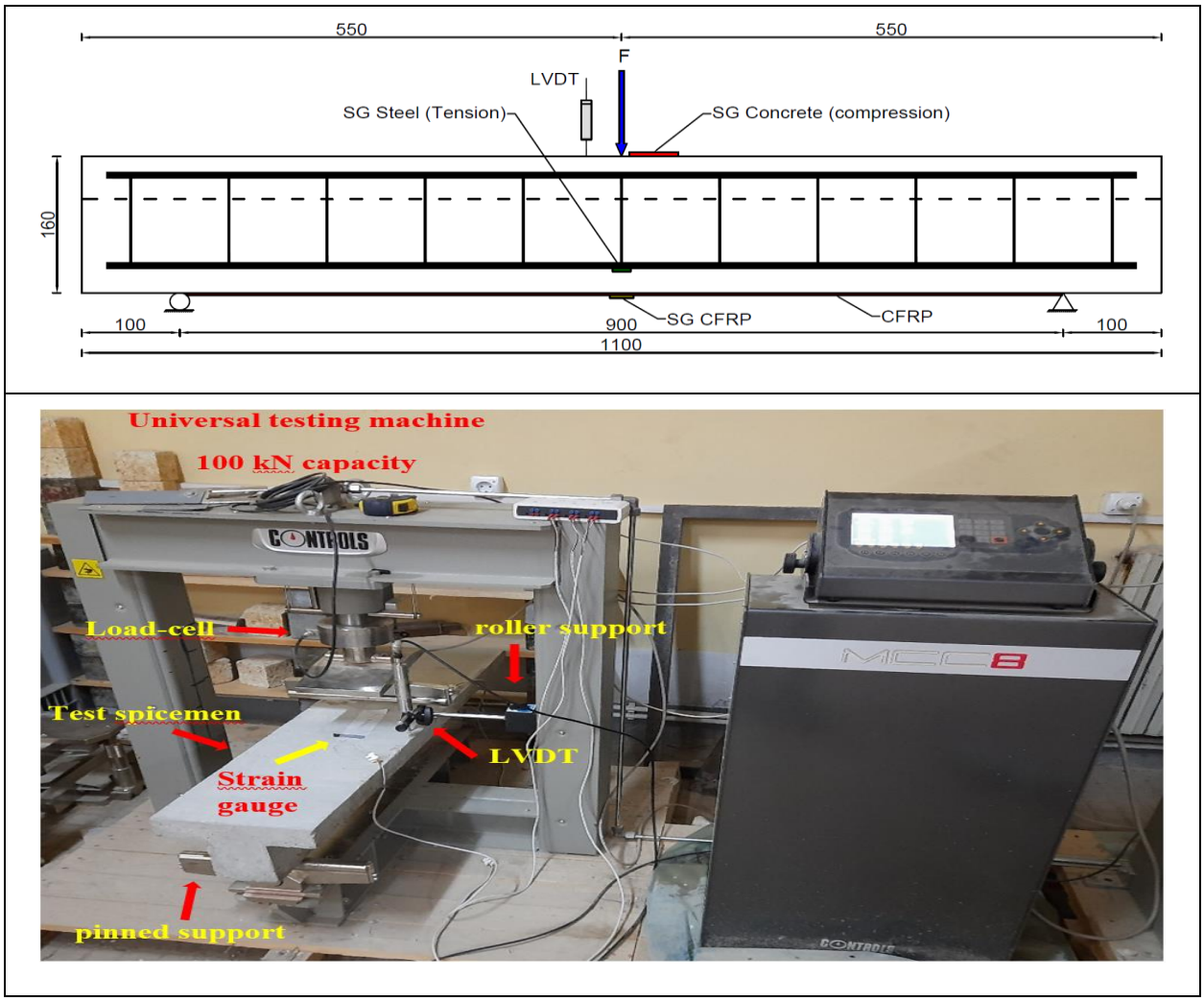

Figure III-17. Test setup and instrumentation (all dimensions in mm)

Chapter IV

EXPERIMENTAL TESTING AND ANALYSIS RESULTS

Chapter IV. Experimental Testing and Analysis Results

IV.1. Introduction

All the RC T-beams produced underwent comprehensive evaluation through a rigorous three-point bending test, as outlined in the previous chapter. This test served as a critical avenue for delving into the beams' flexural performance, enabling us to meticulously examine various aspects of their behavior. In this chapter, our investigation encompassed the determination of crucial parameters, including the first cracking load, yielding, ultimate load, crack patterns, failure modes, load-displacement profiles, and the Load-Strain response. Our exploration into these facets is at the core of this chapter, providing valuable insights into the performance and structural characteristics of the tested RC T-beams.

IV.2. First cracking load

IV.2.1. First Cracking Load Analysis of strengthened RC T-beam

The first cracking load of the strengthened RC T-beams was thoroughly examined and the results are summarized in **Table IV-1**. In comparison to the control solid RC T-beam, CB, the first cracking load of the control hollow RC T-beam, HCB, was found to be reduced by 24%. This reduction can be attributed to the loss of flexural rigidity caused by the longitudinal opening, leading to a decrease in the moment of inertia.

However, for the strengthened solid beams, there was a remarkable increase in the first cracking load. Specifically, the first cracking load of the strengthened solid beams, SCB, experienced a substantial 170% increase when compared to their respective control beam, CB. Similarly, the SHB beams, strengthened and hollow, exhibited a commendable 137% increase in first cracking load compared to their control counterpart, HCB. These results underscore the significant effectiveness of CFRP laminate in enhancing the first cracking load by substantially increasing flexural rigidity.

It is noteworthy that the improvement in first cracking load for the strengthened solid beams when compared to their controls was more pronounced than the improvement observed in the strengthened hollow beams when compared to their controls. This discrepancy suggests that the presence of the longitudinal aperture exerts a negative influence on the first cracking load of the strengthened hollow beams.

Furthermore, the strengthened beams also displayed an increase in the first load cracking deflection, which can be attributed to the heightened flexural rigidity achieved through the

strengthening process. This finding further highlights the positive impact of CFRP strengthening on the structural performance of the T-beams, as indicated in **Table IV-1**.

Table IV-1. Cracking Load and Deflection Comparison for Strengthened and Control RC T-Beams

Beam	Cracking load (KN)	cracking deflection (mm)	Cracking load increasing (%)	cracking deflection increasing (%)
CB	14.53	0.97	-	-
HCB	11.1	0.59	-23,61	-39.18
SCB	39.23	1.97	170	103
SHB	26.31	1.21	137	105

IV.2.2. First Cracking Load Analysis of Retrofitted RC T-Beams

The table below presents the first cracking load and deflection data for both repaired and control RC T-beams:

Table IV-2. Cracking Load and Deflection Comparison for Strengthened and Control RC T-Beams

Beam	Cracking load (KN)	cracking deflection (mm)	Cracking load increasing (%)	cracking deflection increasing (%)
CB	14.53	0.97	-	-
HCB	11.1	0.59	-23,61	-39.18
RCB80	36.84	2.53	153.54	160.82
RHB80	27.1	1.6	144.14	171.19
RCB100	-	-	-	-
RHB100	24.433	2.46	120.12	316.95

In line with the observations made for the strengthened beams, SCB and SHB, the repaired beams, RCB80 and RHB80, also exhibited notable improvements in both first cracking load and cracking deflection after the application of CFRP laminate, as depicted in **Table IV-2**.

It's worth noting that the first cracking deflection of the repaired beams, RCB80 and RHB100, was reduced by 20% and 17%, respectively, when compared to the solid beams SCB and SHB. This reduction can be attributed to the loss of flexural rigidity resulting from the pre-existing cracks in the repaired beams. Nevertheless, these results underscore the effectiveness of CFRP laminate in the repair of hollow beams that have been subjected to preloading-induced cracking.

The findings emphasize the significant impact of CFRP laminate in enhancing the structural performance of repaired RC T-beams and its potential for rehabilitating damaged structures.

IV.3. Ultimate Load and Deflection Analysis

IV.3.1. Ultimate Load and Deflection Analysis of Strengthened RC T-Beams

The **Table IV-3** below summarizes the ultimate load and deflection data for both control and strengthened RC T-beams:

Table IV-3. Comparison of Ultimate Load and Deflection for Strengthened and Control RC T-Beams

Beam	Ultimate load (KN	ultimate deflection (mm)	Ultimate load increasing (%)	ultimate deflection increasing (%)
CB	43.55	14,99	-	-
HCB	41.42	16,90	-4.89	12.74
SCB	58.17	3,44	33.58	-77.05
SHB	52.96	8.08	27.85	-52.19

In this analysis, we examine the ultimate load and deflection behavior of both control and strengthened RC T-beams.

For the control beams, it's noteworthy that the ultimate load of HCB was reduced by 4.89% compared to CB. This reduction is attributed to the decrease in flexural rigidity resulting from the longitudinal opening, which led to a reduction in the moment of inertia in the hollow RC T-beam. However, despite this reduction in ultimate load, the ultimate deflection of the hollow control beam HCB increased by approximately 12.74%. This increase in ultimate deflection can be explained by the decrease in bending stiffness, resulting in greater elasticity of the hollow beam compared to the solid beam.

In contrast, for the strengthened beams, SCB and SHB exhibited remarkable increases in their ultimate loads, with a respective 33.58% and 27.85% increase compared to their control beams, CB and HCB. This significant improvement in ultimate load is attributed to the effective use of CFRP laminate, which substantially enhances the beams' stiffness.

Despite the increased stresses in the tension zone of hollow beams compared to solid beams, causing them to fail earlier, the ultimate load of SHB was only reduced by 9% compared to SCB. This minor reduction underscores the effectiveness of CFRP laminate in strengthening hollow beams.

However, the ultimate deflection exhibited a considerable decrease of 77.05% and 52.19% in SCB and SHB compared to their control counterparts, CB and HCB, respectively. This reduction can

be attributed to the longitudinal opening, which renders hollow beams more flexible. Interestingly, despite this reduction, it is important to note that the deflection of hollow beams remains non-significantly different from that of solid beams, which is a positive factor contributing to the overall ductility of structures.

These results provide valuable insights into the structural behavior of CFRP-strengthened RC T-beams, emphasizing the significant impact of CFRP laminate in enhancing ultimate load and stiffness while maintaining favorable deflection characteristics, particularly in the context of hollow beams.

IV.3.2. Ultimate Load and Deflection Analysis of Retrofitted RC T-Beams

In this section, we focus on the ultimate load and deflection behavior of repaired RC T-beams, which underwent pre-loading at 80% and 100% of their failure load before being repaired with a single layer of CFRP laminate on their tension side.

For the beams pre-loaded at 80%, a noticeable increase in ultimate load was observed in RCB80 and RHB80, with a respective 30.01% and 12.68% gain compared to their corresponding control beams, CB and HCB. This substantial improvement in ultimate load can be attributed to the reinforcement provided by the CFRP laminate. However, it's important to note that the ultimate deflection of RCB80 and RHB80 decreased significantly, with reductions of 73% and 82%, respectively, when compared to the deflection of the control beams, CB and HCB. It is worth mentioning that the lower ultimate load of RHB80, which is 17.54% less than RCB80, as shown in the table, played a role in this difference.

For the beams pre-loaded at 100%, the ultimate load exhibited a substantial increase of 36.3% and 9.15% in RCB100 and RHB100 compared to their control counterparts, CB and HCB. However, it's noteworthy that the high stresses in the tension zone of RHB100 T-beams, as compared to RCB100, led to the repaired hollow beam reaching its failure load before the repaired solid beam. This result indicates the need for further refinement in the repair method employed for hollow beams. Additionally, the ultimate deflection of RCB100 and RHB100 decreased significantly, with reductions of 68.65% and 59.17%, respectively, when compared to CB and HCB. This reduction in deflection can be attributed to the substantial damage sustained by the hollow beam during preloading, rendering it more flexible than the solid preloaded beam.

These findings provide valuable insights into the effectiveness of the CFRP repair method for RC T-beams subjected to preloading, highlighting the impact on both ultimate load capacity and stiffness, with a specific focus on the unique behavior of hollow beams.

The results are summarized in **Table IV-4**.

Table IV-4. Comparison of Ultimate Load and Deflection for Repaired and Control RC T-Beams

Beam	Ultimate load (KN)	ultimate deflection (mm)	Ultimate load increasing (%)	ultimate deflection increasing (%)
CB	43.55	14,99	-	-
HCB	41.42	16,90	-4.89	12.74
RCB80	56.61	4,00	30	-73.32
RHB80	46.68	3,09	12.69	-81.72
RCB100	59.36	4,70	36.30	-68.65
RHB100	45.21	6,90	9.15	-59.17

IV.4. Crack Patterns and Failure Modes

Crack patterns and failure modes are integral aspects of structural analysis, providing valuable insights into the behavior of reinforced concrete (RC) elements and the effectiveness of various strengthening techniques. Understanding how cracks propagate and identifying the modes of failure is essential for assessing structural integrity, safety, and the potential for improvements or reinforcements.

In this section, we delve into an exploration of crack patterns and failure modes, particularly in the context of RC T-beams. By examining the behavior of both control and CFRP-strengthened beams, we aim to shed light on the impact of longitudinal openings, strengthening methods, and other factors that influence the structural response.

Our investigation will not only highlight the typical crack patterns and failure modes observed but also provide a deeper understanding of the underlying mechanisms driving these behaviors. This knowledge is fundamental for engineers and researchers seeking to optimize the performance of RC structures, enhance their load-bearing capacity, and ensure their long-term durability.

Through the analysis of crack patterns and failure modes, we embark on a journey to uncover the intricacies of structural behavior, ultimately contributing to safer and more resilient infrastructure.

IV.4.1. Crack Patterns and Failure Mode of Control RC T-Beam

The control beams, CB and HCB, exhibited similar crack propagation patterns, suggesting that the presence of a longitudinal opening does not significantly influence the crack propagation process. The initiation of cracks in the concrete tension zone, occurring at the midpoint of the beam due to applied loads, was a common feature. These initial cracks were followed by the development of oblique cracks as the applied load intensified. With increasing load, these cracks extended in length and thickness until they intersected with the concrete compression zone at the flange. It's at this stage that flexural failure occurred, as depicted in **Figure IV-1**.

During flexural failure, several key mechanisms came into play. The compressive flange of the beam underwent softening, resulting in a downward shift of the center of rotation of the sections and a reduction in the internal lever arm. Ductile flexural failure ensued when the ultimate capacity of the concrete compressive zone was reached.

It's important to note that flexural failure is primarily governed by concrete crushing after the yielding of the steel. Typically, the deformation capacity of the steel is not a critical factor in this failure mode. Interestingly, in the case of hollow beams, a more pronounced amount of concrete crushing was observed compared to solid beams. This phenomenon can be attributed to the reduction in concrete volume due to the longitudinal opening, resulting in decreased concrete strength and, consequently, an increase in the volume affected by the final damage.

In summary, understanding crack patterns and failure modes in both control and CFRP-strengthened RC T-beams is pivotal for assessing structural performance and the effectiveness of strengthening techniques. The presence of longitudinal openings appears to have a limited influence on crack propagation patterns, while concrete crushing plays a crucial role in flexural failure, particularly in hollow beams.

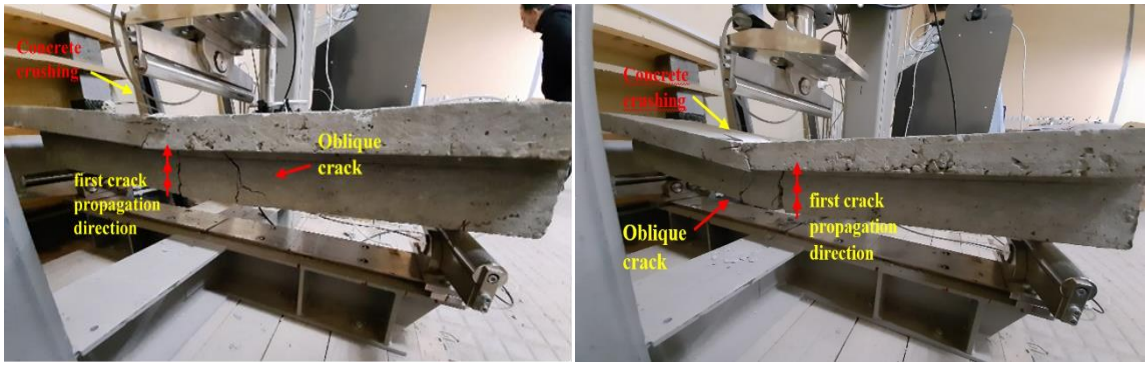

(a) (b)

Figure IV-1. Crack Propagation and Failure Modes of Control Beams: (a) CB; (b) HCB

IV.4.2. Crack Patterns and Failure Mode in Strengthened RC T-Beams

In contrast to the control beams, CB and HCB, the strengthened RC T-beams, SCB and SHB, exhibited distinct crack propagation and failure mode patterns. Notably, cracks in SCB and SHB extended diagonally from the upper center of the beam towards the support. The primary cause of failure in both SCB and SHB was the separation of the concrete cover, resulting in the detachment of the CFRP laminate, as visually depicted in **Figure IV-2**.

The occurrence of concrete cover separation failure can be attributed to the elevated interfacial shear and peeling stresses that developed at the end of the CFRP laminate. These heightened shear stresses, situated near or at the FRP plate's end, induced the formation of cracks within the concrete. These cracks propagated vertically, aligning with the level of the tension steel reinforcement, before extending horizontally along that level of reinforcement. This sequence of events led to the separation of the concrete cover [45]. It is important to note that previous research studies have reported similar instances of this failure mode [71], [72], [73].

Furthermore, it is worth highlighting that the extent of concrete cover separation observed in SHB exceeded that in SCB. This difference can be attributed to the higher ultimate load carried by SHB, despite having a lower moment of inertia compared to SCB, as illustrated in **Figure IV-2**.

In summary, the analysis of crack patterns and failure modes in strengthened RC T-beams, as opposed to control beams, underscores the significance of concrete cover separation as a predominant failure mechanism. The development of diagonal cracks originating from the upper center towards the support is a characteristic feature of this failure mode, resulting from elevated interfacial shear and peeling stresses at the CFRP laminate's end. Understanding this failure mechanism is essential for evaluating the structural performance and effectiveness of CFRP strengthening techniques.

(a) (b)

Figure IV-2. Crack Propagation and Failure Modes of Strengthened Beams: (a) SCB; (b) SHB.

IV.4.3. Crack Propagation and Failure Mode in Retrofitted RC T-Beams

The failure mode observed in the repaired RC T-beams closely resembled that of the strengthened beams, as depicted in **Figure IV-3**. This similarity can be attributed to the use of CFRP for repair, which introduced key alterations in the beams' structural behavior.

One significant alteration was the emergence of a new crack pattern in the repaired beams, accompanied by a delay in the appearance of the first cracks. This deviation from the control beams was a direct result of the CFRP repair process, which effectively counteracted the initial cracks induced by pre-loading. Consequently, the repaired beams remained unaffected by the initial cracks, leading to the continuation of a crack propagation and failure mode akin to that observed in the strengthened beams.

However, it is important to note that the hollow repaired beams subjected to pre-loading exhibited more extensive damage compared to their solid counterparts. This disparity in damage levels can be attributed to the inherent characteristics of hollow beams, which are more vulnerable to structural damage due to their reduced moment of inertia.

In summary, the utilization of CFRP for repair introduced notable changes in the crack propagation and failure mode of RC T-beams. The ability of CFRP to mitigate the impact of initial cracks from pre-loading resulted in a new crack pattern and delayed crack appearance. Additionally, it was evident that the hollow repaired beams experienced greater damage when subjected to pre-loading, underlining the importance of considering beam geometry when implementing repair techniques.

(a) (b)

Figure IV-3. Crack Propagation and Mode of Failure of Retrofitted Girders: (a) RCB80; (b) RHB80

IV.5. Load-Displacement Behavior

IV.5.1. Load-Displacement Behavior of Strengthened RC T-Beam

The load-displacement behavior of the strengthened RC T-beams reveals distinctive stages, as illustrated in **Figure IV-4**:

- **First Stage**: In this initial phase, the stiffness of both the control beams (CB and HCB) and the strengthened beams (SCB and SHB) is identical before reaching a load of approximately 10 kN. During this stage, the absence of concrete cracking keeps beam deflections minimal, and all materials behave linearly elastic.
- **Second Stage**: This stage commences with the appearance of the first cracks and continues up to the yielding load of the control beams, roughly spanning the load range of 10 kN to 34 kN. During this stage, the stiffness of control beams CB and HCB decreases compared to that of strengthened beams SCB and SHB due to the emergence of the first cracks in the concrete tension zone of CB and HCB. Additionally, HCB exhibits a slightly reduced rigidity compared to CB, a consequence of the longitudinal opening's reduction in moment of inertia. Consequently, it can be deduced that the hollow RC T-beam is more flexible than the solid RC T-beam. Throughout this phase, all materials remain within their linear elastic regions until the steel yields. Notably, when compared to CB and HCB, the deflections of SCB and SHB at the yielding load of control beams decrease by approximately 44% and 54%, respectively. This observation suggests that CFRP primarily carries the load at this stage, elucidating the delayed appearance of the first cracks in the strengthened beams.

- **Third Stage**: This phase initiates after the yielding load of the control beams and extends until failure. During this period, control beams CB and HCB undergo plastic deformation leading to failure. HCB, being a hollow beam, experiences slightly greater deflections than solid beam CB due to the reduction in bending stiffness caused by the longitudinal opening. Furthermore, the strengthened beams SCB and SHB experience their first cracks at the onset of this stage. Due to CFRP strengthening, their stiffness slightly decreases in comparison to that of the control beams. Notably, the maximum deflection of SCB and SHB decreases by 77% and 71%, respectively, compared to CB and HCB, owing to the high rigidity achieved through CFRP strengthening of the RC T-beams. Interestingly, the hollow strengthened beam SHB exhibits a larger plastic deformation region than the solid beam. This phenomenon can be attributed to the lower bending stiffness of hollow beams in comparison to solid beams, facilitating optimal utilization of the CFRP plates and thus resulting in larger deflections.

In summary, the load-displacement behavior of strengthened RC T-beams exhibits distinct stages, with CFRP playing a crucial role in load-bearing capacity during the second stage, while the inherent beam geometry influences plastic deformation and deflection characteristics during the third stage. Understanding these behavior patterns is essential for comprehending the effectiveness of CFRP strengthening techniques in RC T-beams.

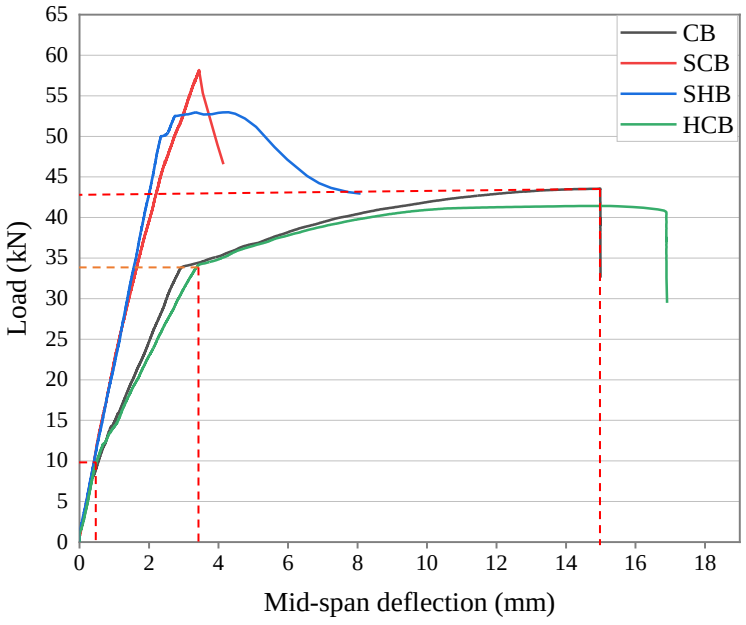

Figure IV-4. Load-Deflection Curves for Control and Strengthened Beams

IV.5.2. Load-Displacement Behavior of Retrofitted RC T-Beams

The load-displacement behavior of retrofitted RC T-beams, enhanced by CFRP laminate, exhibited a pattern similar to that observed in the strengthened beams SCB and SHB. However, there were some notable distinctions worth discussing in detail:

Initial Stiffness: The retrofitted beams initially displayed a slightly lower stiffness compared to the strengthened beams. This disparity can be attributed to pre-load-induced cracking in the retrofitted beams, resulting in approximately a 5% increase in deflection when compared to the strengthened beams.

RHB100 Exception: Among the retrofitted beams, RHB100 stood out due to its lower stiffness and higher deflection. This behavior can be attributed to the significant damage it incurred during pre-loading, which had a pronounced impact on its structural response.

Maximum Deflection: The retrofitted beams, RCB80 and RHB80, exhibited a substantial reduction in maximum deflection, approximately 73% and 82%, respectively, when compared to the deflection of the control beams, CB and HCB. Furthermore, for beams pre-loaded to 100%, the reduction in maximum deflection was approximately 69% and 59%. These findings underscore the effectiveness of CFRP in retrofitting these beams, significantly enhancing their stiffness and reducing deflections.

CFRP Effectiveness: The consistent reduction in deflection by approximately 69% and 59% for beams pre-loaded to 100% demonstrates the remarkable effectiveness of CFRP in retrofitting these beams. This highlights how well CFRP can enhance the structural performance of retrofitted RC T-beams.

In summary, the load-displacement behavior of retrofitted RC T-beams, when enhanced by CFRP retrofitting, closely resembled that of strengthened beams. Despite some variations in initial stiffness and behavior in the case of RHB100, the overall effectiveness of CFRP in reducing deflections and enhancing stiffness in retrofitted beams is evident. These results emphasize the potential of CFRP retrofitting as a viable solution for improving the structural performance of existing RC T-beams.

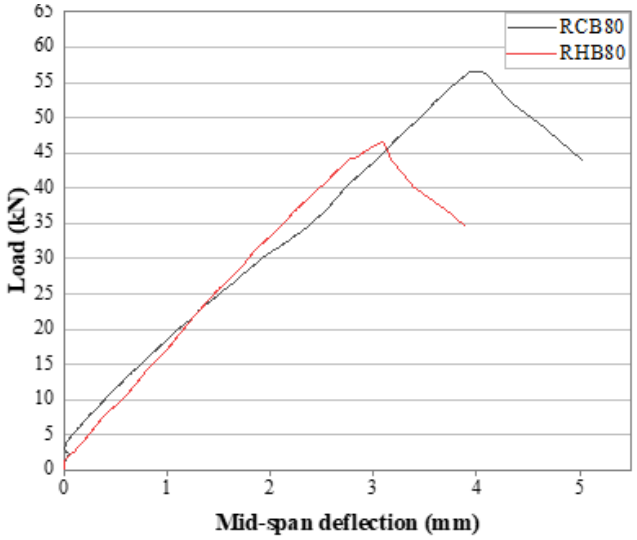

(a)

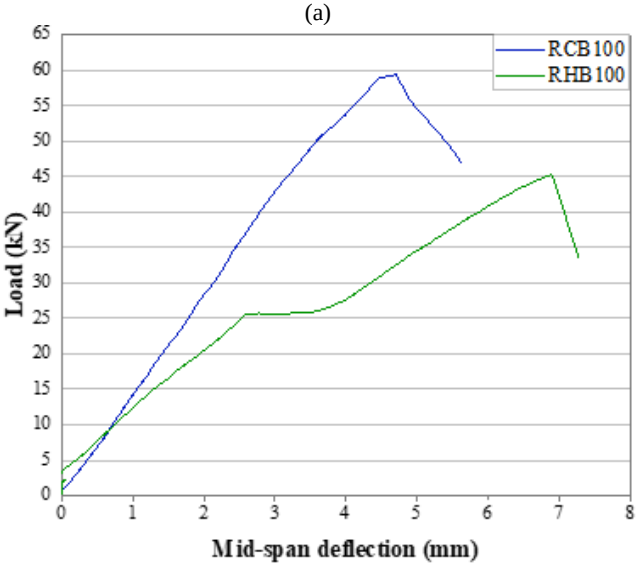

(b)

Figure IV-5. Loading-deflection graphs for retrofitted girders: (a) girders subjected to 80% preload; (b) girders subjected to 100% preload.

IV.6. Load-Strain behaviour

In the evaluation of structural performance and the effectiveness of strengthening techniques for RC T-beams, an in-depth examination of load-strain behavior and concrete strain is crucial. **Table IV-5** presents comprehensive data on the maximum strain values recorded across various components within the beams, including concrete, steel bars, and CFRP. This analysis provides valuable insights into how these beams respond to different loading conditions and highlights the role of CFRP in mitigating concrete strain while enhancing load-bearing capacity.

Table IV-5. Strain Data for Concrete, Steel, and CFRP in RC T-Beams

	Concrete strain (compression)		Steel strain (tension)		CFRP strain (tensile)	
	Solid	**Hollow**	**Solid**	**Hollow**	**Solid**	**Hollow**
Control (CB/HCB)	6138	4447,8	18816	7440.8	-	-
Strengthened (SCB/SHB)	975,2	1883,5	4225.1	2544.7	2569,8	1931
Repair 80 (RCB80/RHB80)	868	661,2	1860	1343,2	2578,9	2051
Repair 100 (RCB100/RHB100)	517,5	105,4	3080	-	2618	2356,6

IV.6.1. Concrete and Steel Strain Behavior in Strengthened RC T-Beams

The analysis of concrete and steel strain behavior within the RC T-beams yielded insightful observations:

A significant distinction in steel strain was evident when comparing CB with HCB. The steel strain within CB was notably higher, as depicted in **Figure IV-6a**. This disparity can be attributed to CB's capacity to support greater loads, resulting in the generation of substantial moments in the beam's midsection. These moments, in turn, made the longitudinal steel bars more resilient, leading to higher strain. However, it is important to note that the compression zone of concrete also experienced an increase in strain due to these elevated moments, as evident in **Figure IV-6b**.

Before any initial concrete cracking occurred, both control and strengthened beams exhibited nearly identical concrete strains, as illustrated in **Figure IV-6b** and **Figure IV-7a**. During this phase, the maximum concrete strain within SCB and SHB decreased by 84% and 58%, respectively, in comparison to CB and HCB. This reduction in concrete strain was a direct result of the incorporation of CFRP, highlighting its effectiveness in minimizing concrete deformation or cracking. A similar effect was observed in the steel strains.

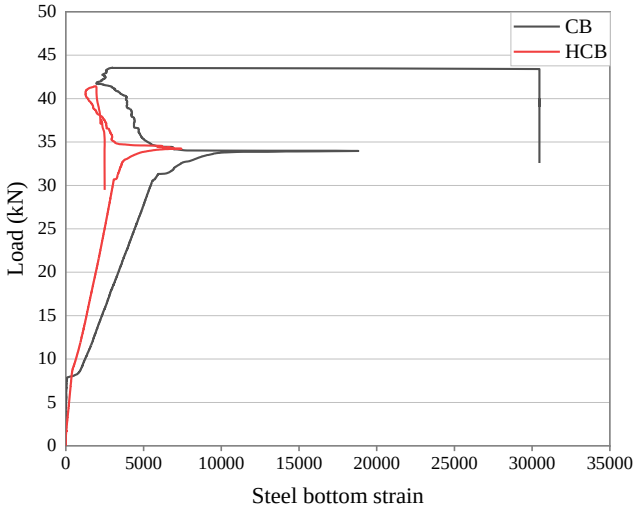

(a)

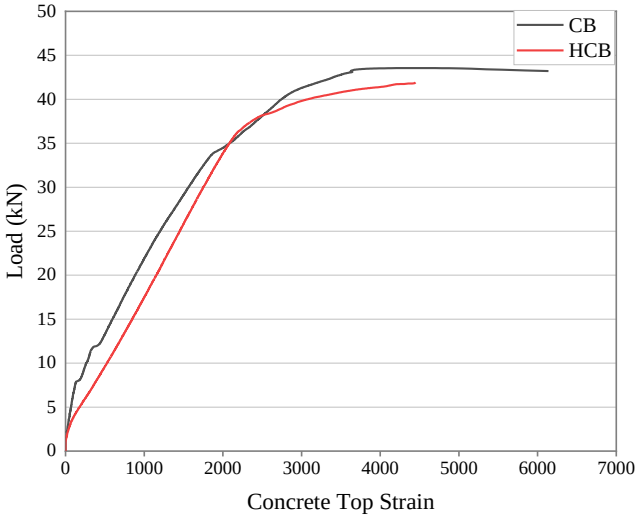

(b)

Figure IV-6. (a) Strain in steel for CB and HCB control girders; (b) Strain in concrete for CB and HCB control girders (με).

Despite SCB's greater load-carrying capacity compared to SHB, the maximum concrete strain in SHB was significantly higher, by approximately 93%, as demonstrated in **Figure IV-7a**. This can be attributed to SHB's lower moment of inertia relative to SCB. The lower moment of inertia made SHB more capable of withstanding the substantial moments generated by the higher load, leading to increased compression strain. Additionally, the maximum steel strain in SHB decreased by 40% in comparison to SCB. This decrease was a result of the longitudinal steel bars in SCB offering greater resistance to the moments generated by the higher load, thus producing higher strain, as shown in **Figure IV-7b**.

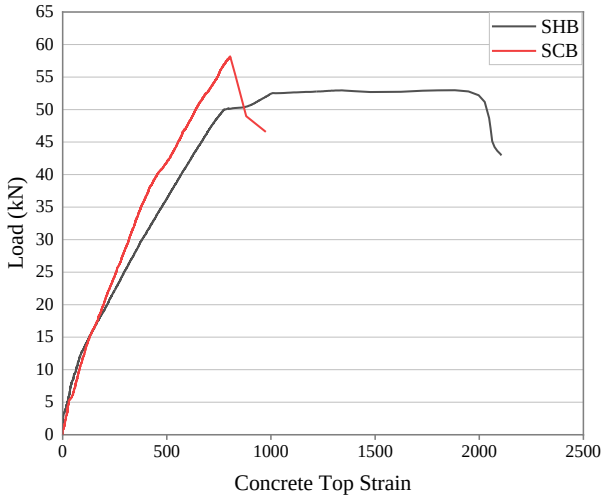

(a)

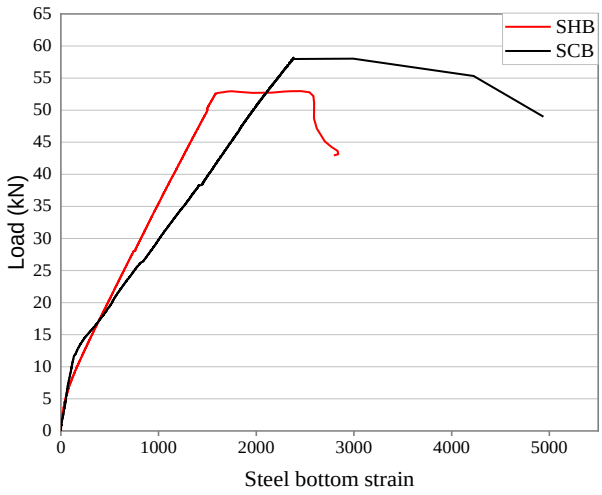

(b)

Figure IV-7. (a) Concrete strain, and (b) Strain in steel for strengthened girders SCB and SHB (με).

IV.6.2. Concrete and Steel Strain Behavior in Retrofitted RC T-Beams:

The load–strain behavior observed in retrofitted RC T-beams mirrored the trends observed in strengthened RC T-beams, as depicted in **Figure IV-8** and **Figure IV-9** However, it's important to note that the steel-bar strain in the RHB100 beam could not be recorded.

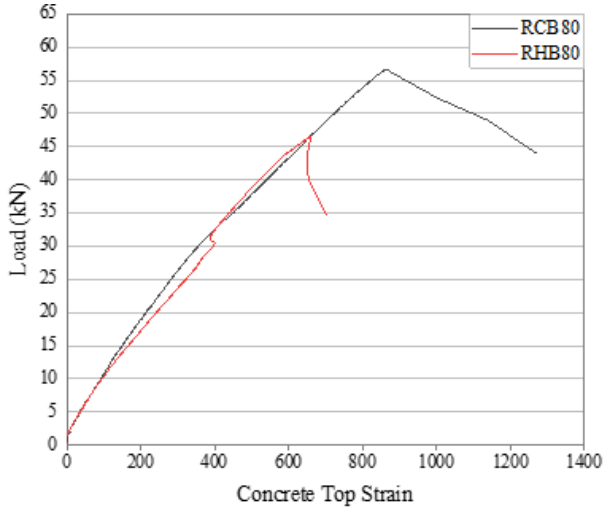

(a)

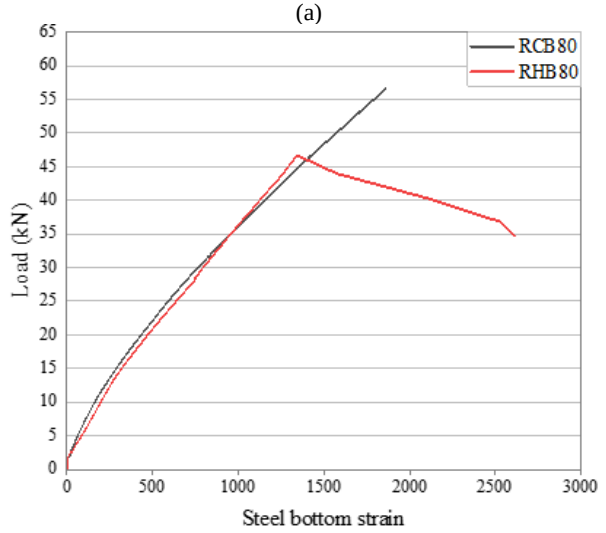

(b)

Figure IV-8. (a) Concrete strain, and (b) Strain in the steel for RCB80 and RHB80 (με).

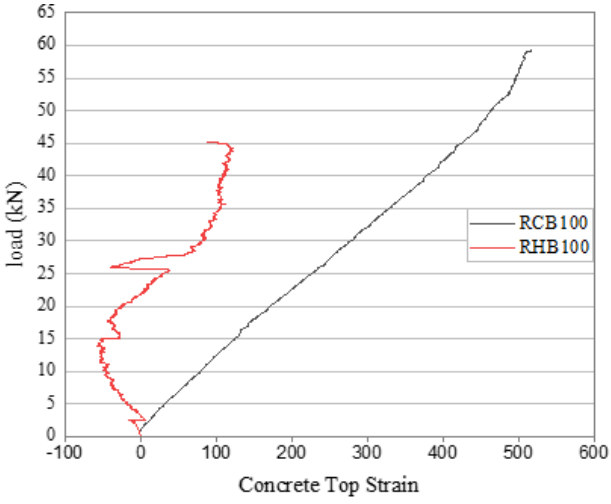

(a)

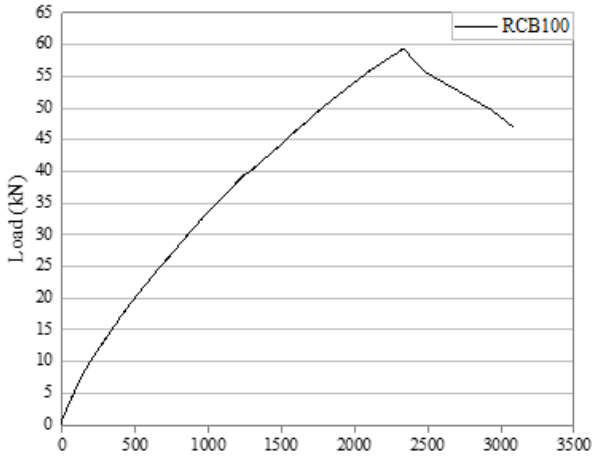

(b)

Figure IV-9. (a) Concrete strain, and (b) Strain in the steel for RCB100 and RHB100 (με).

In summary, the examination of concrete strain behavior in RC T-beams highlights the profound impact of CFRP reinforcement in reducing concrete strain even under substantial loads. These findings underscore the pivotal role of CFRP in enhancing the structural performance of these beams by effectively managing strain and fortifying their load-bearing capacity. Furthermore, the consistent behavior observed in both strengthened and retrofitted beams underscores the versatile utility of CFRP in augmenting the performance of existing RC T-beams.

IV.6.3. CFRP Strain Behavior in Strengthened and Retrofitted RC T-Beams:

The CFRP load–strain curves for all RC T-beams unequivocally demonstrate that the CFRP material remained within its linear elastic range, as indicated by **Figure IV-10**, **Figure IV-11**, and **Figure IV-12**. This behavior can be attributed to the abrupt failure of the concrete and the absence of an anchoring system. Furthermore, the maximum CFRP strain in the hollow RC T-beams (SHB, RHB80, and RHB100) was 25%, 20%, and 10% lower, respectively, compared to the solid RC T-beams (SCB, RCB80, and RCB100). This variance can be attributed to the greater loads borne by the solid RC T-beams, resulting in higher moments at their mid-span. These heightened moments necessitated greater resistance from the CFRP, leading to increased strain in the solid RC T-beams compared to their hollow counterparts.

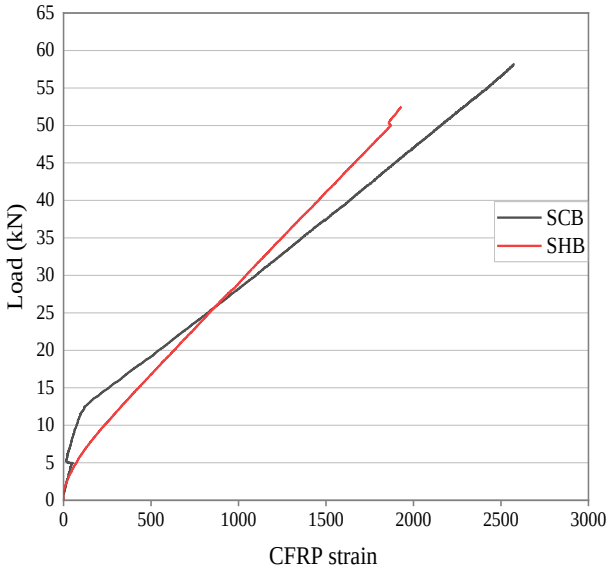

Figure IV-10. strain in CFRP in SCB and SHB (με).

The maximum CFRP strain in RCB100, as depicted in **Figure IV-12**, was the most significant among all tested RC T-beams. This can be attributed to its higher ultimate load capacity. Consequently, preloading emerges as a strategy to enhance the CFRP strain, potentially mitigating the risk of concrete failure.

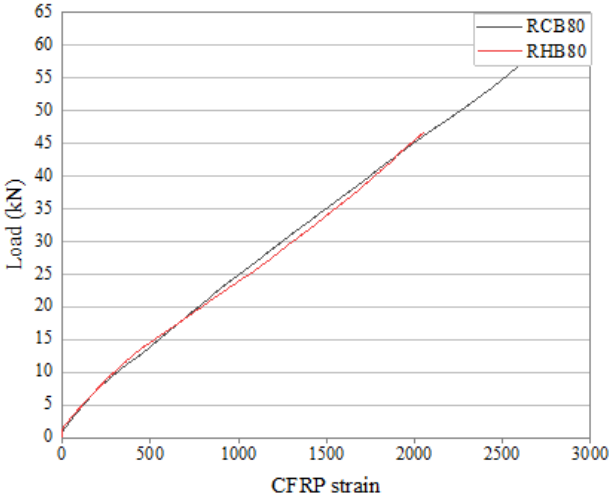

Figure IV-11. strain in CFRP in RCB80 and RHB80 (με).

Furthermore, when RC T-beams were subjected to higher preloads, indicating greater damage prior to retrofitting, the CFRP strain increased significantly, while the concrete strain decreased.

This phenomenon is illustrated in **Table IV-5** and suggests that the presence of cracks resulting from preloading enhances the transfer of loads to the CFRP laminate. Consequently, the CFRP bears more of the applied load, ensuring the structural stability of the beams even in the presence of initial damage.

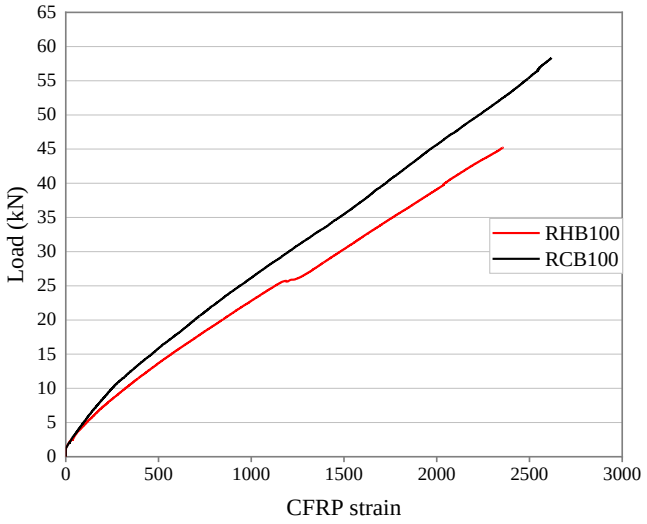

Figure IV-12. strain in CFRP in RCB100 and RHB100 (με).

In summary, the CFRP strain behavior in RC T-beams reveals its remarkable capacity to operate within its linear elastic range, preserving structural integrity. The variations in CFRP strain between solid and hollow RC T-beams underscore the material's adaptability in managing diverse load distributions. Additionally, preloading serves to increase CFRP strain, offering a potential strategy for averting concrete failure and ensuring the structural robustness of RC T-beams.

Chapter V
Numerical Analysis

Chapter V. Numerical Analysis

V.1. Introduction

This study delves into the comprehensive analysis of CFRP-strengthened RC hollow T-beams, with a specific focus on the numerical modeling and parametric investigations aimed at uncovering the intricate interplay of various factors affecting their structural performance. Through finite element (FE) modeling and a parametric study, we examine key parameters such as longitudinal opening position, longitudinal hole size, and shear strengthening using different CFRP wrapping configurations.

The findings presented herein offer valuable insights into the behavior of CFRP-strengthened RC hollow T-beams under a range of conditions and configurations. These insights not only contribute to the fundamental understanding of these structural elements but also provide practical guidance for engineers and designers seeking to optimize the performance of such beams in construction projects. Ultimately, this research contributes to the ongoing efforts to advance the field of structural engineering and construction practices by harnessing the potential of innovative materials and methodologies.

V.2. ABAQUS Software

ABAQUS is a renowned finite element analysis (FEA) software package that holds a prominent place in the field of structural analysis and simulation. It is widely recognized and utilized by engineers and researchers across various industries for its robust capabilities in simulating complex mechanical behavior, conducting structural analyses, and solving engineering problems. In the context of this research, ABAQUS plays a pivotal role in the numerical modeling and analysis of CFRP-strengthened RC hollow T-beams.

Significance in Structural Engineering:

ABAQUS holds immense significance in the realm of structural engineering and research. Its robust capabilities empower engineers and researchers to:

- Conduct detailed and accurate structural analyses.
- Optimize designs for enhanced performance and safety.
- Explore the behavior of complex structures under various loads and conditions.
- Investigate the effects of different materials and strengthening techniques on structural performance.

- Make informed decisions in structural design, retrofitting, and rehabilitation projects

V.3. Numerical Modeling

V.3.1. Finite Element Modeling

to replicate the behavior of the tested girders, a 3D FE model was constructed with ABAQUS software. The concrete material was modeled using an eight-node linear brick element (C3D8R), whereas the inner reinforcement was characterized by a two-node 3D linear lattice element (T3D2). CFRP components were modeled as shell structures with three layers oriented in various orientations (0°, 45° and 90°). To assure that there is no relative movement between CFRP and concrete during their interaction, a bond stress was applied.

To identify the best mesh size, a sensitivity analysis was carried out and different mesh sizes were tested. Subsequently, a mesh of 25 mm was selected as the most suitable for further modelling. The numerical findings, in particular the load-deflection curve, were then checked against the laboratory results. **Figure V-1** provides a visual representation of the beams within the 3D FE model.

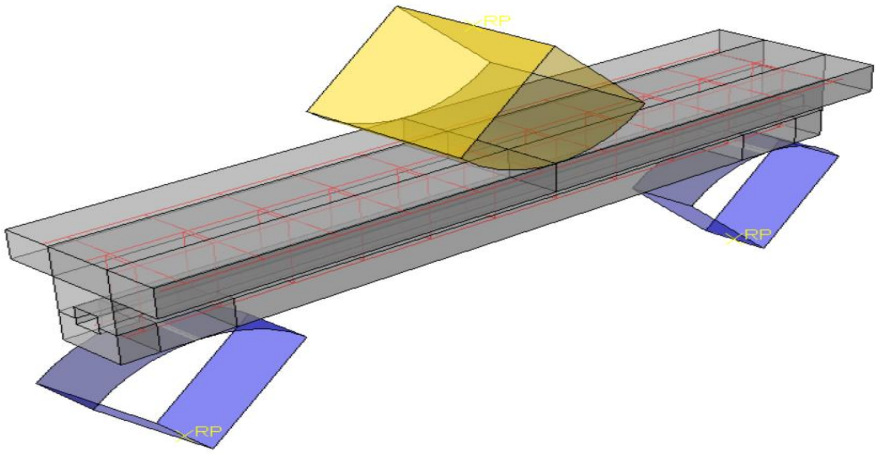

Figure V-1. Modeling T-Girders and Defining Boundary Conditions

V.3.2. Material Modeling

In this section, the material modeling approach used for the study is described. The concrete material was represented using the damaged plasticity (CDP) model implemented in ABAQUS, The CDP model employed in this study incorporated isotropic damaged elasticity, as well as

isotropic tensile and compressive plasticity, to capture the overall behavior of the concrete material. The model accounted for two primary failure mechanisms observed in concrete: tensile cracking and compressive crushing.

For the CDP model, specific material parameters were defined. The dilatation angle (ψ) was selected as 35°, a value falling within the recommended range of 20–45° [74], [75] , representing the friction angle within concrete. An eccentricity parameter (ε) of 0.1 was adopted, a value in accordance with recommendations [76]. The stress ratio (σ_{bo}/σ_{co}) was set to the default value of 1.16, representing the ratio of biaxial compressive and uniaxial compressive yield stresses. The factor K, responsible for establishing initial yield stresses within the deviatoric plane, was set to the default value of 2/3.

Regarding the steel reinforcement bars, an elastic-plastic behavior model was employed, considering strain hardening in both compression and tension. This behavior was characterized by a bilinear stress-strain relationship. In the simulation of the reinforced concrete (RC) beams, three steel plates were incorporated. Two of these plates were positioned at the support points, while the third plate was placed at the loading point to ensure an even distribution of applied loads.

V.3.3. Validation of the Finite Element Model

In order to rigorously assess the accuracy and effectiveness of our numerical models, a series of experimental tests were conducted on a carefully selected set of beams, each featuring distinct hollow configurations. The intent was to establish a robust foundation for comparing and validating the results obtained from both experimental and numerical approaches. This crucial validation process is instrumental in ensuring the reliability and predictive capability of our finite element (FE) model.

The comparison of load-deflection curves, as depicted in **Table V-1**, reveals a striking and gratifying congruence between the outcomes derived from the numerical simulations and those acquired through experimental testing. This close alignment between the two sets of results underscores the fidelity of our FE model in capturing the intricate nonlinear behavior exhibited by RC T-beams.

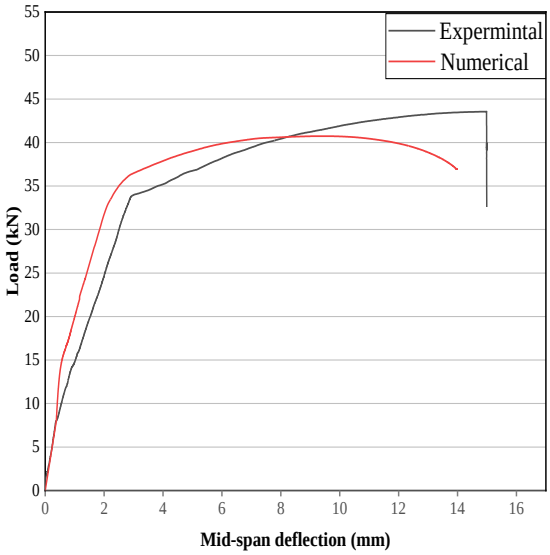

(a) Control solid beam CB

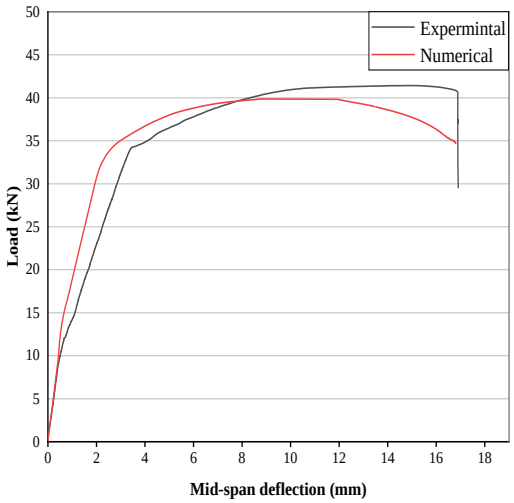

(b) Control hollow beam HCB

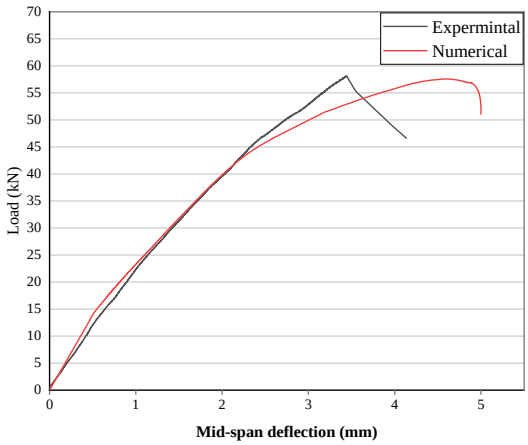

(c) Strengthened solid beam SCB

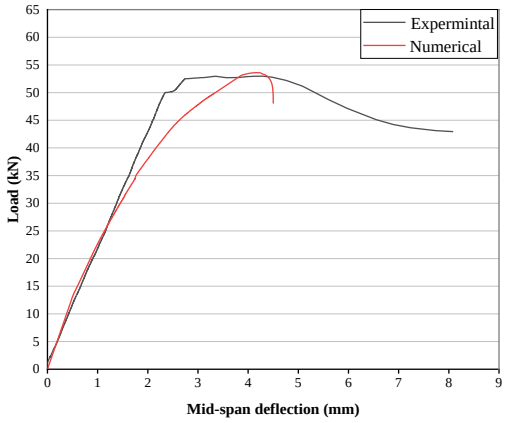

(d) Strengthened hollow beam SCB

Figure V-2. Experimental and numerical model comparison

The behavior of these structural elements can be conceptually dissected into three distinct phases. The initial phase corresponds to the linear response observed during the elastic phase of the constituent materials, wherein the beams deform proportionally to the applied load. The second phase marks a linear response characterized by the formation and propagation of cracks, as guided by the established crack profile within the material. Finally, the third phase heralds the onset of nonlinear behavior, driven by the emergence and development of cracks within each material component.

For a comprehensive evaluation of the ultimate loads, **Table V-1** presents a detailed comparison between the values obtained through experimentation and those predicted by our numerical model. Remarkably, the disparities between the experimental and numerical outcomes remain consistently within a narrow range, spanning from 1.03% to 6.45%. It is worth highlighting that the majority of the newly developed numerical model results closely mirror the experimental data, indicating a

high level of accuracy and reliability. The most substantial deviation, approximately 6.45%, was observed in the case of beam CB, while the smallest deviation of 1.03% was found for the SCB beam.

Table V-1. Comparison of Experimental and Numerical Ultimate Loads.

Beam	Experimental	Numerical	Difference %
CB	43.55	40.74	6.45
HCB	41.42	39.87	3.74
SCB	58.17	57.57	1.03
SHB	52.96	53.62	1.25

In summation, the results of this validation exercise underscore the numerical model's proficiency as a dependable tool for forecasting the complex behavior exhibited by CFRP-strengthened RC hollow T-beams, affirming its suitability for engineering applications and structural analysis.

V.4. Parametric Study

In this section, we delve into the details of our parametric analysis, which encompassed a comprehensive exploration of various variables that significantly impact the structural behavior of the T-beams under investigation. The key parameters considered in our study included the longitudinal opening position relative to the upper concrete fibers, the longitudinal opening size, and the type of shear strengthening achieved through different CFRP wrapping configurations on the T-beams. These parameters were systematically varied to assess their influence on the beams' performance and response. **Table V-2** outlines the specific details of these parametric variations.

Table V-2. Parameters for the Parametric Study

Group	Beam	Holl position (mm)	Holl size (mm)	Strengthening scheme
	Control	105	40×30	3 Layer in tension side
opening position	H105	105	40×30	3 Layer in tension side
	H62,5	62,5	40×30	3 Layer in tension side
	H60	60	40×30	3 Layer in tension side
opening size	B30	62,5	40×30	3 Layer in tension side
	B50	62,5	40×50	3 Layer in tension side
	B70	62,5	40×70	3 Layer in tension side
opening size + Flexural strengthening	SB30	62,5	40×30	3 Layer in tension side
	SB50	62,5	40×50	3 Layer in tension side
	SB70	62,5	40×70	3 Layer in tension side
shear strengthening	CUW	105	40×30	3 Layer in tension side + continuous U-wrapping
	DUW	105	40×30	3 Layer in tension side + discontinuous strip U-wrapping

These carefully defined parameters allowed us to explore the influence of opening position, opening size, and different strengthening schemes on the structural response of the T-beams. The reinforcing steel bars remained consistent across all trials to ensure a controlled experimental setup. The subsequent analysis and findings provide valuable insights into optimizing the structural performance of CFRP-strengthened RC hollow T-beams under various conditions and configurations.

V.4.1. Longitudinal Opening Position

In this section, we delve into the effect of varying longitudinal opening positions on the behavior of the T-beams, a crucial aspect of our parametric study. Three distinct longitudinal opening positions were meticulously considered and illustrated in **Figure V-3**:

- **H105 (105 mm from Upper Concrete Fibers)**: This position is situated beneath the neutral axis of the beam.
- **H62.5 (62.5 mm from Upper Fibers)**: This position aligns with the neutral axis of the beam.
- **H60 (60 mm from Upper Fibers)**: This position is located above the neutral axis of the beam.

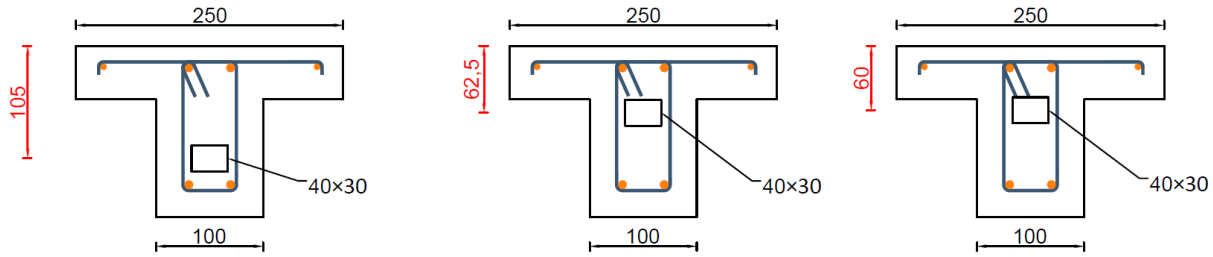

Figure V-3 Longitudinal opening positions.

The purpose of this investigation was to discern the impact of these varying opening positions on the structural behavior of the beams. To facilitate this assessment, we compared the ultimate load and deflection of each beam configuration with those of the control solid beam (CB), as depicted in **Figure V-4**.

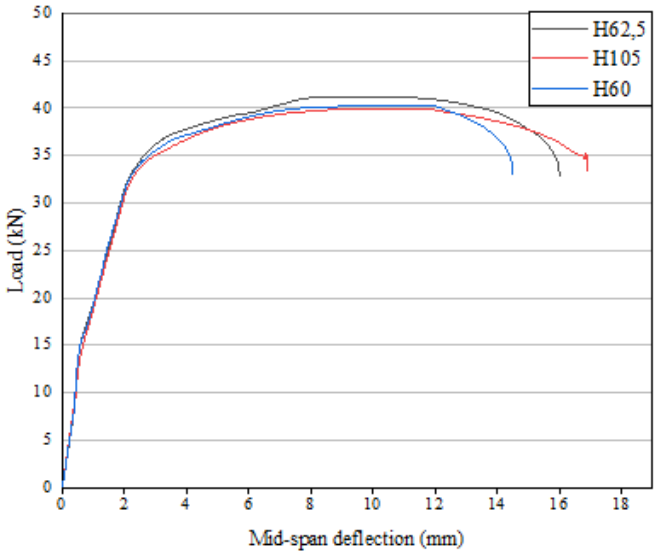

Figure V-4. Load-Deflection graphs for girders with various longitudinal aperture locations

The findings, as summarized in **Table V-3**, unequivocally indicate that the longitudinal opening position plays a pivotal role in shaping the beams' behavior. As the opening position deviates further from the neutral axis, the adverse effects intensify, resulting in a reduction in both the ultimate load capacity and deflection.

- **H105 Girder**: This configuration, positioned below the neutral axis, experienced the greatest decrease in both ultimate load (8.45%) and deflection (41.23%) when compared with the control girder.

- **H60 Girder**: Positioned above the neutral axis, the H60 girder showed reductions of 7.69% in ultimate load and 38.69% in deflection, showcasing a substantial impact.
- **H62.5 Girder**: Situated precisely at the neutral axis, the H62.5 girder had a more moderate impact, achieving reductions of 5.35% in ultimate load and 32.23% in deflection versus the control girder..

These findings underscore the critical role of longitudinal opening position in determining the structural response of the T-beams, emphasizing the need for careful consideration and optimization in beam design and strengthening strategies.

Table V-3. Ultimate Loads and Deflections of Beams with Various Longitudinal Opening Positions

Beam	Ultimate load (kN)	Ultimate deflection (mm)	Ultimate load gain %	Ultimate deflection gain %
Control (CB)	43,55	14,99	-	-
H105	39,87	8,81	-8,45	-41,23
H62,5	41,22	10,1	-5,35	-32,23
H60	40,2	9,19	-7,69	-38,69

V.4.2. Size of longitudinal openings

In this section of our study, we focus on the pivotal role of longitudinal hole size in shaping the structural behavior of the T-beams. We conducted experiments on 3 hollow girders, strategically placing longitudinal apertures precisely in the neutral axis of the cross-section. The openings were systematically resized, as illustrated in **Figure V-5**.

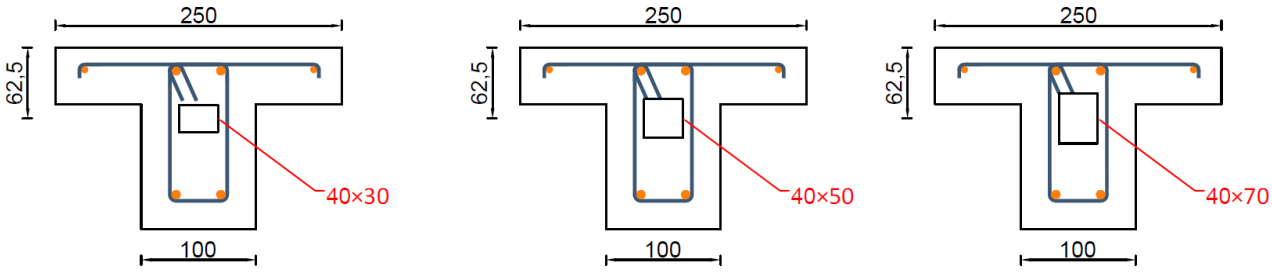

Figure V-5. Various Longitudinal Hole Sizes

The ultimate load and ultimate deflection results, in comparison to those of a solid experimental section, are summarized in **Table V-4** and depicted in **Figure V-6**.

Table V-4. Ultimate Loads and Deflections of Beams with Various Longitudinal Hole Size

Beam	Ultimate load (kN)	Ultimate deflection (mm)	Ultimate load gain %	Ultimate deflection gain %
Control (CB)	43,55	14,99	-	-
B30	41,22	10,1	-5,35	-32,23
B50	40,38	9,27	-7,28	-38,16
B70	39	7,92	-10,45	-47,16

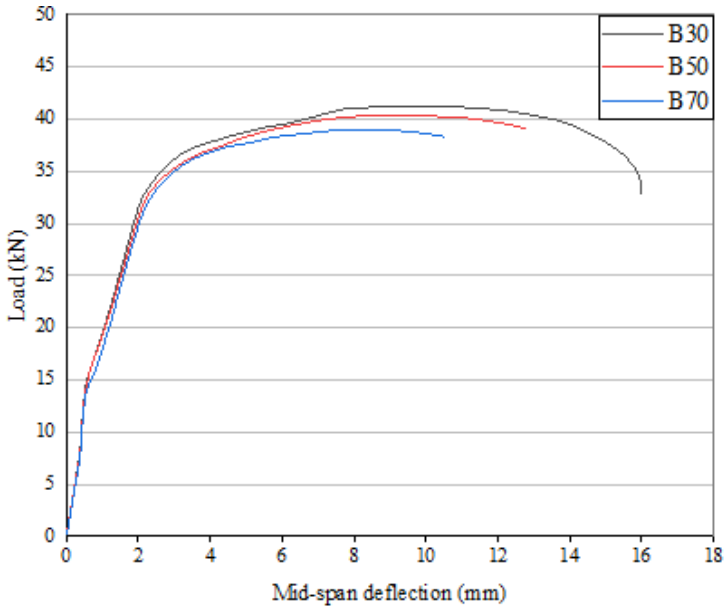

Figure V-6. Load-Deflection graphs for girders with various sizes of longitudinal openings

A discernible trend emerges from our findings: as longitudinal aperture size grows, so too does the adverse impact on both the ultimate load and ultimate deflection. This translates into a reduction in the beams' ability to withstand external loads effectively. Specifically, the ultimate load decreased by 5.35%, 7.28%, and 10.45%, and the ultimate deflection decreased by 32.23%, 38.16%, and 47.16% for the configurations labeled as B30, B50, and B70, respectively, when compared to the solid control beam CB.

This phenomenon can be attributed to the fact that the longitudinal opening in the beam diminishes the effective cross-sectional area, thereby compromising the beam's capacity to resist external loads. Moreover, it introduces stress concentrations at the edges of the opening, further exacerbating its structural performance. As the size of the opening expands, the amount of material contributing to the effective cross-sectional area dwindles, resulting in a commensurate reduction in the beam's load-bearing capacity.

To mitigate the adverse effects of these longitudinal openings, we subsequently reinforced these hollow beams with CFRP in the tension zone. The results indicate a significant increase in the ultimate load capacity of the strengthened beams, ranging from 18.23% to 28.13% compared to that of the control beam CB. However, there was a trade-off, as the ultimate deflection capacity of the strengthened beams diminished substantially, with reductions ranging from 70.45% to 79.65% compared to CB, as shown in **Figure V-7** and **Table V-5**.

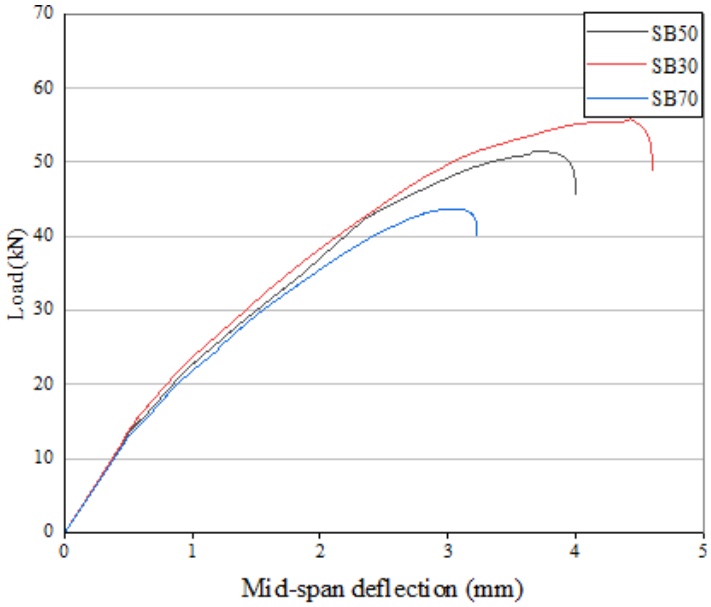

Figure V-7. Load-Deflection graphs for strengthened girders with various sizes of longitudinal openings

It is noteworthy that the beam featuring a longitudinal opening of 30 × 70 mm did not exhibit a significant improvement after CFRP strengthening in the tension zone. This can be attributed to the large size of the opening, which led to premature failure, rendering the CFRP reinforcement ineffective. This underscores the paramount importance of meticulous consideration when determining both the size and location of openings in the design of hollow beams.

Table V-5. Ultimate Loads and Deflections of Strengthened Beams with Various Longitudinal Hole Sizes

Beam	Ultimate load (kN)	Ultimate deflection (mm)	Ultimate load gain %	Ultimate deflection gain %
Control (CB)	43,55	14,99	-	-
SB30	55,8	4,43	28,13	-70,45
SB50	51,49	3,7	18,23	-75,32
SB70	43,72	3,05	0,39	-79,65

V.4.3. Shear Strengthening with Different CFRP Wrapping Configurations

In this section, we explore the impact of shear strengthening using two distinct CFRP wrapping configurations, namely continuous U-wrapping (CUW) and discontinuous U-wrapping (DUW), on the load-deflection behavior of our T-beams. These configurations were chosen based on previous studies [77], [78] and their schematic representations are provided in **Figure V-8**.

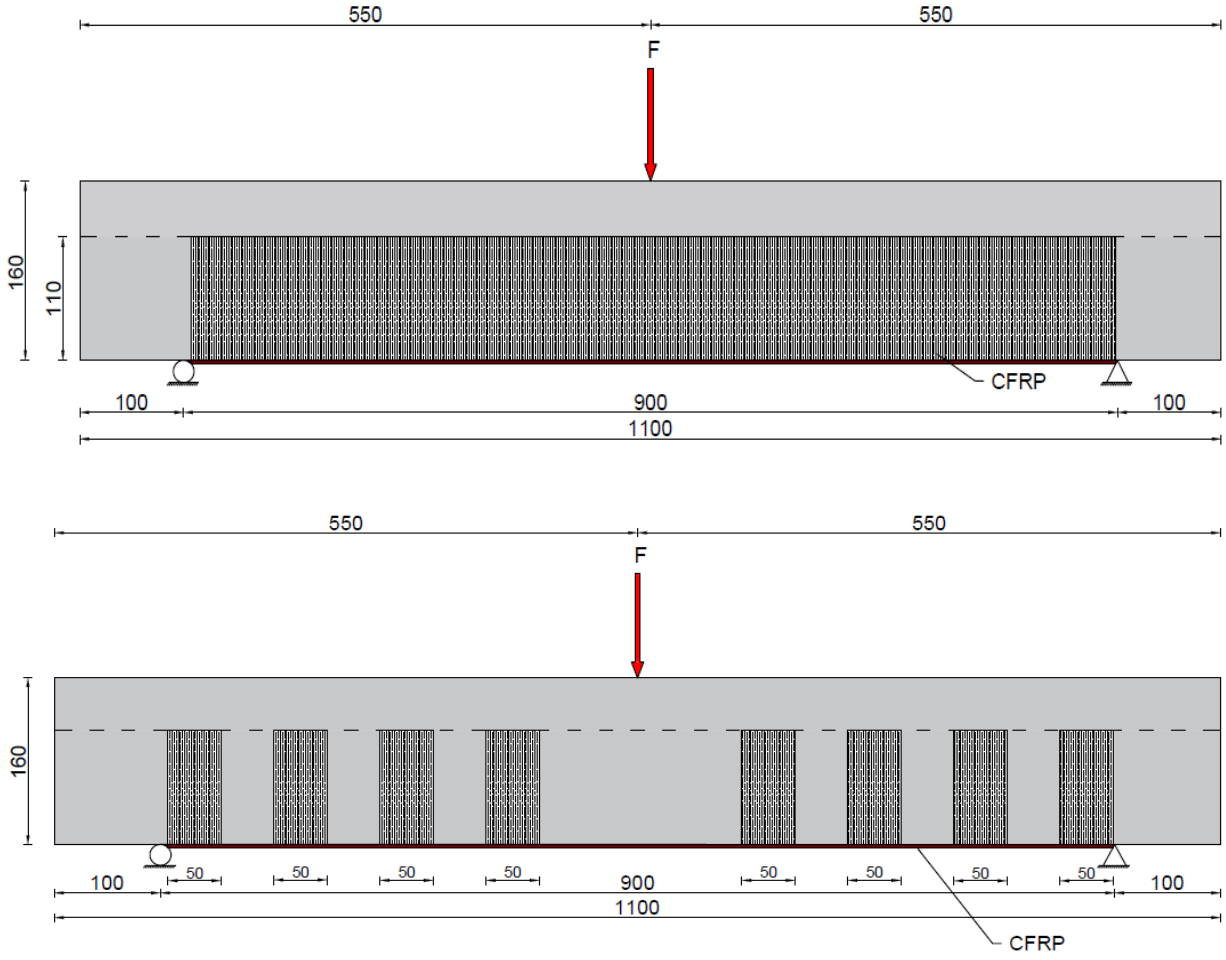

Figure V-8. Various Wrapping configurations: (a) continuous U-wrapping, and (b) discontinuous strip U-wrapping

The introduction of CFRP wrapping configurations represented a pivotal enhancement, resulting in a substantial augmentation of both ultimate load capacity and ultimate deflection when compared to the strengthened solid beam (SCB) without shear strengthening, as illustrated in **Figure V-8**.

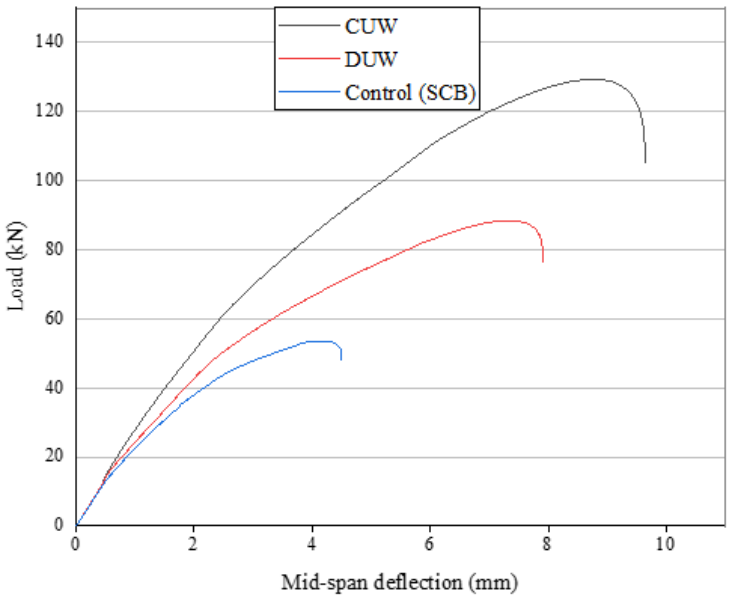

Figure V-9. Load-deflection graphs for strengthened girders with various wrap patterns

Remarkably, the CUW configuration emerged as the most effective, delivering an impressive 122.33% increase in ultimate load capacity. Conversely, the DUW configuration, while still providing a significant boost, exhibited a comparatively lower gain in ultimate load capacity at 52% as illustrated in **Table V-6**.

Table V-6. Ultimate Loads and Deflections of Strengthened Beams with various wrapping configurations

Beam	Ultimate load (kN)	Ultimate deflection (mm)	Ultimate load gain %	Ultimate deflection gain %
CUW	129,33	8,74	122,33	154,07
DUW	88,41	7,31	52	112,5
Control (SCB)	58,17	3,44	-	-

In addition, the two CFRP cladding patterns significantly enhanced the girders' ductility by improving the ultimate deflection. This is a critical aspect in evaluating a girder's capability to withstand structural damage and retain its load-bearing capability under severe conditions. Once again, the CUW layout proved to be the superior choice, elevating the ultimate deflection by a

remarkable 153.49%. Meanwhile, the DUW layout, though offering substantial enhancement, achieved a slightly lower gain at 112.5% in final deflection than the SCB configuration with no wrapping.

The findings underscore the efficacy of CFRP shear strengthening configurations in improving the load-carrying capacities and ductilities of T-girders, with the continuous U-wrapping (CUW) configuration emerging as the most advantageous choice for achieving these structural improvements. These insights provide valuable guidance for engineers and designers when considering shear strengthening strategies for similar structural elements.

CONCLUSION

AND

PERSPECTIVES

Conclusion

As our research reaches its conclusion, it becomes evident that this work encapsulates a comprehensive journey through the realm of reinforced concrete structures, the challenges they face, and innovative strategies to enhance their durability. We believe that this exploration contributes significantly to the ongoing efforts to advance the field of structural engineering and construction practices. The potential of innovative materials and methodologies, such as CFRP, lies at the heart of this research, and we aspire for it to shape the future of structural engineering, ensuring structures that are not only robust and resilient but also sustainable and long-lasting. In our concluding chapter, we will synthesize the insights gained from our multifaceted research and propose recommendations that can further enrich the field.

Important conclusions drawn from the section on "**Durability of reinforced concrete structures**" are as follows:

1. The durability of reinforced concrete structures is essential to ensure their long-term functionality. Various environmental factors, including mechanical, physical, chemical, and structural, can impact their durability.
2. Mechanical factors, such as abrasion, significantly affect the durability of concrete structures. Preventative measures include using suitable materials, optimizing mix composition, and proper construction techniques.
3. Freeze-thaw cycles can lead to concrete deterioration, including microcracking and surface spalling. To enhance freeze-thaw durability, controlling pore structure, using non-freezing aggregates, and curing concrete effectively are essential.
4. Exposure to high temperatures, such as in a fire, can cause thermal instability in concrete. Different types of thermal damage, including explosive spalling and surface spalling, can occur. Design, fire-resistant materials, and construction techniques are key to mitigating such effects.
5. Alkali-aggregate reaction (AAR), specifically the alkali-silica reaction (ASR), can lead to the deterioration of concrete structures. Using nonreactive aggregates, low-alkali cement, and pozzolans can help prevent ASR-related damage.
6. Concrete structures are vulnerable to acid attack, which can lead to erosion and structural damage. Using appropriate aggregates, coatings, and additives can protect against acid attack.

7. Sulfate attack, caused by sulfates in groundwater and soils, can degrade concrete. Measures include adhering to design standards, modifying cement content, and using protective coatings.
8. Structural factors, such as overloading and cyclic loading, can lead to cracking and other forms of concrete damage. Proper structural design and concrete composition are key to mitigating these issues.
9. Settlement cracks, caused by differential settlement of concrete, can be reduced by using additives, such as fibers, lightweight aggregates, and proper curing techniques.
10. Corrosion of reinforcement, triggered by carbonation and chloride attack, can lead to cracking, spalling, and reduced structural integrity. Preventative measures include proper concrete cover, protective coatings, and the use of corrosion-resistant materials.

These conclusions highlight the importance of considering and mitigating various factors that can impact the durability of reinforced concrete structures, ensuring their long-term performance and structural integrity.

Key findings derived from the "**Strengthened RC beams**" section include:

1. Strengthening reinforced concrete (RC) beams is essential for repairing and improving the structural integrity of these elements.
2. Traditional methods of repairing RC structures, such as lining with additional concrete, have disadvantages like increased weight, the need for structure decommissioning, and difficulties in achieving good adhesion between old and new concrete.
3. Using composite materials, particularly Fiber Reinforced Polymers (FRP), for strengthening RC beams is a more effective and less invasive technique.
4. The adhesion of FRP materials to concrete surfaces changes the structural behavior, enhancing strength, stiffness, and durability, which is crucial for beams subjected to bending or shear stresses.
5. FRP composites consist of two key components: reinforcing fibers (e.g., glass, aramid, carbon) and a polymeric matrix (usually epoxy).
6. Proper interfacial adhesion between FRP layers and concrete is essential for the success of strengthening. Surface energy and interfacial tensions play a significant role in adhesion.
7. There are different forms of plating beams: tension face plates, side plates, and compression face plates.

8. Tension face plates maximize flexural capacity but are more prone to debonding, while side plates can be more ductile and resistant to debonding.
9. Compression face plates enhance ductility and vertical shear resistance. Extending tension face plates into the compression faces is a common technique.
10. Plates can be adhesively bonded to RC beams or bolted. Bolting provides the full strength of the plate but may be more expensive to install.
11. Wrapping is an effective method to transfer force into a plate in reinforced concrete beams.
12. Different wrapping types include fully wrap, partially wrap, and compromise wrap.
13. Fully wrapped sections are particularly effective in improving vertical shear capacity but can be challenging to implement.
14. Several failure modes include concrete crushing, FRP rupture, shear failure, intermediate crack (IC) debonding, critical diagonal crack (CDC) debonding, concrete cover separation failure, and plate-end interfacial failure.
15. Factors affecting the durability of FRP-concrete systems include glass transition temperature, moisture, freeze-thaw effects, alkalinity/acidity, fatigue, impact, lightning, and galvanic corrosion.
16. Adequate surface preparation and correct implementation are essential for long-term durability.
17. Encapsulation of concrete in FRP may be beneficial in some conditions but risky in others.
18. Hollow RC beams exhibit different behavior and performance compared to solid beams.
19. Hollow beams can be more flexible but have lower cracking loads compared to solid beams.
20. The size and depth of cavities affect the behavior of hollow beams.
21. Hollow beams can be strengthened with CFRP sheets to improve their performance.

The investigation of longitudinal openings in hollow RC T-beams in the "**Experimental Part**" and "**Parametric Study**" sections revealed several significant findings that are crucial for designers and engineers seeking to use such beams in their projects. These findings are as follows:

1. Longitudinal openings had an adverse impact on the first cracking load of hollow RC T-beams, while the application of CFRP laminates improved the first cracking load in both solid and hollow RC T-beams.
2. The ultimate load was significantly increased by strengthening or retrofitting hollow T-beams with CFRP, especially when the beams were heavily preloaded.

3. Two types of failure modes were observed:
   - Bending failure in control specimens without CFRP.
   - Concrete cover separation in strengthened specimens with CFRP debonding.

   Additionally, hollow specimens exhibited more significant concrete damage and separation compared to solid specimens.
4. CFRP effectively decreased strains on the concrete and steel components within the specimens.
5. The application of CFRP to strengthen and retrofit specimens substantially enhanced their mechanical characteristics, culminating in amplified capacity for carrying loads and heightened resistance failure and deformation.
6. Hollow spicemens strengthened with CFRP and incorporating a 5% hollow cavity area located 105 mm from the upper fiber, demonstrated behavior akin to strengthened solid spicemens. Nevertheless, retrofitted spicemens exhibited diminished bending effectiveness following preloading in comparison to retrofitted solid spicemens.
7. Positioning the opening on the neutral axis is preferred to reduce its adverse effects, while positioning it above the neutral axis is inadvisable as it leads to premature damage to the concrete in the compression area.
8. The increase in opening size resulted in a proportional adverse effect on both the maximal force and displacement.
9. Increasing the aperture size has enhanced the efficiency of the CFRP by increasing maximum force and reducing displacement.
10. The bending performance of reinforced hollow spicemens with CFRP was notably influenced by the dimensions and position of the longitudinal aperture.
11. The use of CFRP in a U-shaped winding configuration across the entire length of the bay showed superior performance for the structural parameters evaluated, including ultimate strength and ductility. This configuration guarantees the structures' security and impact resistance, even under heavy load situations.

These results underline the significance of the appropriate location of longitudinal openings in reinforced concrete hollow T-beams for ensuring structural integration and global performance. Consideration of the size and position of apertures when planning cavity sections is essential to preserve the load-bearing properties and stiffness.

Perspectives

Based on my research findings, I recommend that future studies in this field consider expanding the scale of their investigations. Specifically, researchers should focus on enlarging the scope of their experiments by incorporating larger-scale specimens, especially in terms of beam dimensions resembling real-life structural elements. This expansion will provide a more comprehensive understanding of the behavior of reinforced concrete beams with openings and their response to strengthening techniques such as CFRP laminates. Additionally, investigating a wider range of parameters, such as varying opening sizes, locations, and CFRP strengthening configurations, would contribute to a more nuanced comprehension of structural performance and inform practical design guidelines for engineers and practitioners.

Another recommendation for further work in this field is to conduct additional laboratory experiments aimed at mitigating early concrete failure by incorporating shear strengthening. This would involve studying the effectiveness of various shear strengthening techniques, such as adding different CFRP wrapping configurations, to enhance the structural integrity and durability of reinforced concrete beams. Additionally, exploring innovative approaches to address shear-related challenges in concrete structures can contribute valuable insights to the field and advance the development of more resilient infrastructure systems.

BIBLIOGRAPHIC REFERENCES

Bibliographic References

[1] A. K. H. Kwan and H. H. C. Wong, “Durability of Reinforced Concrete Structures, Theory vs Practice.”

[2] “Durability of Reinforced Concrete Structures.”

[3] L. Bertolini, *Corrosion of steel in concrete : prevention, diagnosis, repair*. Wiley-VCH, 2004.

[4] J. F. Lamond and J. H. Pielert, “Significance of Tests and Properties of Concrete and Concrete-Making Materials STP 169D,” 2006. [Online]. Available: http://www.copyright.com/.

[5] ACI Committee 201. and American Concrete Institute., *Guide to durable concrete*. American Concrete Institute, 2008.

[6] B. D. Scott and M. Safiuddin, “Abrasion Resistance of Concrete-Design, Construction and Case Study,” 2015. [Online]. Available: www.crl.issres.net

[7] Y. W. Liu, T. Yen, and T. H. Hsu, “Abrasion erosion of concrete by water-borne sand,” *Cem Concr Res*, vol. 36, no. 10, pp. 1814–1820, Oct. 2006, doi: 10.1016/j.cemconres.2005.03.018.

[8] S. Macdonald, D. Watt, and P. Swallow, “Concrete Building Pathology.”

[9] M. Hang, L. Cui, J. Wu, and Z. Sun, “Freezing-thawing damage characteristics and calculation models of aerated concrete,” *Journal of Building Engineering*, vol. 28, Mar. 2020, doi: 10.1016/j.jobe.2019.101072.

[10] U. M. El, B. El, I. de Bordj, and B. Arréridj, “Pathologies des Constructions,” 2019. [Online]. Available: https://www.researchgate.net/publication/336287624

[11] Noumowé A, “Effet de hautes températures (20-600°C) sur le béton. Cas particulier du béton à hautes performances,” Institut National des Sciences Appliquées de Lyon, Lyon, 1995.

[12] Xing Z, “Influence de la nature minéralogique des granulats sur leur comportement et celui du béton à haute température,” Université de CergyPontoise, 2011.

[13] “Draft Technical Report ?? Assessment, design and repair of fire-damaged concrete structures Final draft,” 2008.

[14] 7 Author, K. J. Folliard, M. D. A. Thomas, B. Fournier, K. E. Kurtis, and J. H. Ideker, "Interim Recommendations for the Use of Lithium to Mitigate or Prevent Alkali-Silica Reaction (ASR) 6. Performing Organization Code Contracting Officer's Technical Representative (COTR): Fred Faridazar, HRDI-11 Unclassified Unclassified," 2006.

[15] J. E. Gillott, "ALKALI-AGGREGATE REACTIONS IN CONCRETE," 1975.

[16] M. G. Alexander, A. Bentur, and S. Mindess, *Durability of concrete : design and construction, 2017*.

[17] "ATTAQUES CHIMIQUES." [Online]. Available: www.belzona.com/tcc

[18] M. Çullu and M. Arslan, "The effects of chemical attacks on physical and mechanical properties of concrete produced under cold weather conditions," *Constr Build Mater*, vol. 57, pp. 53–60, Apr. 2014, doi: 10.1016/j.conbuildmat.2014.01.072.

[19] Victoria Interval, "Concrete Cracks: An Overview of Types of Cracking/Deterioration and Their Implications." [Online]. Available: https://crspgh.com/about-concrete-repair-services/causes-of-concrete-cracks/

[20] T. C. Powers, *The Properties of Fresh Concrete*. John Wiley and Sons, Inc. NY, 1968.

[21] Sidney Mindess, J. Francis Young, and David Darwin, *Concrete (2nd Edition)*, 2nd ed. Prentice-Hall, Englewood Cliffs, 2002.

[22] R. Combrinck, "Cracking of Plastic Concrete in Slab-Like Elements," PhD Thesis, Stellenbosch University, Stellenbosch, 2016.

[23] W. J. Weiss and J. Olek, "Assessing the settlement of fresh concrete using a non-contact laser profiling approach Investigation of use of recycled concrete aggregate (RCA) in pavement concrete. View project New Approaches to Mixture Development for Concrete Durability and Service Life View project," 2005. [Online]. Available: https://www.researchgate.net/publication/228436720

[24] D. P. Bentz *et al.*, "Plastic shrinkage cracking in internally cured mixtures made with pre-wetted lightweight aggregate." [Online]. Available: https://www.researchgate.net/publication/228912590, January 2010.

[25] Euro-International Committee for Concrete., *Durable concrete structures design guide*. Telford, 1997.

[26] A. M. Neville, *Properties of Concrete*, 4th edition. Longman Group Limited, 1995.

[27] ACI Committee 222. and American Concrete Institute., *Design and construction practices to mitigate corrosion of reinforcement in concrete structures*. American Concrete Institute, 2011.

[28] E. Chen, S. Tang, and C. K. Y. Leung, "Corrosion-induced cracking in reinforced concrete due to chloride contamination and ingress," *ACI Mater J*, vol. 116, no. 5, pp. 99–111, 2019, doi: 10.14359/51716831.

[29] C. Krasniqi, A. Sadikaj, S. Bublaku, N. Kabashi, A. Muriqi, and H. Morina, "CORROSION IN CONCRETE UNDER SULPHATE AND CHLORIDE ATTACKS," 2017. [Online]. Available: https://www.researchgate.net/publication/316440930

[30] Ze Yi Wu, "ETUDE EXPERIMENTALE DU COMPORTEMENT DES POUTRES COURTES EN BETON ARME PRE-FISSUREES ET RENFORCEES PAR MATERIAUX COMPOSITE SOUS CHARGEMENT STATIQUE ET DE FATIGUE," Français, 2004. Accessed: Aug. 30, 2022. [Online]. Available: https://pastel.archives-ouvertes.fr/pastel-00001266

[31] M. Ansley and et al., "Thermo-Mechanical Durability of Carbon Fiber Reinforced Polymer Strengthened Reinforced Concrete Beams. Final Report, Florida DOT, Project No. BD550-06," 2009.

[32] A. Nanni, "Fiber Reinforced Polymer Composites for Infrastructure Strengthening-From Research to Practice."

[33] A. Elarbi, "Durability Performance of FRP Strengthened Concrete Beams and Columns Exposed to Hygrothermal Environment, PhD Dissertation," Wayne State University, Detroit, MI, 2011.

[34] Hwai-Chung Wu and Christopher D. Eamon, *Strengthening of Concrete Structures Using Fiber Reinforced Polymers (FRP)*, 1st ed. Woodhead Publishing, 2017.

[35] P. Mallick, *Fiber-Reinforced Composites-Materials, Manufacturing, and Design, third ed*, 3rd ed. CRC Press, 2007.

[36] Meier U, "Strengthening of structures using carbon fibre/epoxy composites," *Construction and Building Materials, 9(6)*, pp. 341–351, 1995.

[37] O. Buyukozturk and B. Hearing, "Failure behaviour of precracked concrete beams retrofitted with FRP," *J. Compos. Construct. 2 (3),* pp. 138–144, 1998.

[38] C. Mikami, H. C. Wu, and A. Elarbi, "Effect of hot temperature on bond strength of FRP bonded concrete," *Constr. Build. Mater. 91*, pp. 180–186, 2015.

[39] M. Anson, J. M. Ko, and E. S. S. Lam, *Advances in building technology : proceedings of the International Conference on Advances in Building Technology, 4-6 December, 2002, Hong Kong, China*. Elsevier, 2002.

[40] R. Al-Mahaidi and R. Kalfat, "FRP Anchorage Systems," in *Rehabilitation of Concrete Structures with Fiber-Reinforced Polymer*, Elsevier, 2018, pp. 331–376. doi: 10.1016/b978-0-12-811510-7.00008-2.

[41] A. M. Remennikov, N. Sheikh, A. Remennikov, M. Goldston, and M. Neaz Sheikh, *Composite railway sleepers View project Static and Dynamic testing of tendons using double shear apparatus View project Impact performance of concrete beams externally bonded with carbon FRP sheets*. 2016. [Online]. Available: https://www.researchgate.net/publication/313030086

[42] T. Aljaafreh, E. Beneberu, and N. Yazdani, "Anchorage Effect on Flexural Fiber Reinforced Polymer (FRP) Laminate Strengthening of Lightweight Concrete Beams," *Journal of Engineering and Architecture*, vol. 6, no. 1, 2018, doi: 10.15640/jea.v5n2a2.

[43] J. G. Teng and J. Yao, "Plate end debonding in FRP-plated RC beams-II: Strength model," *Eng Struct*, vol. 29, no. 10, pp. 2472–2486, Oct. 2007, doi: 10.1016/j.engstruct.2006.11.023.

[44] H. Pham and R. Al-Mahaidi, "Assessment of available prediction models for the strength of FRP retrofitted RC beams," *Compos Struct*, vol. 66, no. 1–4, pp. 601–610, Oct. 2004, doi: 10.1016/j.compstruct.2004.05.008.

[45] R. Al-Mahaidi and R. Kalfat, "Strengthening Members in Flexure Using FRP," in *Rehabilitation of Concrete Structures with Fiber-Reinforced Polymer*, Elsevier, 2018, pp. 25–119. doi: 10.1016/b978-0-12-811510-7.00005-7.

[46] S. Tudjono, H. A. Lie, and B. S. Gan, "An integrated system for enhancing flexural members' capacity via combinations of the fiber reinforced plastic use, retrofitting, and surface treatment techniques," *International Journal of Technology*, vol. 9, no. 1, pp. 5–15, 2018, doi: 10.14716/ijtech.v9i1.298.

[47] J. G. Teng, S. T. Smith, J. Yao, and J. F. Chen, “Intermediate crack-induced debonding in RC beams and slabs,” in *Construction and Building Materials*, Sep. 2003, pp. 447–462. doi: 10.1016/S0950-0618(03)00043-6.

[48] S. K. Sharma, M. S. M. Ali, D. Goldar, and P. K. Sikdar, “Investigation of critical diagonal crack debonding in plated RC beams,” *Compos B Eng*, vol. 39, no. 3, pp. 570–584, Apr. 2008, doi: 10.1016/j.compositesb.2007.02.021.

[49] J. G. Teng and J. F. Chen, “DEBONDING FAILURES OF RC BEAMS STRENGTHENED WITH EXTERNALLY BONDED FRP REINFORCEMENT: BEHAVIOUR AND MODELLING,” 2007.

[50] Fédération internationale du béton., *Externally bonded FRP reinforcement for RC structures : technical report on the design and use of externally bonded fibre reinforced polymer reinforcement (FRP EBR) for reinforced concrete structures*. International Federation for Structural Concrete, 2001.

[51] P. Kelley, F. Isley, M. Vatovec, and Mack J, “Sika CarboDur structural strengthening system, engineering guidelines for design and application,” 1999.

[52] G. Lubin and P. Donohue, “Real life ageing properties of composites,” in *Proceedings of 35th Annual Technical Conference of the Reinforced Plastics and Composites Institute, Section 17E, 21.*, 1980.

[53] V. and H. I. Karbhari, “Effect of composite wrap architecture on strengthening of concrete due to confinement: II-Strain and damage effects,” *Journal of Reinforced Plastics and Composites, 16(2)*, 1997, doi: https://doi.org/10.1177%2F073168449701601105.

[54] H. Kaiser, “Strengthening of reinforced concrete with CFRP plates, Ph.D. dissertation,” ETH Zürich (in German)., 1989.

[55] S. R. , I. M. and M. B. Tysl, “Effect of surface delamination on the freeze/thaw durability of CFRP-reinforced concrete beams,” in *Durability of Fibre Reinforced Polymer (FRP) Composites for Construction CDCC ’98*, Sherbrooke, Canada, 1998, pp. 317–324.

[56] K. Yagi, T. Tanaka, H. Sakai, and H. Otaguro, “Durability of carbon fiber sheet for repair and retrofitting,” in *Non-Metallic (FRP) Reinforcement for Concrete Structures, Proceedings of the Third International Symposium, 2, Sapporo, Japan*, 1997, pp. 259–266.

[57] K. A. Soudki and M. F. Green, “Freeze-thaw response of CFRP wrapped concrete,” in *Concrete International, 19,* 1997, pp. 64–72.

[58] H. Toutanji and P. Balaguru, “Durability characteristics of concrete columns wrapped with FRP tow sheets,” *Journal of Materials in Civil Engineering, ASCE, 10(1),* pp. 52–57, 1998.

[59] A. Pantuso, U. Neubauer, and F. S. Rostasy, “Effects of thermal mismatch between FRP and concrete on bond,” in *Minutes of 4th ConFibreCrete Meeting, Lille, France.*, Lille, France., 2000.

[60] M. Deuring, “Strengthening of RC with prestressed fiber reinforced plastic sheets. EMPA Research Report 224, Dübendorf, Switzerland (in German),” 1993.

[61] R. Barnes and G. Mays, “Fatigue performance of concrete beams strengthened with CFRP plates,” *ASCE Journal of Composites for Construction, 3(2),* pp. 63–72, 1999.

[62] M. Erki and U. Meier, “Impact loading of concrete beams externally strengthened with CFRP laminates,” *ASCE Journal of Composites for Construction, 3(3),* pp. 117–124, 1999.

[63] A. S. Alnuaimi, K. S. Al-Jabri, and A. Hago, “Comparison between solid and hollow reinforced concrete beams,” *Materials and Structures/Materiaux et Constructions*, vol. 41, no. 2, pp. 269–286, Mar. 2008, doi: 10.1617/s11527-007-9237-x.

[64] A. S. Elamary, I. A. Sharaky, and M. Alqurashi, “Flexural behaviour of hollow concrete beams under three points loading: Experimental and numerical study,” *Structures*, vol. 32, pp. 1543–1552, Aug. 2021, doi: 10.1016/j.istruc.2021.03.094.

[65] H. M. Abdulhusain and M. A. Ismael, “Flexural Behaviour of Hollow Reinforced Concrete T-Beams,” *IOP Conf Ser Mater Sci Eng*, vol. 1090, no. 1, p. 012133, Mar. 2021, doi: 10.1088/1757-899x/1090/1/012133.

[66] A. A. Abbass, S. R. Abid, F. H. Arna’ot, R. A. Al-Ameri, and M. Özakça, “Flexural response of hollow high strength concrete beams considering different size reductions,” *Structures*, vol. 23, pp. 69–86, Feb. 2020, doi: 10.1016/j.istruc.2019.10.001.

[67] A. Murugesan and A. Narayanan, “Deflection of Reinforced Concrete Beams with Longitudinal Circular Hole,” *Practice Periodical on Structural Design and Construction*, vol. 23, no. 1, p. 04017034, Feb. 2018, doi: 10.1061/(asce)sc.1943-5576.0000356.

[68] A. Sirisonthi *et al.*, "Structural Behavior of Large-Scale Hollow Section RC Beams and Strength Enhancement Using Carbon Fiber Reinforced Polymer (CFRP) Composites," *Polymers (Basel)*, vol. 14, no. 1, Jan. 2022, doi: 10.3390/polym14010158.

[69] C. Hamza, S. Bouchra, B. Mostapha, and B. Mohamed, "Formulation of ordinary concrete using the dreux-gorisse method," in *Procedia Structural Integrity*, Elsevier B.V., 2020, pp. 430–439. doi: 10.1016/j.prostr.2020.10.050.

[70] S. Carbodur®, "Notice produit Sika® CarboDur® S NOTICE PRODUIT," 2020.

[71] K. W. Al Shboul, M. M. Raheem, and H. A. Rasheed, "Debonding characterization for all-lightweight RC T-Beams strengthened in flexure with FRP," *Journal of Building Engineering*, vol. 44, Dec. 2021, doi: 10.1016/j.jobe.2021.103377.

[72] F. Ceroni, "Experimental performances of RC beams strengthened with FRP materials," *Constr Build Mater*, vol. 24, no. 9, pp. 1547–1559, Sep. 2010, doi: 10.1016/j.conbuildmat.2010.03.008.

[73] R. Kotynia, "Ductility and failure mode of RC Beams Strengthened for Flexure with CFRP / Odkształcalność i sposób zniszczenia żelbetowych belek wzmocnionych na zginanie materiałami CFRP," 2003. [Online]. Available: https://www.researchgate.net/publication/315409104

[74] M. Rezazadeh, I. Costa, and J. Barros, "Influence of prestress level on NSM CFRP laminates for the flexural strengthening of RC beams," *Compos Struct*, vol. 116, no. 1, pp. 489–500, Sep. 2014, doi: 10.1016/J.COMPSTRUCT.2014.05.043.

[75] P. Kmiecik and M. Kamiński, "Modelling of reinforced concrete structures and composite structures with concrete strength degradation taken into consideration," 2011.

[76] R. H. K. and S. Inc. ; 2012. Pawtucket, *ABAQUS user's manual version 6.12*.

[77] B. Dutta, A. Kumari, and A. N. Nayak, "Shear behaviour of RC deep beams retrofitted with externally bonded GFRP fabrics: Experimental and numerical study," *Structures*, vol. 46, pp. 1–16, Dec. 2022, doi: 10.1016/j.istruc.2022.10.042.

[78] L. K. Amaireh and A. Al-Tamimi, "Optimum Configuration of CFRP Composites for Strengthening of Reinforced Concrete Beams Considering the Contact Constraint," in *Procedia Manufacturing*, Elsevier B.V., 2020, pp. 350–357. doi: 10.1016/j.promfg.2020.02.284.